Construction and Calibration of Large-Scale Rainfall Simulators

by

Jacob Allen Etheridge

A thesis submitted to the Graduate Faculty of
Auburn University
in partial fulfillment of the
requirements for the Degree of
Master of Science in Civil Engineering

Auburn, Alabama
May 6, 2023

Keywords: rainfall simulation, erosion control, stormwater,
raindrop size distribution, runoff

Approved by

Michael A. Perez, Chair, Assistant Professor of Civil and Environmental Engineering
Wesley N. Donald, Research Fellow of Civil and Environmental Engineering
Xing Fang, Professor of Civil and Environmental Engineering

ABSTRACT

Large-scale rainfall simulation offers valuable insight into the effectiveness of erosion control practice. While small and intermediate-scale apparatuses can analyze the effects of splash and sheet erosion on a slope, large-scale plots allow the formation of rills, which better represent real applications on long slopes such as highway embankments. Construction and calibration methods for large-scale rainfall simulators are standardized by ASTM D6459-19. As part of Phase II of "Evaluation of ALDOT Erosion Control Practices using Rainfall Simulation on Various Soil Types and Slope Gradients," twelve ASTM D6459-19 rainfall simulators were constructed, calibrated, and used to obtain soil erodibility factors in bare-soil testing. Efficient construction practices for ASTM D6459-19 rainfall simulators include using pre-made tanks for catchment basins, using lumber for plot borders, and creating a portable rainfall simulation system with a manifold for flow distribution. These techniques along with others included in this work can reduce the cost of constructing large-scale rainfall simulators, which allows for increased ability to test on various slopes and soils.

Calibration analysis was performed to evaluate direct measurement of runoff for intensity calibration. The results indicate that the runoff volume method produced statistically different results than the ASTM D6459-19-recommended rainfall gauge method. The runoff from the impermeably covered plot was 27.8% to 32.8% less than the rainfall gauges predicted. Furthermore, there was not enough evidence to conclude that 20 and 6 observation rainfall gauge setups were statistically different. Photography was investigated for determining raindrop characteristics including size and velocity. Results indicated that the photography method

represented a greater proportion of raindrops smaller than 1.68 mm diameter than the ASTM D6459-19 flour pan method. The photography method yielded a raindrop erosivity factor 32.8% less than the flour pan method for the center of the plot. Raindrop velocity results of the photography method yielded statistically different velocities than theoretically predicted based on drop size and fall height. The photographically determined velocities were calculated as the distance traveled by a raindrop over the time the camera captured the photograph, called the shutter speed, and the photographs yielded 25.8% lower velocities than predicted on average.

The twelve new rainfall simulators at AU-SRF were calibrated and tested using ASTM D6459-19 methods. Using the same sprinkler design as the original AU-SRF rainfall simulator, the theoretical rainfall erosivity factor (*R*) with target intensities was 148.5. The first three bare soil control tests on the new rainfall simulator plots yielded soil erodibility factors (*K*) of 0.18, 0.06, and 0.02 for ASTM sand, loam, and clay, respectively.

This thesis includes documentation and analysis of rainfall simulator construction, calibration methods, and control testing. The continuity of rainfall simulator methodology is critical to the continued precise evaluation of erosion control practices at Auburn University-Sediment Research Facility and other facilities.

ACKNOWLEDGEMENTS

The author thanks Dr. Michael Perez and Dr. Wesley Donald for their continued support and guidance. In addition, he thanks the Auburn Stormwater research team and specifically Christy Manning and Jack Cater, who worked with him on separate stages of the rainfall simulator project. He would also like to thank the many undergraduate workers without whom this project would not have been possible. He thanks Dr. Xing Fang and Dr. Jeffrey LaMondia for their guidance and the Alabama Department of Transportation for their financial support of the rainfall simulator project. Finally, he thanks his father, Allen, his mother, Suzanne, his sister, Adrian, his significant other, Liza, and his grandparents, Katherine, Young, Linda, and Charlie for their love and support throughout his studies.

TABLE OF CONTENTS

LIST OF TABLES

LIST OF FIGURES

CHAPTER 1: INTRODUCTION

1.1 BACKGROUND

For decades, soil erosion originating on construction sites has been identified as a significant source of sediment and suspended solids in runoff in the United States (Hagman, 1980). Soil erosion has devastating, well-recorded effects, including sedimentation in streams and rivers, which can cause clogging and destroy riparian ecosystems. In 1917, pioneers at the University of Missouri established the precursor to rainfall simulation plots. They discovered that cultivation of slopes leads to large losses of soil; however, cropping methods could reduce these losses *(*Gantzer et al., 2018). Now, numerous erosion control practices are used to reduce slope erosion.

In erosion control, various forms of straw and mulch are used on bare soil to aid the establishment of vegetation and prevent soil loss. While straw is cheap and effective for this purpose, manufactured products can be more effective when properly installed (Horne, 2017). Erosion control blankets, or ECBs, are one of the most effective products for erosion control on slopes. ECBs evolved from straw applications due to increasing regulation at the introduction of the Clean Water Act of 1972. The demand for ECBs in transportation system construction has risen significantly in the last century due to the signage of the Federal-Aid Highway Act of 1956, which commissioned 41,000 miles (66,000 km) of interstate and lead to the construction of numerous other roadways (Kaszynski, 2000), which require countless miles of slope stabilization, especially on the embankments of superelevated sections that tend to have steep and long slopes.

Other methods for slope protection on construction sites include topsoiling, surface tracking, vegetation, and mulching. Topsoiling is the spreading of in-situ or imported topsoil on disturbed or excavated areas to promote successful vegetation growth. Surface tracking is a method

of compaction using heavy equipment by driving up and down slopes. Vegetation used on sites varies greatly by region; however, in Alabama, Bermuda and Fescue are commonly used grass species for the warm and cold seasons, respectively. Mulching includes straw applications, hydromulches, and the use of other mulching materials. Straw and other mulch products like woodchips protect the soil surface from raindrops, reduce runoff velocity, increase infiltration, slow soil moisture loss, prevent soil crusting, moderate soil temperature, and improve conditions for seed germination and vegetation growth. When slopes are steep and inaccessible to equipment, fibers with tackifier and mineral binders can be sprayed out of a hose, which is called hydromulching. Often, they contain seed, fertilizer, mulch, and a tackifier in liquid form. The evaluation of the efficacy of these products requires rigorous testing.

1.2 RAINFALL SIMULATION

One concept for testing erosion control products is to measure the amount of soil displaced by rainfall on a bare slope and a protected slope and compare the difference. To obtain consistent results, rainfall events can be simulated using testing apparatuses rather than relying on natural rainfall events. Rainfall simulators are preferable to natural events because they produce consistent rainfall intensity, drop size distribution, and test duration. Rainfall simulator plot sizes, slopes, soils, raindrop delivery methods, target rainfall intensities, calibration techniques, test methods, and analysis methods vary; however, the most prevalent guidance for large-scale rainfall simulation is ASTM D6459-19.

ASTM International offers guidance on the construction and calibration of large-scale rainfall simulators via standard D6459-19, “Determination of RECP Performance in Protecting Hillslopes from Rainfall-Induced Erosion” (ASTM, 2019). Rainfall simulators are used to test product installations versus bare soil control conditions to determine the effectiveness of various

products and practices for protecting topsoil on these sites to prevent soil pollution. The calibration of these rainfall simulators is critical to their success so that correct results may be obtained.

1.3 RESEARCH OBJECTIVES

The primary purpose of this research is to disseminate effective practices for constructing, calibrating, and testing on ASTM D6459-19 rainfall simulators. Additionally, novel techniques for calibration were investigated to develop rainfall simulator calibration with current technology. The novel techniques for calibration can be used to articulate the testing environment that practices and products are tested under by determining performance evaluation characteristics of the rainfall simulator.

Documentation on time and cost-effective construction methods for large-scale rainfall simulators meeting ASTM D6459-19 specifications is sparse. By experimenting with the efficacy of various practices during the construction of twelve rainfall simulators in 2021 and 2022, this thesis seeks to establish a basis for overcoming the many challenges that accompany the task of constructing a large-scale rainfall simulator. This work is key for refining standardization among large-scale rainfall simulators so that studies may be easily juxtaposed. Currently, rainfall simulator research varies by plot size, which substantially affects results (Ricks, 2020). Therefore, the size of the plot and the construction methods applied are variables that must be considered when comparing studies using different designs. Large-scale rainfall simulators require more construction effort than small-scale apparatuses, but they may provide more useful results for practical applications. Therefore, efficient rainfall simulator construction techniques specifically targeting ASTM D6459-19 are necessary to construct large-scale apparatuses that can generate more widely comparable results.

Furthermore, this work evaluated various calibration methods including the usage of runoff for the measurement of rainfall intensity and videography for raindrop size and raindrop velocity calibration. These methods may offer improved precision for their respective parameters compared to standard ASTM D6459-19 methods such as rainfall gauges and the flour pan method. Statistical analysis was used to compare the alternative methods to ASTM D6459-19 methods and recommendations were made based on the significance of differences between the methods and the feasibility of the alternative methods.

Lastly, control testing is key to proper evaluation of products, and documentation on the methodology and results of the first round of bare soil tests on the twelve new slopes is included. While further testing is required to determine the effects of various slopes and soils on soil loss, preliminary results are provided and discussed.

Therefore, the objectives of this thesis are as follows:

1. Document the construction of twelve ASTM D6459-19 rainfall simulators on various slopes and soils,

2. Investigate alternative methods for rainfall intensity, raindrop size, and raindrop velocity calibration, and

3. Provide control test results from calibrated rainfall simulators. Additionally, this work contains relevant literature review including testing of hydromulch, relevant soil analysis, and initial control tests for the new plots.

The project was separated into the following tasks to accomplish these objectives:

1. Construct twelve rainfall simulators and stockpiling of soils for testing,

2. Verify the original AU-SRF ASTM D6459-19 rainfall simulator for renewal of accreditation from Geosynthetic Accreditation Institute,

3. Investigate novel calibration techniques including runoff to determine intensity and photography for rainfall characteristics including drop size distribution and raindrop velocity,

4. Calibrate new rainfall simulators including the flour pan test for rainfall drop size distribution and theoretical rainfall erosivity factor calculation, and

5. Perform initial testing on new rainfall simulators on bare soil with preliminary soil erodibility factor calculations.

1.4 ORGANIZATION OF THESIS

This thesis communicates numerous results which are grouped into several sections. In *Chapter 2: Literature Review*, topics include ASTM D6459-19, the Revised Universal Soil Loss Equation (RUSLE), alternative plot designs, alternative calibration methods, and hydromulch testing methods. *Chapter 3: Construction Methodology* details the many steps for constructing an ASTM D6459-19 rainfall simulator plot. *Chapter 4: Calibration and Testing Methodology* contains procedures for each calibration practice examined as well as the procedures utilized for ASTM D6459-19 bare soil testing on the new rainfall simulators. *Chapter 5: Results and Discussion* summarizes construction findings and contains statistical analyses of alternative intensity calibration methods versus standard practices. This includes the comparison of ASTM D6459-19 recommended methods for intensity, raindrop size, and raindrop velocity determination

to alternative methods including measuring maximum runoff and utilizing photography for raindrop size and velocity. Furthermore, this section contains the findings of the first bare soil tests on the new rainfall simulator plots. Finally, *Chapter 6: Conclusions* contains a summary of results and offers recommendations for future work.

CHAPTER 2: LITERATURE REVIEW

2.1 EROSION CONTROL PRACTICES

Erosion control products are commonly applied on bare slopes such as newly constructed roadway embankments and in small channels. They are installed with seed to promote vegetation for permanent stabilization and prevent sediment runoff by shielding soil particles from being dislodged and transported by raindrops and overland flow. They are often fabricated from natural fibrous materials such as cotton, straw, wood, or coconut, which are plant-based and sustainable materials (City of Springfield, 2008). ECBs protect against wind and water induced erosion while also increasing infiltration rates and decreasing soil crusting and compaction (City of Springfield, 2008). Most ECBs are made from biodegradable materials that decompose to further support vegetation growth. One type of rolled erosion control product, or RECP, that is commonly confused for an ECB is a turf reinforcement mat (TRM). However, TRMs are synthetic and permanent (MPCA, 2012). Slope stabilization is a necessary step for transitioning from the construction phase of transportation infrastructure to the post-construction phase, and biodegradable ECBs can help to accomplish this task sustainably. Roadways in particular benefit from bare soil protection practices because roadway runoff can reach high velocities while moving over pavement and because embankments often have relatively steep slopes of 4H:1V, 3H:1V, or greater. Sediment pollution can be prevented at the source with erosion control to protect water quality of ecosystems and save cost by reducing need to filter or dredge downstream bodies of water.

Early precursors to ECBs such as mulch are vulnerable to erosion during the germination of the vegetation, and contractors did not have external incentives to use more effective products before federal regulations (Hanrahan, 2015). While inexpensive materials such as straw can protect bare soil to an extent, pressure from environmental agencies forced demand for better-performing manufactured products. The company American Excelsior claims to have invented the first erosion control blanket in 1974 as a response to pressure and regulations by the EPA with the introduction of the National Pollutant Discharge Elimination System (NPDES) in 1972 (Kelsey, 2014). The modern erosion control blanket and method of manufacture is patented by Timothy Prunty and Wendell E. Johnson. The patent was filed February 3, 1997, and granted on July 28, 1998. It describes the generalized function of modern rolled erosion control blankets as shields for the earth (Prunty et. al, 1997). The manufacturing includes the mat, made of wood wool or similar, being longitudinally passed under a bonding agent spray with at least one designed surface (Prunty et. al, 1997). Contemporary ECBs are extremely effective at soil loss prevention with around 95% reduction in soil loss compared to a bare slope (Faulkner, 2020).

Biodegradable ECBs are used where vegetation requires only temporary support to be established (MPCA, 2012). For example, slopes that are 3H:1V or steeper benefit greatly from stabilization by preventing seed washout that would otherwise occur with a rainfall event and may not be prevented by straw. In most states, ECBs are used with fast-growing grass seed on newly constructed roadway embankments with straw being used for flatter slopes (Barkley, 2004). A synthesis on highway practice by the National Cooperative Highway Research Program (NCHRP) describes how ECBs can be used for low-volume roads, which represent 75% of miles (kilometers) of road in the U.S. (Fay et. al, 2012). Low-volume roads often cut corners at the end of construction by omitting slope protection and can be susceptible to embankment erosion (Fay et. al 2012). ECBs

can be a part of the appropriate stormwater management plan for each site because they are low-cost and highly effective. The general procedure for sustainable embankment practices should include using vegetation whenever possible, considering mulch and soil amendments to promote growth, saving and reusing topsoil, and considering erosion control blankets for application at every site on any disturbed surface (Fay et. al, 2012).

The general installation procedure for installing an ECB is described by the Erosion Control Technology Council (ECTC) in an installation guide for RECPs (ECTC, 2017). Several methods for securing ECBs are described. One notable method is to excavate a 6.0 in. by 6.0 in. (150 mm by 150 mm) anchor trench after spreading topsoil and seed. Then, the erosion control blanket can be stapled to the bottom of the trench and the trench can be backfilled to the previous soil level. Then, the blanket can be stapled uniformly to the soil. The blanket should be in contact with the ground at all points so that runoff does not undermine the blanket and cause the topsoil and seeds to wash out.

Other erosion controls include pellets, jute, and polyacrylamide (PAM). Rainfall simulator research at Auburn University found that jute with gypsum could be as effective as erosion control blankets for stabilizing bare slopes and had a cover factor, *C*, of 0.12 (Manning, 2021). However, there are variable factors to consider when determining cover factor experimentally. Ji et. al found that rainfall erosion is significantly affected by water quality factors such as sodium adsorption ratio and conductivity (2017). Since initial water quality is not accounted for in the standard RUSLE equation, water quality may quietly influence comparisons between research at various testing facilities.

Erosion control is critical to transitioning from construction to post-construction on sites. Erosion control impacts can be difficult to measure because practices are proactive in reducing non-point source pollution and preventing sediment loss. While rainfall simulator studies have already demonstrated that erosion controls can be effective, there is still a substantial need for testing erosion control effectiveness in a standardized method (Kumarasinghe, 2021). One such project funded is taking place at Auburn University where twelve rainfall simulators will follow the ASTM D5964-19 standard to test various erosion control practices under rainfall simulation such as ECBs, hydromulches, and straw applications on three different types of soil and two different slopes (Schussler et. al, 2022). The results of this work may yield new insight on how different soils may benefit from different soil stabilization products. This thesis includes the construction, calibration, and early testing of the rainfall simulators for the use in ALDOT-funded erosion control research.

2.2 ASTM D6459-19

Research at Auburn University led to the development of a working rainfall simulator following ASTM D6459 (Horne, 2017., Faulkner, 2020, Ricks, 2020). Faulkner re-analyzed sprinkler layout and the apparatus remains calibrated via ASTM methods to Faulkner's design, including ten sprinkler risers. This layout is calibrated to produce at least 80% Christiansen uniformity and intensity of 2.0, 4.0, and 6.0 in./hr (51, 102, and 152 mm/hr) (Faulkner, 2020). Another group using ASTM D6459 for large-scale rainfall simulation is Early et al. at American Excelsior Company's ErosionLab (American Excelsior Earth Science Division, 2022). Both facilities use RUSLE in their analysis.

The design render of an ASTM D6459-19 plot at Auburn University is shown in Figure 2.1 and with a description to follow.

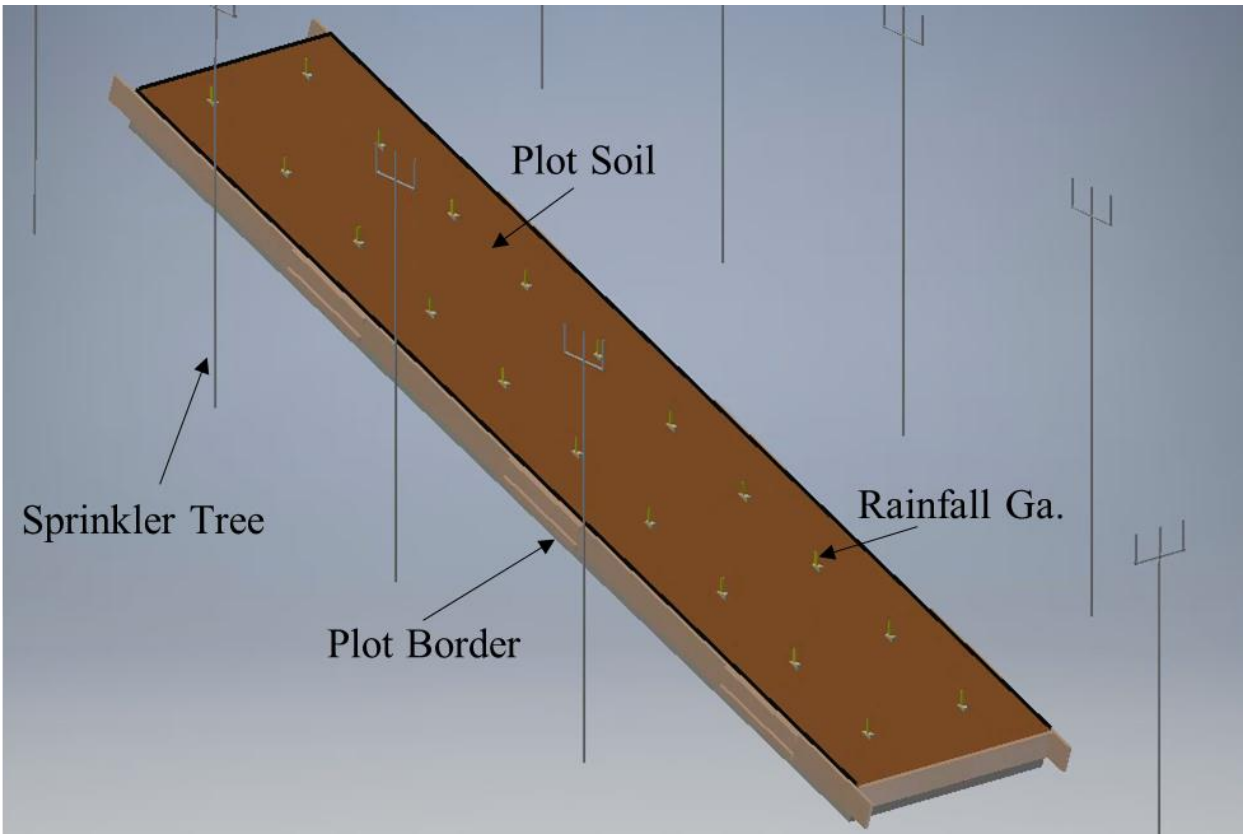

FIGURE 2.1: ASTM6459-19 Plot Render.

The plot is 40.0-ft (12.2-m) long by 8.0-ft (2.4-m) wide with minimum 1.0-ft (30-cm) soil depth. The specified slope is 3H:1V. Importantly, the sprinkler layout section of ASTM D6459-19 specifies that pressurized sprinklers be used to meet specific drop size parameters with a raindrop fall height of 14 ft (4.3 m). Barriers must be in place on the borders to prevent flow from running onto the plot. Lawn edging is suggested for this task. Construction methods are not specified in the document and may be unique to each site. However, a key parameter to obtain useful results is soil compaction, which must be within 90 ± 3 % of standard Proctor Density in accordance with ASTM D698, “Laboratory Compaction Characteristics of Soil” (2021).

During calibration, the rainfall intensity is calculated by placing twenty rainfall gauges in a uniform pattern on the plot as shown in Figure 2.2 and recording intensity after 15 min of rainfall for each desired intensity under conditions of uniform pressure and 1.0 mi/hr (1.6 km/h) wind or less (ASTM, 2017).

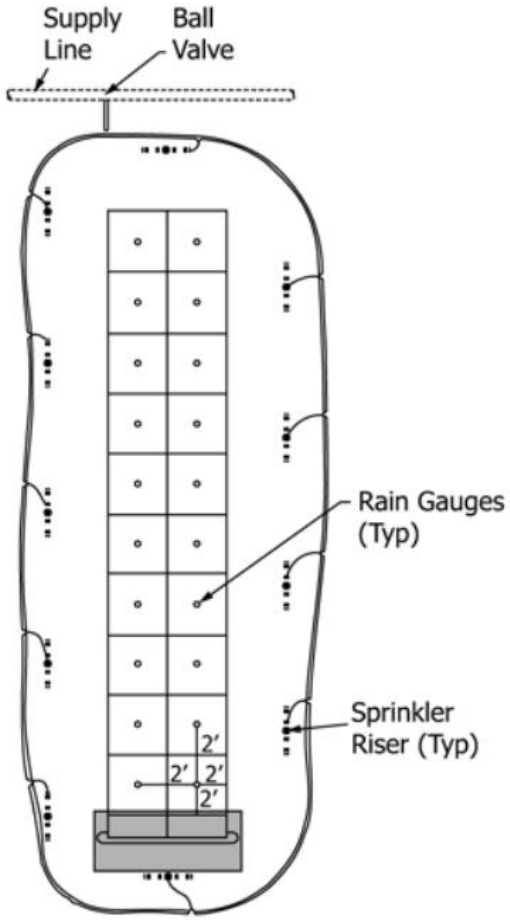

FIGURE 2.2: ASTM6459-19 Rainfall Gauge Layout.

To calculate intensity from rainfall gauge heights, the readings are averaged and normalized for cm/hr units in Equation 2.1 (ASTM, 2019).

$$i = 60[\sum_{j=1}^{J} P_j \div Jt] \quad (2.1)$$

where,

i = rainfall intensity, cm/hr

P_j = depth of rainfall, cm

J = number of rain gauges

t = time of test

Christiansen Uniformity is utilized to determine the even distribution of rainfall intensity on the plot. In the ASTM6459-19 standard, twenty rainfall gauges are required to apply this equation, and 80% uniformity is the requirement for calibration. It is shown below in Equation 2.2:

$$C_u = 100\ [\ 1.0 - \sum |d| \div n\,\overline{\mathrm{X}}\ ] \tag{2.2}$$

where,

C_u = Christiansen Uniformity Coefficient

d = X_i - $\bar{X}$

n = number of rain gauges

X = average depth in rainfall gauge, cm

X_i = depth in each rainfall gauge, cm

Drop size calibration is also included in ASTM D6459-19. For this metric, the flour pan method is used. To perform this test, three pie pans are filled with sifted flour and struck off to obtain a smooth surface. Along the centerline of the test plot at the three-quarter points, the pie pans are uncovered for 2 to 4 sec to produce pellets in the flour. Then, the pans are dried for a minimum of 12 hr and sieved through a 70-mesh to remove loose flour. Total weight of the hard flour is recorded, and the pellets are sieved through standard soil sieves for two min. The flour pellets caught in each sieve size are weighed and counted. Finally, the kinetic energy departed by the rainfall simulator is obtained by summing the energy of each drop size group and multiplying by the percentage of energy that drop size makes up of the total distribution. The flour pan method bases energy calculations on drop size and raindrop fall height. The kinetic energy equation is shown in Equation 2.3.

$$KE_{total} = \sum 0.5\, m\, v^2 \tag{2.3}$$

where,

KE_{total} = rainfall intensity, cm/hr

m = mass of drop, kg

v = velocity of drop at soil surface, m/s

Terminal velocity used in this equation is derived from Figure 2.3.

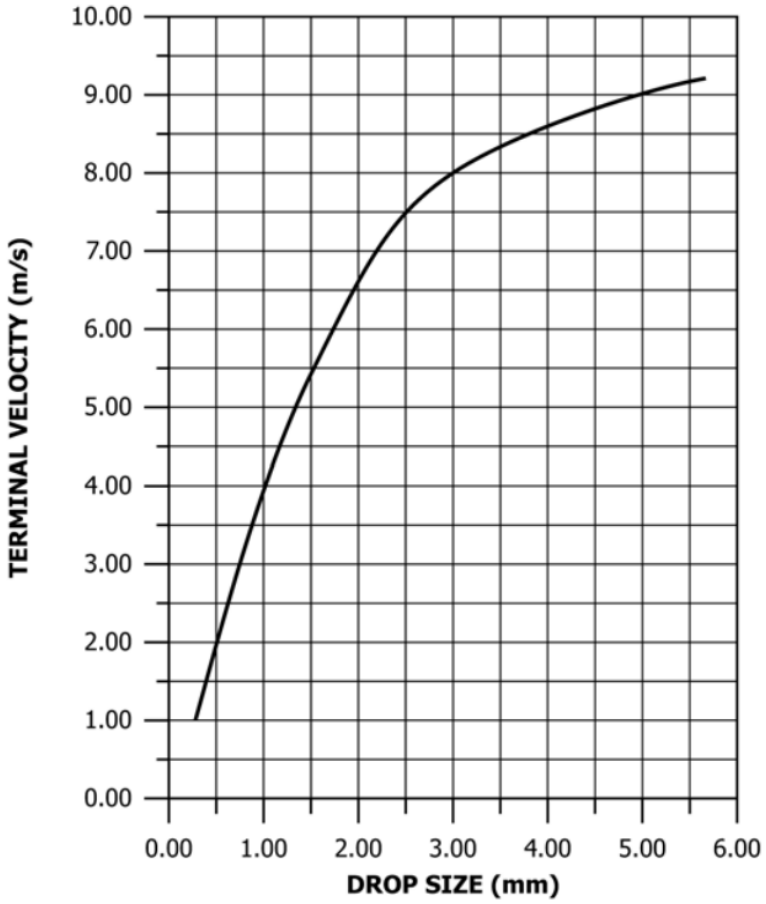

FIGURE 2.3: Drop Size to Terminal Velocity Correlation (ASTM, 2017).

For test preparation, ASTM D6459-19 offers specific guidance. Test plot preparation includes adding soil in 6-in. (15-cm). lifts and meeting the previously mentioned compaction requirements. Moisture content affects compaction substantially; therefore, the moisture content must be within 4% of optimum moisture content for maximum compaction. Also included are specific test preparation practices for RECPs and TRMs including documentation of installation procedures and accounting for vegetation with TRMs.

During each test, numerous measurements are collected. Runoff is collected separately for each target intensity and rainfall gauge heights are recorded. Additionally, sample bottles and volume readings are collected every 30 sec to 180 sec depending on runoff rate. Following a test, ASTM D6459-19 specifies that deliverables include runoff hydrographs, sediment concentration curves, Curve Number computed from total runoff volume, the Rational coefficient as used for peak discharge in the Rational Equation, and cover factor using the total sediment yield and comparing to bare soil tests. Cover factor is the ratio of soil loss when the plot is protected to soil loss when the plot is bare.

2.3 REVISED UNIVERSAL SOIL LOSS EQUATION

RUSLE is used in rainfall simulator research to compare erosion control products. RUSLE stems from the Universal Soil Loss Equation, or USLE. One motivation for the development of USLE was the Dust Bowl of the 1930s, which ravaged crops due to extreme wind erosion. The rigorous and continued testing done by university faculty and federal scientists in the United States over the next decades led to the development of USLE in 1965 in the USDA Agricultural Handbook (USDA, 2016). One of the main studies in USLE was at the University of Missouri, where numerous plots were constructed with various slopes and lengths to measure erosion from rainfall events. Many of the plots were 6.0 ft (1.8 m) wide and 72.6 ft (22.0 m) long. Now, RUSLE is a computerized version of USLE with improvements in factor estimates and was released in 1992 for public use by the USDA.

$$A = R * K * LS * C * P \tag{2.4}$$

where,

A = annual soil loss per acre (tons/acre/year)

R = rainfall erosivity factor

K = soil erodibility factor

LS = length of slope steepness factor

C = cover management factor

P = support practice factor

In rainfall simulation, the support practice factor is typically ignored because it accounts for suspended sediment that is removed from runoff before discharge off site. Fixed factors include soil erodibility factor, referred to as *K*-factor, and slope characteristics, *LS*. Rainfall erosivity factor, referred to as *R*-factor, is determined through the calibration procedures described in section 2.2. The equation for incremental rainfall energy for determining *R*-factor is found by Equation 2.5. This equation demonstrates that *R*-factor represents the total rainfall energy on the plot area. The contains a unit conversion from ft^2 (m^2) to ac (ha) for the 320 ft^2 (29.7 m^2) plot area of the ASTM D6459-19 design. $KE_{totalrainfall}$ is obtained from Equation 2.3.

$$Incremental\ E = KE_{totalrainfall} / (\frac{320}{43560}) \tag{2.5}$$

where,

$Incremental\ E$ = incremental rainfall energy by drop size class, ft-tonf/ac

$KE_{totalrainfall}$ = total estimated kinetic energy of all rainfall, ft-tonf

Finally, *R*-factor can be determined for a rainfall simulator test by calculating the erosion index.

$$Test\ EI_{30} = \sum Incremental\ E * 0.01 * (i_{4\ in./hr} * 10 + i_{6\ in./hr} * 20) / 30 \tag{2.6}$$

where,

$Test\ EI_{30}$ = Erosion index, or *R*-factor, hundreds of ft-tonf-in./ac-hr

$i_{4\ in./hr}$ = Rainfall intensity during 4.0 in./hr (102 mm/hr) target intensity

$i_{6\ in./hr}$ = Rainfall intensity during 6.0 in./hr (152 mm/hr) target intensity

Annual soil loss per acre, which is represented by *A* in the RUSLE equation, is measured or estimated by the rainfall simulation experiment from the total soil loss per intensity. The *K*-factor is calculated by conducting tests with bare soil where cover factor is 1.0. Finally, cover

factor, *C*, is the unknown variable that is obtained by comparing bare soil test soil loss to covered test soil loss using the calculated *K*-factor.

The benefit of numerous rainfall simulator plots is that the typically fixed variables of *K*-factor and length of slope steepness factor, *LS*, are made variable. The twelve plots at Auburn University provide three options for soil with a sand, a clay, and a loam, which all meet particle size and plasticity index requirements as stipulated by ASTM D6459-19 and shown in Table 2.1 (ASTM, 2019). Additionally, the inclusion of six 3H:1V slopes and six 4H:1V slopes means that the slope steepness can be variable.

TABLE 2.1: ASTM6459-19 Soil Requirements

Particle Size (mm)	Sand	Loam	Clay
D_{100}	$25 > D_{100} > 3.0$	$10 > D_{100} > 0.3$	$3.0 > D_{100} > 0.02$
D_{85}	$4.0 > D_{85} > 0.8$	$0.8 > D_{85} > 0.08$	$0.08 > D_{85} > 0.003$
D_{50}	$0.9 > D_{50} > 0.2$	$0.15 > D_{50} > 0.015$	$0.015 > D_{50} > 0.0008$
D_{15}	$0.3 > D_{15} > 0.01$	$0.03 > D_{15} > 0.001$	$D_{15} < 0.002$
Plasticity Index	N/A (nonplastic)	$2 < PI < 8$	$10 < PI$

1 mm = 0.039 in.

2.4 ALTERNATIVE RAINFALL SIMULATOR DESIGNS

Rainfall simulators can have different dimensions, slopes, and soils, which hinders the ability to compare and verify results between studies. A study in Alberta, CA found that, for a rainfall simulator to test the efficacy of vegetation on reclaimed sand slopes near oil sand mines, a large plot size was necessary because of the effects of the edge of the plot on the runoff flow (Sawasky, 1996). Therefore, the effect of plot size on rainfall simulator results may stem from not only allowing the formation of highly erosive rills due to increased slope length but also the effect of plot width on flow patterns. A study at the University of Tennessee titled "*Performance Base Testing for Erosion Prevention and Sediment Control (EPSC) Devices*" found that there is little quantitative performance testing for sediment reduction practices that consider diverse conditions

(Wilson, C., 2019). Conditions that commonly differ between studies are slope, slope length, soil type, and rainfall intensity.

In a study at Istanbul Technical University reported 82% to 89% uniformity in "A rainfall simulator for laboratory-scale assessment of rainfall-runoff-sediment transport processes over a two-dimensional flume" (Aksoy et al., 2012). The apparatus is indoors with "up to 20%" slope. Limited specific soil data and test results are recorded. This medium scale rainfall simulator attempts to address some issues of smaller scale plots by artificially adding rills. However, these rills are not naturally formed by flow over bare soil and may not represent real conditions. It uses 10 VeeJet pressurized sprinklers with 1.8, 2.6, 3.3, and 4.1 in./hr (45, 65, 85, and 105 mm/hr) intensities. The height of the sprinklers is 8.0 ft (2.4) and the rainfall diameters are between 2.2 mm and 3.1 mm. One conclusion of the study is that experiments resulted in typical rainfall-induced hydrographs.

Many facilities do not follow ASTM recommendations for plot size, which means they cannot employ the ASTM D6459-19 rainfall gauge arrangement. Research at the University of Tennessee uses a smaller 8.0-ft (1.8-m) long 3H:1V slope (C. Wilson, 2021) while research in Alberta, Canada includes testing on a nearly 50-ft (15-m) slope on a 2.5H:1V hillside (Sawatsky et. al, 1996). Another research facility in Texas uses both 30-ft (9.1-m) indoor slopes and 50 to 70 ft (15 to 21 m) outdoor slopes (Ming-Han et al., 2014). Ming-Han et al. conclude that their indoor and outdoor apparatuses are consistent with one another despite differences in plot size, compactness, rainfall duration, and intensity. However, Ricks concludes that small and intermediate plots underrepresent soil erosion and runoff and are less viable for RUSLE analysis (Ricks, 2020). This is due to the formation of rills being limited by slope length. Therefore, Ricks recommends utilizing large-scale plots for rainfall simulation for evaluating erosion control

products. Standardization of plot size may allow datasets to be more easily compared by rainfall gauge techniques. Alternatively, rainfall intensities on plots of different sizes can be compared by runoff rate instead of rainfall gauges.

2.5 ALTERNATIVE CALIBRATION TECHNIQUES

Calibration techniques vary between facilities. This section describes various techniques for rainfall intensity and drop size distribution measurement. These measurement techniques can be used to design sprinkler systems capable of meeting design criteria of standard rainfall simulator designs.

2.5.1 Intensity Calibration

Sawatsky et al. use four methods for intensity calibration. These include a variation of the ASTM D6459-19 method using rainfall gauges, a turbine meter on the supply line, a tipping bucket, and four troughs at four widths of the plot (Sawatsky et al., 1996). However, many facilities use rainfall gauges like ASTM D6459-19 recommendations. However, the spacing of rainfall gauges is seldom recorded, which may affect intensity results. At Auburn University, the ASTM D6459-19 setup yields 79 to 81% uniformity with rainfall gauges 2.0 ft (0.6 m) from the plot sides (Horne, 2017). Low uniformity can indicate that intensity is variable across a plot.

Researchers including Cottenot et al. used alternative methods for drop formation (Cottenot et al., 2021). Earlier work at Auburn University used an intermediate-sized plot to evaluate methods for applying straw and hydromulches (Wilson, W.T., 2010). This apparatus had a single sprinkler for two 2.0 ft (0.6 m) by 4.0 ft (1.2 m) plots and was able to achieve an 83% to 88% Christiansen Uniformity (Shoemaker, 2008). Drop formation techniques and rainfall gauge spacing vary between these apparatuses; therefore, rainfall gauges may not provide effective comparison to ASTM D6459-19 apparatuses for uniformity.

Ricks presents a raster projection for rainfall intensity, which suggests that rainfall gauges may misrepresent rainfall intensity because intensity can vary across the plot (2020). Furthermore, from a study at the University of Tennessee, C. Wilson concludes that runoff is the greatest erosivity factor rather than other factors including rainfall intensity (2021). This means that measuring maximum runoff volumes may be a better metric for calibration than rainfall intensity since runoff is the greatest determining factor for erosion.

One issue with pressurized sprinklers is that they can be observed to have "hot spots" which deliver excess volumes of water to the central areas of the plots, which presents a problem for the rainfall gauge methods. Only six rainfall gauges are used to calculate the intensity for one factor in the RUSLE analysis, which is critical to the results of each product and bare soil test. One way to address these concerns is to remove the rainfall gauges from the calibration and instead measure the runoff when the plot cover is impermeable. Mirroring the method used to collect and store runoff during product testing, the runoff can be collected at the bottom of the plot and pumped into a tank to determine the intensity based on the volume of runoff generated by the sprinklers. However, this method must be evaluated and its correlation to well-established rainfall gauge methods.

2.5.2 Drop Size Calibration

The flour pan method, which samples raindrops sizes by creating raindrop fossils in flour to determine raindrop size distribution, is prevalent within rainfall simulation and is described in ASTM D6459-19. While the establishment of this method provides potential for continuity between research facilities, the flour pan method cannot directly measure raindrop velocity. Alternative methods for determining raindrop parameters can provide more accurate measurements. Several methods are explored in "Comparing Raindrop Size and Velocity

Measurement Accuracy Using Shadowgraphy, Disdrometry, and Pie Pan Measurement Techniques" (Tullis, 2016). Tullis's shadowgraphy system, which utilized photography with a film to create shadows of raindrops, achieved 2.86% uncertainty and served as the comparative standard versus the flour pan method and the disdrometer method. The disdrometer, which is a laser instrument capable of measuring raindrop size and velocity, slightly underestimated raindrop size. Most importantly, the pie pan method overestimated raindrop size by 41%. For raindrop velocity, the disdrometer underestimated raindrop velocity but was the only viable method for directly measuring velocity of the three available methods according to Tullis. Since the flour pan method greatly overestimates raindrop size, the calculation for determining raindrop velocity is also affected. For example, according to ASTM D6459-19, a 3 mm drop at 14-ft (4.3-m) drop height impacts at 6.75 m/s (2019). However, if the drop size were overestimated by 41%, the true velocity at impact would be 5.60 m/s. Furthermore, in Equation 2.3, this erroneous velocity would be squared for each raindrop size class, further compounding the error used to determine the total kinetic energy of the raindrops. Therefore, photography and disdrometry are worthy of investigation as alternatives for determining drop size and even direct measurement of raindrop velocity.

Each alternative for raindrop parameter determination has negative aspects. Photography entails using a camera to capture photographs of a raindrop, and this method can be highly accurate as demonstrated by Tullis. However, since a single focal point is used, error may arise from the determination of the distance of a raindrop from the camera lens. Drop height was varied with drop sizes ranging from 3.8 mm to 4.0 mm. Disdrometer raindrop sizing allows for the collection of thousands of datapoints easily while the flour pan and photography methods are more laborious. Tullis collected 15,000 raindrop data points with over 95% of the data points determining drop

size between 3.8 and 4.0 mm. However, this method was less accurate than the shadowgraphy method. The least accurate method was the pie pan method, which followed ASTM D6459. The disdrometer presents the most viable alternative for easily collecting large amounts of data; however, the cost for these products is roughly $8,000 to $12,000 each. Therefore, a low-cost and accurate solution for applying photography methods to rainfall simulators may be more practical.

The accuracy of photography for determining raindrop size allows the calculation in Equation 2.3 to be much more accurate than the pie pan method. Additionally, disdrometers underestimate raindrop velocity by nearly 70% (Tullis, 2016). While Tullis does not explore the usage of shadowgraphy for the direct measurement of raindrop velocity, another apparatus for determining raindrop velocity with a similar photographic method may be possible and able to directly compare with raindrop velocities calculated from drop size by the shadowgraphy and the pie pan methods. Photography methods present promise for the determination of raindrop parameters in rainfall simulation because of their mild cost when compared to disdrometers and potential for high accuracy.

2.5.3 Additional Considerations

Ji et. al found that rainfall erosion is significantly affected by water quality (2017). The study found that water quality's greatest impact is on erosion. The magnitude of the effect is greatly dependent on soil properties such as clay particle percentage, sodium adsorption radio, and conductivity. The experiment was performed on a 5% slope for all tests. Various loam and silt soils were used, and tests were performed with fully saturated soil. Water varied between natural precipitation, natural hydrops, and tap water. Raindrop diameter was 297±0.5 mm while uniformity was 94%. Rainfall height was 8.66 in. (220 mm) and the plot was 5.7 in. (145 mm) by 5.7 in. (145 mm) by 1.6 in. (40 mm) deep. The key findings in the report are that infiltration was

significantly affected by water quality and that erosion decreased with increased salt concentrations. While this study was intended for agricultural applications and used a small plot, the conclusions introduce questions about whether water quality used in rainfall simulators should be standardized.

2.6 HYDROMULCH EXPERIMENTAL EVALUATION METHODS

Hydromulch is a liquid combination of fertilizer, seed, and mulch in a mixing tank which is sprayed on soil surfaces as an alternative to traditional dry seeding. Hydromulch supports germination of grass seed (Kowk et al., 2008) while also functioning as a protective erosion control to prevent seed washout. It is cheaper than temporary erosion control blankets according to a study at Texas Agricultural and Mechanical University (McFalls et al., 2007). The same study found that erosion prevention by the hydromulch used in the study had variable difference to temporary erosion blankets depending on the soil. Mulch products performed best in sandy soils.

Methods designed to be used for testing ECBs may not fairly represent the effectiveness of hydromulches. While ASTM D6459-19 is the preeminent method for large-scale rainfall simulation testing, other ASTM designations including D8297 “Determination of Erosion Control Products (ECP) Performance in Protecting Slopes from Sequential Rainfall-Induced Erosion Using a Tilted Bed Slope” and ASTM D8298 “Determination of Erosion Control Products (ECP) Performance in Protecting Slopes from Continuous Rainfall-Induced Erosion Using a Tilted Bed Slope” differ from ASTM D6459-19 and may be more suitable for hydromulch testing.

The two alternative methods, ASTM D8297 and ASTM D8298, are very similar except that they utilize sequential and continuous rainfall, respectively. These methods use an adjustable slope which can vary from 2H:1V to 4H:1V and 2.5H:1V to 4H:1V, respectively. While ASTM

D6459-19 relates specifically to RECPs, these designations use broader language with the intent of applying to all ECPs. These designations contain specifications for a hydroseeding apparatus to apply hydromulch, which implies that the tests are designed for testing hydromulch products. In contrast to ASTM D6459-19, which calls for the variation of rainfall intensity over one hour at 2.0, 4.0, and 6.0 in./hr (51, 102, and 152 mm/hr), ASTM D8297 specifies rainfall at a static intensity of 3.5 in./hr (89 mm/hr) for 30 min per day over three days for a total of 90 min. Like ASTM D6459 in that it is also continuous, ASTM D8298 is a one-hour test with two 30-min periods with target intensity between 4.0 and 5.0 in./hr (102 and 127 mm/hr). ASTM D8297 and D8298 allow for various techniques for simulating rainfall including sprinklers, nozzles, and drop emitters while ASTM D6459-19 specifically mentions using sprinklers selected on ability to model natural raindrop sizes. For both D8297 and D8298, runoff is collected separately for each period of simulated rainfall to obtain soil loss weights and samples are taken for turbidity and sediment concentration, like ASTM D6459-19. However, D6459-19 requires bottle samples every thirty sec to 180 sec while the two ECP standards only stipulate sampling every 15 min. One additional requirement of ASTM D8297 and D8298 that D6459-19 does not implement is turbidity testing for the water supply.

The three-day length of ASTM D8297 presents challenges to operators that do not exist for users of ASTM D6459 and ASTM D8298. While outdoor apparatuses are allowed by the standard, indoor plots may be necessary to comply with the test's lengthy schedule. Natural rainfall may interfere with the results and apparatus in between 30-min sessions with an outdoor apparatus. Additionally, a sufficient workforce is required over three days rather than only one day.

In addition to differences in testing procedures, the designations differ in apparatus design. D6459-19 specifies a raindrop fall height of 14 ft (4.3 m) while D8297 and D9298 only specify a

minimum height of 8.0 ft (2.4 m). This provides an opening for the usage of variable sprinkler heights between testing facilities, which affects raindrop fall velocity and total rainfall energy. All designations include flashing, runoff collection, and holding tanks. However, the test plots vary greatly. ASTM D6459 requires 12 in. (30 cm) of soil while D8297 and D8298 require only 9 in. (23 cm) depth. While ASTM D6459 requires 40 -ft (12-m) by 8.0-ft (2.4-m) borders, ASTM D8297 and D8298 utilize metal trays with perforated bottom sheets with geotextile for soil underlay, which means that the entire soil installation must be redone periodically to replace the geotextile. D8297 and D9298 do not have specific plot size requirements. Instead, the minimum plot size is 30-ft (9-m) by 6-ft (1.8-m) with a necessary length-to-width ratio of 5:1. Therefore, these standards leave opportunity for differences between apparatuses, which limits the possibility of comparing results between facilities despite sharing the same ASTM designation guidance.

The three designations share many similarities in plot preparation. Soil selection requirements, soil preparation practices, ECB application, and wind requirements are similar or identical. Each designation requires that wind be less than 1.0 mi/hr (1.6 km/hr) for a test. Additionally, each designation contains strict rainfall uniformity requirements. All standards use Christiansen Uniformity with ASTM D6459 requiring 80% uniformity and the other designations requiring 90% uniformity. All designations use the flour pan method three times along the centerline of the plot at quarter points; however, ASTM D8297 and D8298 specifically mention that Pillsbury Best all-purpose flour be used. Rainfall intensity calibration is also similar between the methods. Each designation requires uniform placement of rainfall gauges. However, ASTM D8297 and D8298 go into additional detail on covering and uncovering rainfall gauges as the sprinklers are running to ensure that rainfall gauges receive rainfall for identical lengths of time.

The testing procedures are similar despite the differences in the length of tests and requirements of specific intensities. ASTM D6459 does not specify time for the settling of runoff before measurement while the other two designations require a minimum of 12 hr. Research at Auburn University uses a minimum 24-hr settlement with ASTM D6459-19 (Faulkner, 2020). Furthermore, ASTM D8297 and D8298 contain a procedure for representative sampling as well as basic equations for determining cover factor, which ASTM D6459 does not explicitly provide.

In summary, ASTM D8297 and D8298 share many similarities to each other and ASTM D6459-19; however, they allow variation in plot apparatus within the standards while ASTM D6459-19 provides exact dimensions. Importantly, ASTM D8297 and D8298 use static rainfall intensities while ASTM D6459 increases rainfall intensity throughout the test. The last major difference between the method types is that ASTM D8297 is performed over three days, which necessitates that the rainfall simulator be indoors, which may not be practical for all testing facilities. Table 2.2 summarizes the comparison between the designations.

TABLE 2.2: Comparison of Rainfall Simulator ASTM Designations

Designation	D6459-19	D8297	D8298
Rainfall Intensity, in./hr (mm/hr)	2.0, 4.0, and 6.0 (51, 102, and 152)	3.5 (89)	4.0 and 5.0 (102 and 127)
Christiansen Uniformity, %	80%	90%	90%
Drop-forming technique	Sprinklers	Sprinklers, nozzles, or drop-emitters	Sprinklers, nozzles, or drop-emitters
Plot Dimensions, ft (m)	40 by 8 (12 by 2.4)	Min. 30 (9) by 6 (1.8) with 5:1 L:W ratio	Min. 30 (9) by 6 (1.8) with 5:1 L:W ratio
Soil Depth, in (cm)	12 (30)	9 (23)	9 (23)
Slope	3H:1V	2H:1V to 4H:1V	2.5H:1V to 4H:1V
Drop Size Distribution Calibration Method	Flour pan	Flour pan	Flour pan
Bottle Sampling Gap Time, Min	0.5 to 3	15	15
Runoff Minimum Settling Time, hr	Unspecified	12	12
Maximum Wind, mi/hr (km/hr)	1.0 (1.6)	1.0 (1.6)	1.0 (1.6)
Total Test Time, hr	1.0	1.5	1.0
Notable Requirements	Variable intensity	Geotextile underlay on metal tray Tested over 3 days	Geotextile underlay on metal tray

2.7 SUMMARY

The field of large-scale artificial rainfall simulation is diverse. Many plot sizes, slopes, intensities, and calibration methods are used. ASTM D6459-19 provides the clearest parameters for determining cover factor in the RUSLE equation. However, ASTM D6459-19 is designed for RECP testing, and other designations such as D8297 and D8298 offer designs that have specifications for hydromulch evaluation. These designations differ by many metrics from D6459-

19 including by plot size, test period, and target rainfall intensity, but they also share many practices including using the flour pan test, limiting maximum wind, and requiring minimum Christiansen uniformity.

Rainfall gauges and the flour pan method are most often used for determining rainfall parameters such as intensity and drop size distribution. However, since runoff is the greatest determining factor for erosion (C. Wilson, 2021), direct measurement of runoff may be viable for determining intensity instead of using rainfall gauges. Additionally, one study found that the flour pan technique overrepresents drop size by 41% (Tullis, 2016). Since drop size is also used to determine rainfall velocity by traditional methods, overrepresented drop size could create compound errors in raindrop energy calculations. Therefore, greater investigation is required for alternative methods for drop size measurement such as photography and disdrometry.

CHAPTER 3: CONSTRUCTION METHODOLOGY

3.1 INTRODUCTION

Twelve rainfall simulators with varied slopes and soils were constructed at the Auburn University - Stormwater Research Facility (AU-SRF). Six plots were built on 3H:1V slopes while the other six were built on 4H:1V slopes. The plots were split into pairs, each containing matching soil: ASTM clay, loam, and sand sourced from Montgomery, AL, Auburn, AL, and Abbeville, AL, respectively. The array of soils sought to represent most of the state. A map from the United States Soil Conservation Service (SCS) is displayed in Figure 3.1 with soil groups in Alabama and locations of soil sources for the rainfall simulator project.

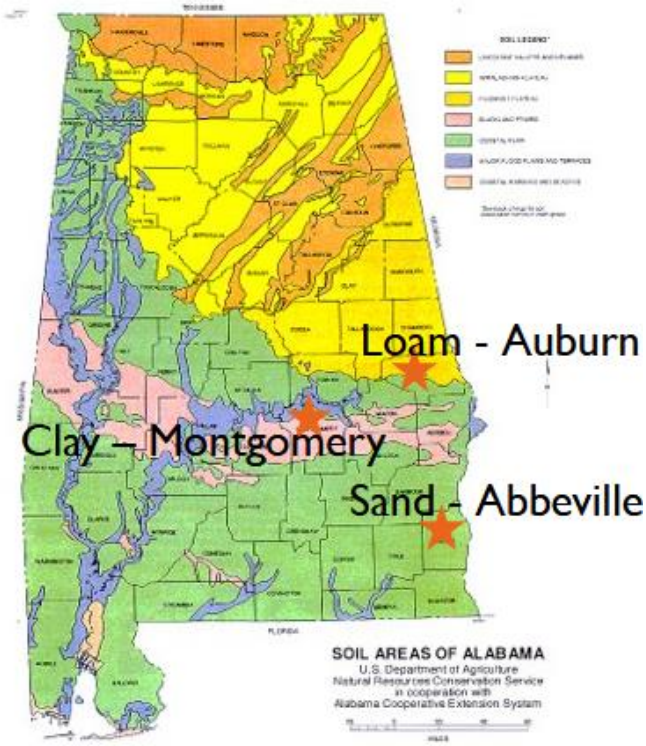

FIGURE 3.1: Rainfall Simulator Soil Source Locations (SCS, 1986).

The design and methodology for constructing these plots is described in this chapter.

3.2 RAINFALL SIMULATOR LAYOUT

The layout of the plots, which allows for at least 10 ft (3.0 m) of space between plots for equipment accessibility, was devised and is displayed in Figure 3.2.

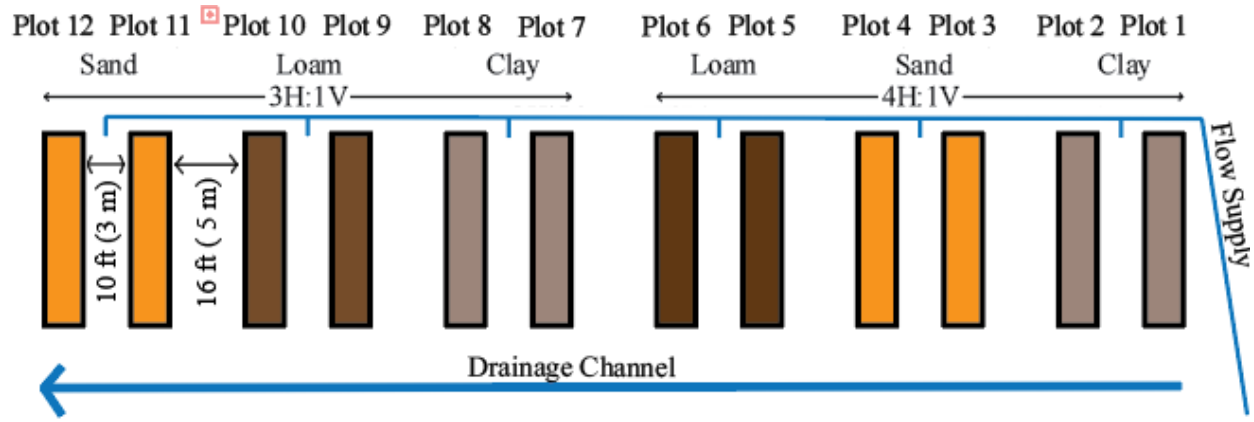

FIGURE 3.2: Rainfall Simulator Plot Layout.

A Trimble S6 Robotic Total Station was used to grade the area alongside heavy equipment. The rainfall simulators were planned along the embankment of the facility access road. This was both convenient and reflective of the purpose of the project.

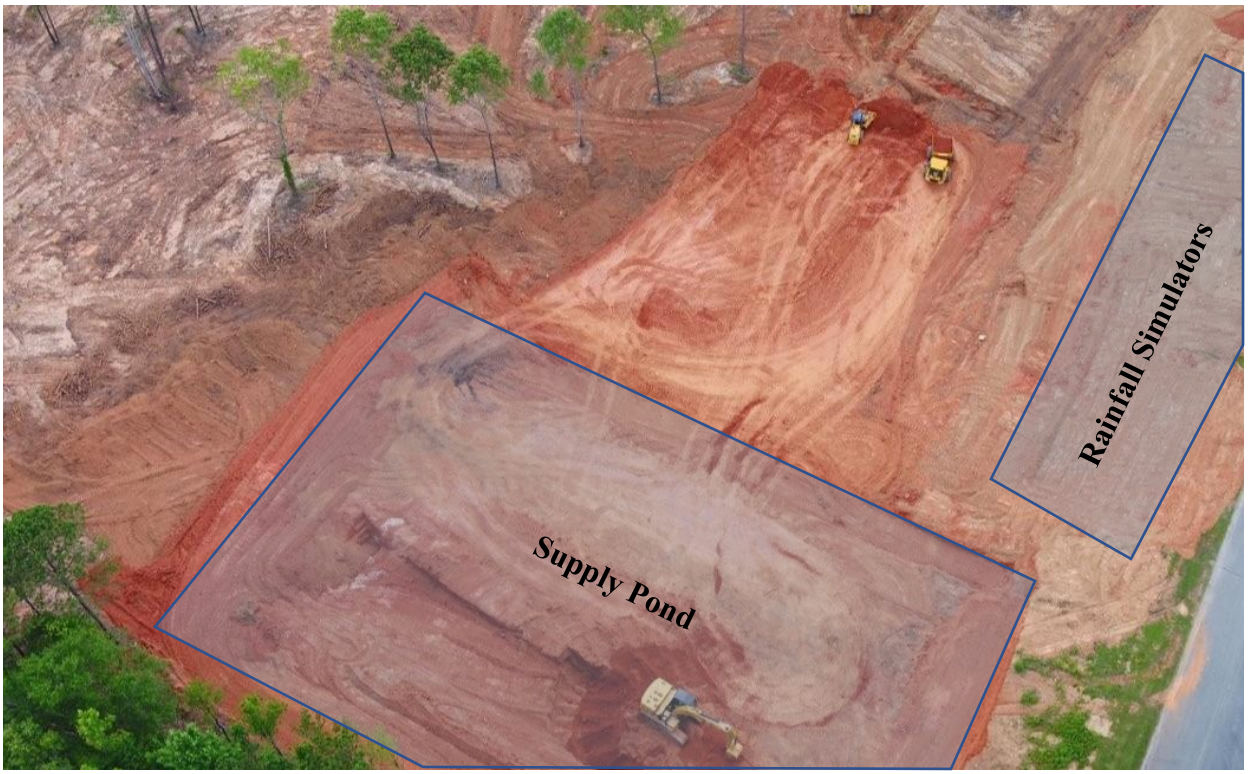

FIGURE 3.3: Rough Grading Aerial View.

The desired coordinates of the corners for all twelve plots were created in the Total Station as a digital terrain model and marked with stakes. Then, the slopes were temporarily seeded. Construction was performed on a maximum of two plots simultaneously to minimize the disturbed area without reducing productivity. This greatly reduced the exposed bare soil during the process of construction.

3.3 EARTHWORKS

Each plot was excavated to 42.0 ft (12.8 m) by 10.0 ft (3.0 m) and 18 in. (46 cm) depth. To make this process safer, a terrace was created in the middle of each plot to park the excavator while digging the upper reaches of the plot rather than parking on the slope. This method allowed all digging to be performed with heavy equipment while minimizing risk to the excavator operator. Elevations at each point on the plot can be checked by the total station by verifying the excavated elevation is 18 in. (46 cm) below the desired final grade.

(a) Plot 8 excavation (b) adding soil to plot with skidsteer

FIGURE 3.4: Plot Earthwork Activity.

After excavation, a team of three workers was used to grade the slope: an excavator operator, a surveyor, and a raker. First, the Total Station was set up above the plot using two control points on the nearby road. The surveyor used the Total Station to determine the difference from the desired grade and communicated it to the equipment operator. In general, the surveyor followed a square grid pattern with 1.0 ft (0.3 m) or less between each consecutive survey grid point. The excavator operator removed or added soil. The third worker manually raked small volumes of soil to obtain a precise grade. The Total Station is key to precise grading in this stage of construction. Next, 6.0 in. (15 cm) of the desired soil for testing was added onto the plot with a Kubota SVL 75-2 skidsteer and compacted. Sufficient compaction was checked with a Proctor compaction test following ASTM 2937-17e2 “Standard Test Method for Density of Soil in Place by the Drive-Cylinder Method” (ASTM, 2018). The first lift was added before the plot borders as a subgrade.

Despite that the rough grading had already been completed, the bottom elevation for the 3H:1V plots was at too high an elevation. These plots require bottom elevations be nearly 3 ft (1 m) lower than the 4H:1V plots due to the difference in steepness of the slopes. The grade beyond the toe of the rainfall simulators declined towards the area of the catchment basins, which meant that the area of the catchment basins was prone to flooding. This flooding was solved by proper drainage and catchment basin installation. However, to install the catchment basins at appropriate heights, machinery with greater capability than a mini-excavator was required to cut significant volumes of soil. A bulldozer, shown in Figure 3.5, was rented, and over the course of one week, the grading was corrected. The cut was used to fill in a gulley in another part of AU-SRF.

FIGURE 3.5: Bulldozer for Regrading.

3.4 PLOT BORDERS

For the plot borders, 2.0 in. (5.1 cm) by 12.0 in. (30.5 cm) (nominal dimensions) weather-rated lumber was used with lawn edging protruding 2.5 in. (6.3 cm) on the inside of the plot. While

ASTM D6459-19 specifies that plots must only be 40.0 ft (12.2 m) long, constructing 42.0 ft (12.8 m) side boards allows tolerance in positioning. The quantities of lumber, lawn edging, and soil required for one plot are shown in Table 3.1.

TABLE 3.1: Rainfall Simulator Plot Material Quantities

Lumber	Quantity
2x12x12	7
2x8x12	2
2x4x12	4
Lawn Edging, ft (m)	90 (27.4)
Soil Volume, ft^3 (m^3)	402 (11.4)

Since the first lift of soil was already placed in the plot during the earthworks, the surveyor displayed 12.0 in. (30.5 cm) below the desired elevation at this point. The side borders were fastened together inside the plot to ease assembly. Finally, 8.0 ft (2.4 m) boards formed the top and bottom of each plot. However, the bottom board was not added until the final two lifts of soil were placed. The plot design including the plot borders is shown in Figure 3.6.

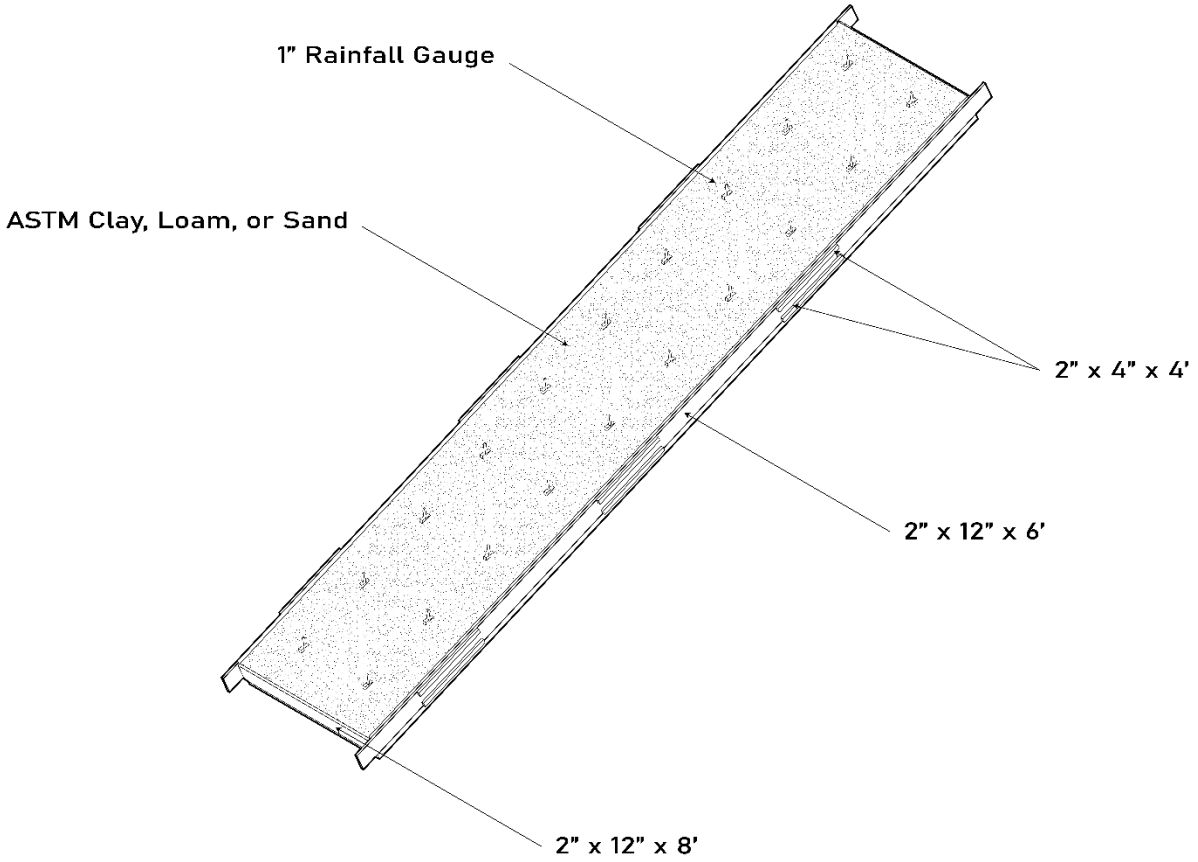

FIGURE 3.6: Plot Design Isometric View.

The squareness of each plot was ensured by checking that the diagonal measurements from opposite corners were equal. After this, the next two lifts of the soil were added and compacted. Compaction was completed using a plate compactor. Backfill was added outside the plot border with the mini excavator after each lift to ensure that the borders stayed in place. Finally, the bottom board was installed. The distance between the inside of the top board and the bottom board was measured as 40.0-ft (12.2-m) to determine the location of the bottom board. This order of operations eases the process of plot construction. For example, using the first lift as a subgrade gives the plot borders support. Additionally, when the bottom board is installed before adding lifts, it is susceptible to damage and shifting from the weight of equipment. These methods allow heavy machinery to do most of the soil installation with minimal soil volume required to be moved manually. At this point, adjacent slopes can be stabilized. Adjacent slopes should be stabilized as

soon as final grades are achieved to minimize the time that bare soil is exposed. Straw erosion control blankets with appropriate mixes of Fescue and Bermuda seed with fertilizer were applied between and beside each plot.

FIGURE 3.7: Completed Plots.

3.5 COMPACTION

The primary compaction method used was a Mikasa Multiquip plate compactor machine, which is displayed in Figure 3.8.

(a) plate compactor (b) driving cylinder

FIGURE 3.8: Compaction Equipment.

To compact each soil layer, the compactor was first placed at the top of the plot. Next, it was started, and the operator guided it laterally across the plot and then down before turning around, moving slightly down the slope, and repeating. All areas of the plot received one pass of the compactor. Then, compaction was checked with the Proctor Compaction method. The Proctor compaction method required several devices including a cylindrical mold, a Proctor rammer, a ruler, a scale, and an oven. First, the mold, shown in Figure 3.8(b), was driven into the soil by the rammer at three locations on the plot. The locations were randomized by envisioning a 30-unit long by 3-unit wide grid on the plot and utilizing a random number generator. Once a sample was collected, it was weighed in the mold and the weight of the mold was subtracted. Additionally, the height of the soil within the cylinder was measured with the ruler. Finally, a sample of soil from the cylinder was taken, weighed for wet weight, dried in the oven, and weighed for dry weight.

The percentage difference of the weights yields the moisture content, which was used in unison with previously generated compaction to moisture content charts unique to each soil to obtain a maximum compaction for the soil based on the moisture content (ASTM, 2008). The equations for Proctor compaction testing are Equation 3.1, 3.2, and 3.3.

$$Wet\ Density = \frac{W_{soil}}{V_{soil}} \tag{3.1}$$

$$Dry\ Density = \frac{Wet\ Density}{(1 + MC)} \tag{3.2}$$

$$Compaction\ \% = \frac{Dry\ Density}{Wet\ Density} \tag{3.3}$$

where,

W_{soil} = weight of soil in cylinder, lb

V_{soil} = volume of soil in cylinder, ft^3

MC = moisture content, %

The charts for maximum dry density were obtained by Christin Manning and are detailed in "Rainfall Simulator Construction and Evaluation of Erosion Control Practices" (Manning, 2021). The three soils, sand, loam, and clay, remain the same in this work as her soil selection.

3.6 DRAINAGE

Seven plots were installed with French drain systems surrounding a plastic tub. The French drain method was not always successful for the 3H:1V plots and was susceptible to failure from flooding. Therefore, an alternate method for securing the catchment basin tubs was devised. For this method, three posts were leveled horizontally and packed with No. 57 stone at the elevation of the bottom of the catchment basin. The tub was placed onto these post anchors and fastened. Using a mini-excavator and the spoil pile from excavation, the gaps around the tub were filled and compacted. This method was substantially less costly than the French drains, which required

drainage pipes, soil fabrics, and additional No. 57 stone. The anchor method was less prone to failure from flooding but still required effective drainage for natural rainfall events.

FIGURE 3.9: Excavation for Catchment Basin and Anchoring.

A drainage system was installed to collect natural rainfall runoff. A trench was spaced 30 ft (9.1 m) from the catchment basins to allow vehicle and equipment access to the bottom of the plots. This spacing was transformed into a gravel road to protect the surface from heavy machinery. Both TRMs and ECBs were applied in this channel. First, the rolled TRM was installed following final earthworks. Next, topsoil was added and graded on top of the TRM and seeded with grass. Finally, a rolled straw ECB was installed to protect the seed.

(a) TRM installation (b) ECB installation

FIGURE 3.10: Construction of Drainage Channel.

A 24-inch (61 cm) diameter pipe was installed underground to improve equipment access and safety. The pipe and drainage ditch are shown in Figures 3.11 and 3.12. The excavation was nearly 8.0 ft (2.4 m) deep maximum, and the pipe was over 100 ft (30 m) long.

FIGURE 3.11: Drainage Pipe Installation.

This pipe was connected to a smaller ditch which drained through another culvert into the lower storage pond. Additionally, this ditch was used as a channel for future sediment research applications.

(a) Plot 7 culvert (b) drainage pipe outlet

FIGURE 3.12: Drainage Pipes.

Due to flooding at the bottom of 3H:1V plots, two culverts were installed near plots 7 and 12 as demonstrated in Figure 3.12. These were installed with 6.0-in. (15 cm) pipe and connect to the main drainage ditch, which routed to the lower pond. The culverts were successful at preventing flooding around the basins. When catchment basins flooded, they were subject to immense pore water pressure and buoyant force, which sometimes displaced them to the surface. Therefore, proper drainage is paramount for rainfall simulator catchment basins. While concrete catchment basins may better withstand flooding, the large reduction in cost by utilizing the plastic tubs allowed for many more apparatuses to be constructed.

3.7 FLOW SUPPLY SYSTEM

A 3.0-in. (7.6-cm) diameter PVC pipe was installed with six outlets and two end valves. Each pair of identical plots had one supply connection in-between them at the top of the slope, which Figure 3.13 demonstrates.

FIGURE 3.13: Supply Pipe Outlet.

The pipe was placed at the top of the slopes for multiple reasons, including that space was limited at the bottom of the slopes with the drainage systems already installed and that the elevation at the bottom of the plots varied while the top of the plots retained a flat grade. Since the pipe was over 300 ft (91 m) long, joints were encased in concrete to form concrete thrust blocks, which prevented damage to the system as the pipe filled.

To distribute flow from the water main to each rainfall tree, a manifold was necessary. The manifold design was 3.0 ft (1.0 m) by 3.0 ft (1.0 m) with previously manufactured 3.0-in. (7.6 cm) by 0.75 in. (1.9 cm) tees. Figure 3.14 contains an overhead concept drawing of the manifold.

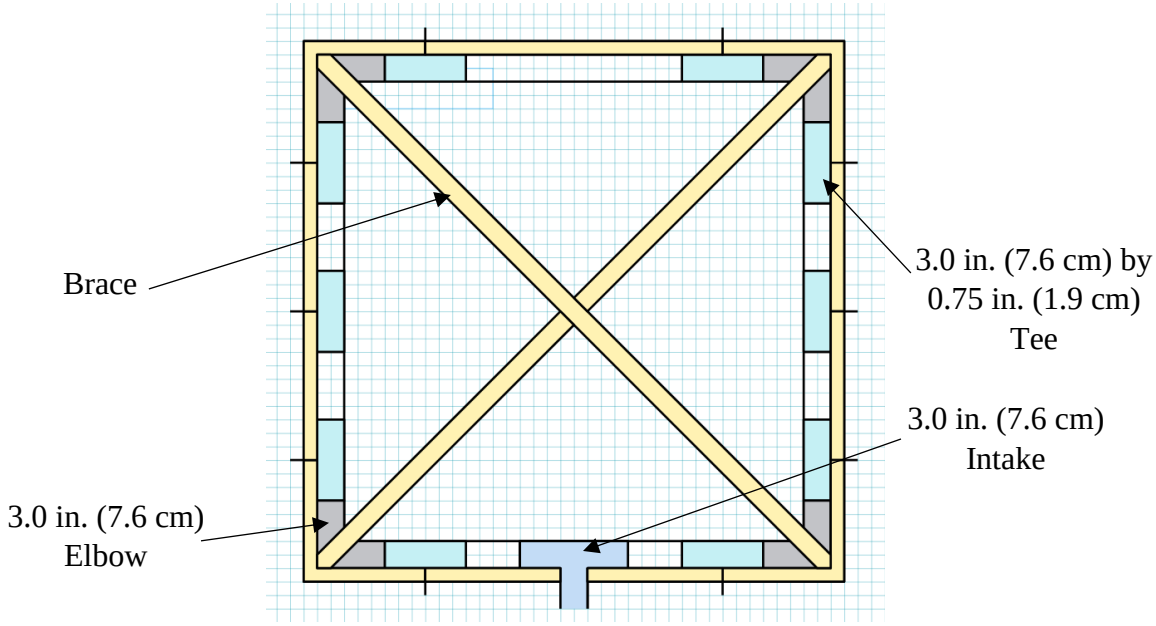

FIGURE 3.14: Manifold Design Concept Drawing.

The manifold was constructed, and the braces were changed from the concept drawing in Figure 3.14 to better support the intake and allow for forklift transport. Figure 3.15 displays the constructed manifold.

FIGURE 3.15: Supply Flow Manifold.

This solution allowed the manifold to sit on either side of the water main stub-outs and to connect to the rainfall trees with hose running down from the top of the hill to each sprinkler. Pumping from the lower pond into the pipe presented multiple challenges. A low water level meant that the pump would intake undesired material such as algae. Furthermore, the intake hose could not always reach the water from the embankment. Therefore, two solutions were implemented. First, an in-line filter was connected to the pipe system at the intake.

FIGURE 3.16: Supply Pipe Intake Debris Filter.

This filter was cleaned each time before starting the pump. To clean the filter, the cylindrical mesh was removed and washed. Figure 3.17 displays effectiveness of the filter by showing the material caught by the filter after only 20 min of pumping at medium throttle from the high-pressure pump while the pond level was low.

FIGURE 3.17 Debris Caught by Filter.

To allow the intake hose to reach the water level, a floating dock was constructed. This dock was tied to the embankment to be able to float up and down with the water level. The pump sat on the dock and connected flexible hose to the filter and intake pipe.

(a) dry supply pond (b) floating dock

FIGURE 3.18: Pond and Floating Dock.

One key cost-saving measure of the plot design of these twelve new rainfall simulators was that the sprinklers were shared between the plots. Rather than requiring a set of sprinklers for each plot, post sleeves were installed into the ground for each plot. Then, the sprinklers and support posts were easily moved between apparatuses. The post sleeves were 2.0 ft (0.6 m) deep and fit 4.0 in. (10 cm) by 4.0 in. (10 cm) posts. One sprinkler system was created initially. The shared sprinkler system ensured continuity between tests and reduced the cost of sprinkler trees by 92%. The gate valves alone cost around $50 each, and since 30 valves are required per sprinkler, this part alone costs roughly $1,500 per sprinkler system. For twelve immovable sprinkler sets, these valves would cost $18,000; however, the portable system saves $16,500 on valve cost. Other costly items for sprinkler systems include 600 ft (183 m) of 4-stand wire, galvanized steel pipe, and

sprinkler components, which have variable costs. Therefore, the shared system eliminates the cost of components and labor for assembling 11 sets of sprinkler trees.

(a) post sleeve with cap (b) post sleeve with post

FIGURE 3.19: Post Sleeve.

3.7 RUNOFF COLLECTION

Some raindrops impacted outside of the plot borders but should be kept out of the catchment basin to ensure accurate runoff volume and sediment capture for the system. To achieve this, several measures were taken. A funnel from the plot to the basin was constructed and installed to both convey the runoff into the basin and to allow for more effective sampling. Additionally, diverters were installed where necessary at the bottom of the plots to prevent flow outside of the plot from flowing into the catchment basin. Plastic sheeting was used to bridge the small gap between the plot and the funnel. Figure 3.20 displays the runoff collection. Finally, an overhead cover kept raindrops from landing in the catchment basin and kept workers dry during tests.

FIGURE 3.20: Runoff Collection.

3.8 ELECTRICAL SYSTEM

To meet the requirements of ASTM D6459-19, which stipulate that intensity must be variable between 2.0, 4.0, and 6.0 in./hr (51, 102, and 152 mm/hr), a system of valves was devised. The system for the twelve new rainfall simulators followed the successful implementation of a similar system on the original AU-SRF rainfall simulator with some improvements. The design included three valves per rainfall tree, which each control flow to a sprinkler. For 2.0 in./hr (51 mm/hr) target intensity, one valve on each sprinkler tree was open and powered. For 4.0 in./hr (102 mm/hr) intensity, two valves were powered. For 6.0 in./hr (152 mm/hr) intensity, all three valves on each sprinkler tree were powered. The improvements were that the electrical controller was portable and that the switches were on the front of the box with lights indicating the target intensity.

The electrical controller was powered by a 12V deep cycle marine battery inside a protective case with a fuse connected to positive and negative splitters. A power switch interrupted the positive wire before reaching the positive splitter. The positive splitter then distributed to three more splitters which corresponded to each set of ten valves with another switch before connection for each of the three positive splitters. Each of the three positive splitters connected to one valve on each rainfall tree. A single negative wire from each rainfall tree that served all three valves on the tree connected to the negative splitter. Figure 3.21 displays the interior of the finished electrical controller box.

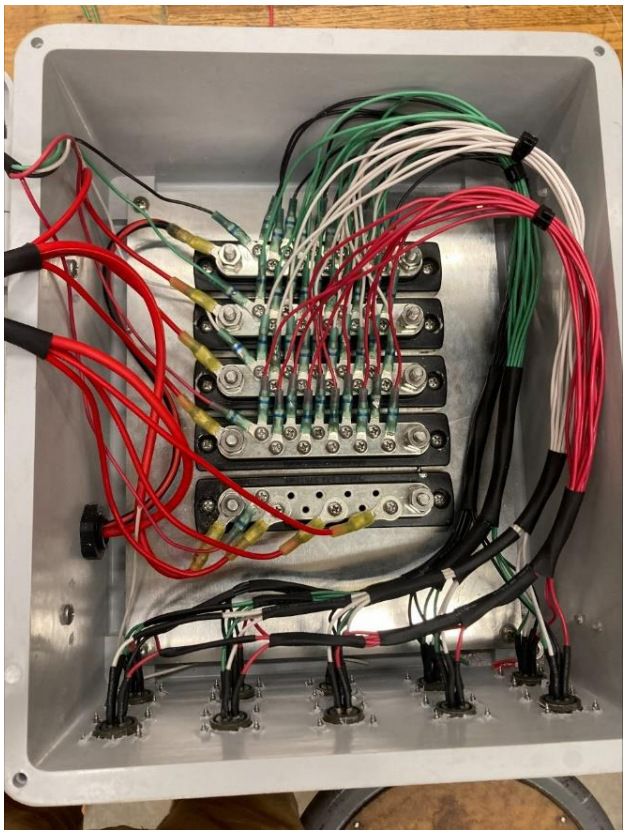

FIGURE 3.21: Electrical Controller.

Each sprinkler required wire to be cut at variable lengths corresponding to its positioning on the plot in order to reach the location of the electrical controller at the bottom of the plot. Wire

lengths are shown below and are derived from the distance from the controller to the bottom of each sprinkler plus 15 ft (4.6 m) for the height of the sprinkler.

TABLE 3.2: Rainfall Sprinkler Tree Wire Lengths

Wire Length, ft (m)	Quantity
90 (27)	1
75 (23)	2
65 (20)	2
55 (17)	2
45 (14)	2
30 (9)	1

Four-strand wire was used. Three positive wires connected to one valve each, and the same negative wire was used for all three valves. The valves were 0.75-in. (1.9 cm) 12V DC electric brass solenoid valves. Wires connected to the electrical box with Military Spec Signal/Power connectors with four poles. Appendix B contains a parts list for the electrical controller box.

3.9 SOIL VERIFICATION AND ACQUISITION

The ASTM sand stockpile was exhausted after the construction of Plots 3 and 4. Therefore, sieve analysis was conducted on the stockpiles from the same source location to verify that the soil was identical (ASTM, 2014). The source was Skipper's Trucking near Abbeville, AL. Additional soil analysis was conducted on soils from Notasulga quarry near Loachapoka, AL and other stockpiles. Ultimately, ten truckloads of soil, totaling 200 yd^3 (153 m^3) were delivered by Skipper's trucking. With this acquisition, all soil quantities required for construction and testing proposed by "Evaluation of ALDOT Erosion Control Products Using Rainfall Simulation on Various Soil Types and Slopes Gradients Phase II" were obtained.

To perform sieve testing, a representative oven-dried sample that weighed approximately 200g was taken and the weight recorded as "Initial sample weight." Next, the #200 "wet sieve"

was used to gently wash fines from the sample with minimal water. The remaining wet sample from the sieve was dried in the oven at 220 F (104 C). Then, it was weighed and recorded as "Weight after wet sieving." The sample was broken up and sieve stack was prepared with No. 4, No. 10, No. 20, No. 40, No. 50, No. 80, No. 120, and No. 200 sieves. The sieves were stacked in order with the largest aperture size at the top and the smallest at the bottom. A pan was placed under all the sieves to collect samples. Then, the empty sieves were weighed individually, and the masses were recorded. The soil was poured into top of the stack of sieves and the lid was secured. The sieve stack with soil was allowed to shake in the sieve shaker for 15 min. Then, the shaker was stopped and the mass of each sieve and retained material was recorded. If the total weight of the finished sample deviated more than 2% from the initial weight, the procedure was redone with new soil, which was required for one sample. Sieves were washed, dried, and re-weighed after each test.

The findings of this sieve testing are discussed in *Chapter 5: Results and Discussion*. These results were used to identify and label as many soil piles as possible, which had become necessary after the expansion of AU-SRF. Signs were constructed out of 0.75 in. (2.0 cm) plywood and wooden stakes. Soil labels containing pertinent information such as soil classification and source were printed and laminated. Finally, the labels were stapled onto the signs, and they were staked into the ground near each soil pile. An example sign is shown in Figure 3.22 which contains the soil classification and the source.

(a) sign at stockpile (b) ASTM sand sign

FIGURE 3.22: Stockpile Signs.

3.10 CONSTRUCTION SUMMARY

While large-scale rainfall simulators can be costly and time-consuming to construct, several efficient practices can reduce the necessary cost and labor. Following the standardized ASTM D6459-19 plot design is key to communicable results, and this research seeks to share in detail the specific techniques for constructing to this standard. Major findings throughout the course of plot construction include that 2.0-in. (5.1-cm) thick lumber is suitable as a material for plot borders and that anchored plastic tubs can be effective for catchment. While French drains were first used for protecting catchment basins from flooding, the anchoring method proved more effective. Drainage channels and culverts were also completed for mitigating flood risk. To ensure that tests were performed with appropriate soils, stockpiles of ASTM sand, clay, and loam were

obtained and labeled. Additional sand identical to previously obtained material was matched by sieve testing.

Methods for successful flow supply and electrical function are not addressed in ASTM D6459-19. The flow supply was implemented for this project using a pipe along the top of all plots with six connections to supply a manifold and two end valves for pressurizing the system. The manifold divided the flow between the ten sprinklers once the system was pressurized by closing both valves. The electrical system was implemented with an electrical control box. While one switch on the box activated power to the controller, the remaining three switches powered one sprinkler valve on each sprinkler tree.

CHAPTER 4: CALIBRATION AND TESTING METHODOLOGY

4.1 VERFICATION OF ORIGINAL AU-SRF RAINFALL SIMULATOR

ASTM D6459-19 bare soil testing was completed on the original rainfall simulator plot with the methods described in this section to renew accreditation with the Geosynthetic Accreditation Institute. The original plot contains loam soil different from the native stockpile used for the new apparatuses. This procedure was used to formulate the procedure for testing on the twelve new rainfall simulators with some modifications. The procedure for the new rainfall simulators is contained in Section 4.5 of this chapter.

4.1.1 Intensity Calibration

To ensure that the rainfall simulator still output the target intensities of 2.0, 4.0, and 6.0 in./hr (51, 102, 152 mm/hr), 15-min calibration tests were performed on a covered surface with a total of 20 rainfall gauges set on the plot on wooden wedges and stapled into the soil. ASTM D6459-19 specifies that the rainfall gauges are spread evenly from each other with 2.0-ft (0.61 m) spacing to borders, as demonstrated by Figure 2.2.

To prevent clogging in the rainfall simulator sprinklers, the pressure gauges on each rainfall tree were disconnected and water was pumped through to wash out the pipes. Next, the pressure gauges were reconnected, and pumping resumed to verify that each sprinkler was working. Valves and sprinkler nozzles for any malfunctioning sprinkler were cleaned and checked for electrical problems. Each sprinkler contained a green nozzle, shown disconnected in Figure 4.1, above the valve and below the disperser. This was the most common location for clogging.

FIGURE 4.1: Sprinkler Clog Location.

Finally, with the sprinklers all working, the calibration test was performed. On a calm day with wind speeds less than 1.0 mi/hr (1.6 km/hr), each intensity ran for 15 min, and rainfall gauge heights were recorded. Intensity in in./hr was calculated by multiplying the average measured rainfall by four to normalize for in./hr units per Equation 2.1. Additionally, Christiansen uniformity, Cu, was calculated using Equation 2.2. The results are shown in Table 4.1.

TABLE 4.1: First Intensity Calibration Test Results

Target Intensity, in./hr (mm/hr)	**2.0 (51)**	**4.0 (102)**	**6.0 (152)**
Average Gauge Height, in. (mm)	0.64 (16)	1.00 (25)	1.50 (38)
Measured Intensity, in./hr (mm/hr)	2.54 (65)	3.98 (101)	5.99 (152)
Cu (%)	76.06	84.97	80.47

The apparatus had three switches to power valves. Each switch corresponded to adding 2.0 in./hr (51 mm/hr) to the target intensity. The switches were aligned vertically. This test used the top switch for the 2.0 in./hr (102 mm/hr) target intensity and added the middle switch for the 4.0 in./hr (102 mm/hr) intensity. All switches were on for the 6.0 in./hr (152 mm/hr) intensity.

(a) during 2.0 in./hr (51 mm/hr) (b) during 4.0 in./hr (102 mm/hr) (c) during 6.0 in./hr (152 mm/hr)

FIGURE 4.2: Rainfall Simulator Calibration.

Since the order of switches activated to add intensity determined which sprinkler on the tree that rainfall ejected from, an experiment to determine which switch was closest to desired for the 2.0 in./hr (51 mm/hr) target intensity on this rainfall simulator was performed. The target metrics were to reach 80% Christiansen uniformity and to be as close to the target intensity as possible. The 4.0 and 6.0 in./hr (102 and 152 mm/hr) tests achieved this with the initial switch pattern while the 2.0 in./hr (51 mm/hr) test did not meet standards for either metric.

For the 2.0 in./hr (51 mm/hr) test, different switches were tested to determine the closest to the target intensity. The results are shown in Table 4.2.

TABLE 4.2: Target Intensity Calibration Test Results Varied by Switch

Switch Location	Top	Middle	Bottom
Average Gauge Height, in. (mm)	0.61 (15)	0.46 (12)	0.56 (14)
Measured Intensity, in./hr (mm/hr)	2.42 (61)	1.84 (47)	2.24 (57)
Cu (%)	80.00	78.91	80.18

The results indicated that the bottom switch should be used for half of the 2.0 in./hr (51 mm/hr) test and the middle switch should be used for the other half. The combined switch method was tested experimentally and yielded an intensity of 2.05 in./hr (52) and a Christiansen uniformity of 82.20%. Therefore, this order of switch activation was utilized for testing on this apparatus to ensure precise rainfall simulation.

4.1.2 Bare Soil Testing

For re-certification of the rainfall simulator, a bare soil test was performed to compare to previous results and ensure that the soil loss yield was similar. Slope preparation began several days before the test by tilling it with shovels. However, it is important to note that for the first bare soil test of the two, the soil was not tilled deeply enough because the appearance of the soil became gravelly following the test. Next, the soil was compacted using the plate compactor one time. However, this over-compacted the soil relative to previous testing. The Proctor Compaction test results for bare soil test 1 are shown in Table 4.3.

TABLE 4.3: Compaction in Verification Test 1

Average Compaction (%)	87.66
Average Moisture Content (%)	19.2

An improved method of supporting the rainfall gauges was desired to not have wooden wedges interfering with flow and soil loss on the plot. Using small wooden stakes, rebar, and rebar clamps, a method of suspending above the ground was devised. During testing, only six rainfall

gauges were used, and they were spaced at 10.0-ft (3.0-m) intervals with the gauges 2.0 ft (0.6-m) from the plot borders.

FIGURE 4.3: Rainfall Gauge Suspension Method.

On test day, several containers were prepared to collect runoff separately including two barrels and two metal troughs. Additionally, an electric sump pump was prepared and placed in the barrels to pump the 2.0 and 4.0 in./hr (51 mm/hr and 102 mm/hr) runoff to separate troughs. Four workers were required for the test. While one worker operated the rainfall simulator, monitored the sprinklers, monitored the pressure within the sprinkler trees, and handled the pumps, one worker collected bottle flow samples for turbidity and total suspended solids (TSS) every 3 min. Another two workers measured flow rate every two min using a stopwatch and 1.0 gal. (3.8 L) container.

The 2.0 in./hr (51 mm/hr) intensity storm ran for twenty min. The sides of the plot were observed to ensure no runoff outside the plot entered the catchment basin. All the runoff for the 2.0 in./hr (51 mm/hr) test was routed into the barrel and as much sediment-laden runoff as possible was pumped to the first trough. At 20 min., the test was paused, and a barrel was placed in the catch basin for the 4.0 in./hr (102 mm/hr) flow. The intensities for the six rainfall gauges were recorded to verify the *R*-factor in the RUSLE equation. The electric pump outlet was switched to the second trough. Then, the second twenty-min portion of the test was performed. Finally, at forty min, the rainfall simulator was turned off again, the barrel was removed, and gauge heights were recorded. For the last twenty min, the 6.0 in./hr (152 mm/hr) flow routed directly into the catch basin, and the pumps were shut off at 60 min so that gauge heights could be recorded. Following the test, the plot was allowed to dry, and all containers were left undisturbed for 24 hr to allow settling.

At the 24-hr mark following the test, supernatant was pumped off using a wet shop vacuum. Then, the sediment was weighed in buckets. Visually distinct strata of sediment were sampled for moisture content and the distinct material was recorded separately for both troughs, both barrels, and the catch basin. The 2.0 in./hr (51 mm/hr) target intensity runoff was in trough 1 and barrel 1, the 4.0 in./hr (102 mm/hr) runoff was in trough 2 and barrel 2, and the 6.0 in./hr (152 mm/hr) runoff was in the catchment basin. The turbidity and total suspended solids of the sample bottles were tested and recorded in the laboratory. All data was compiled in a single spreadsheet to be used for analysis.

4.1.3 Turbidity Testing

To perform turbidity testing, the first step was to calibrate the turbidimeter by standard procedures in the user manual. Next, the sample was shaken in the bottle to reduce any settlement.

Then, part of the sample was added into a beaker suitable for the turbidimeter. The beaker was placed inside the turbidimeter and the NTU of the sample was recorded. If the turbidimeter could not find turbidity due to excessive NTU, the sample was diluted. Typical dilutions required for rainfall simulator bare soil tests ranged from 20 to 120 parts water to 1 part turbidity sample depending on soil characteristics with the Hach TL2300 Tungsten Lamp turbidimeter.

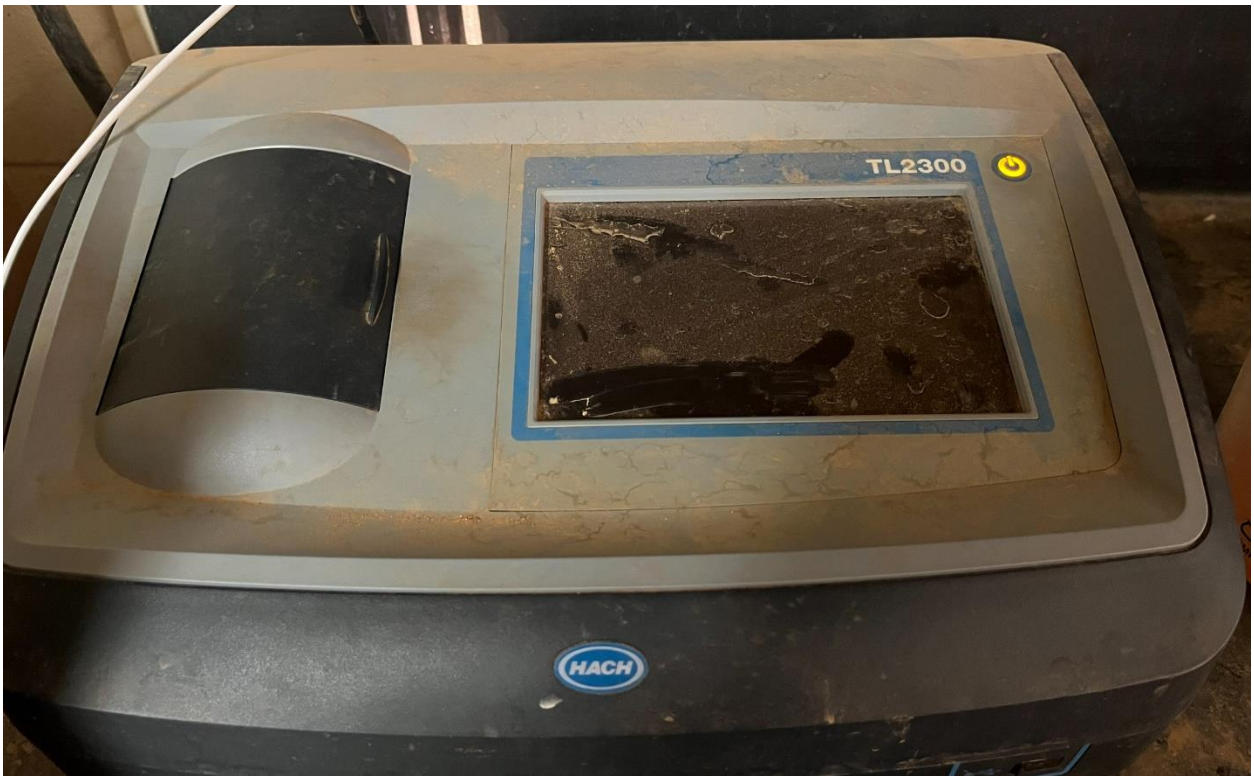

FIGURE 4.4: Turbidimeter.

4.1.4 Total Suspended Solids Testing

The total suspended solids, or TSS, was determined from the same samples as the turbidity. First, the appropriate number of crinkle dishes and filter membranes were prepared. They were washed by spraying deionized water from a bottle onto the dishes and dried. Filters were placed on the crinkle dishes. The filters were handled with tweezers to prevent contamination. Next, the crinkle dishes and filter membranes were dried in the oven for one hour. They were weighed together with a precise balance to the ten-thousandth grams. The filters were placed on the filtering

machine individually. Using a pipette, 10 to 25 mL of the sample sediment-water was transferred onto the membranes. The filtering machine was activated to vacuum the water from the sample for each sample. Once all water was removed from the filter membrane, the filters were removed and placed back in the crinkle dish to be placed back in the oven for at least one hour. Once dry, their dry weights were recorded. The equation for the total suspended solids of a sample is in Equation 4.1. Since the weights were in grams and the volume was in mL, a unit conversion of 1,000,000 was applied in the equation to find TSS in mg/L.

$$TSS = \frac{W_{final} - W_{initial}}{V_{sample}} * 1{,}000{,}000 \tag{4.1}$$

where,

TSS = total suspended solids, mgTSS/L

W_{final} = weight of sample after oven drying, g

$W_{initial}$ = weight of crinkle dish and filter membrane, g

V_{sample} = volume of sample used, mL

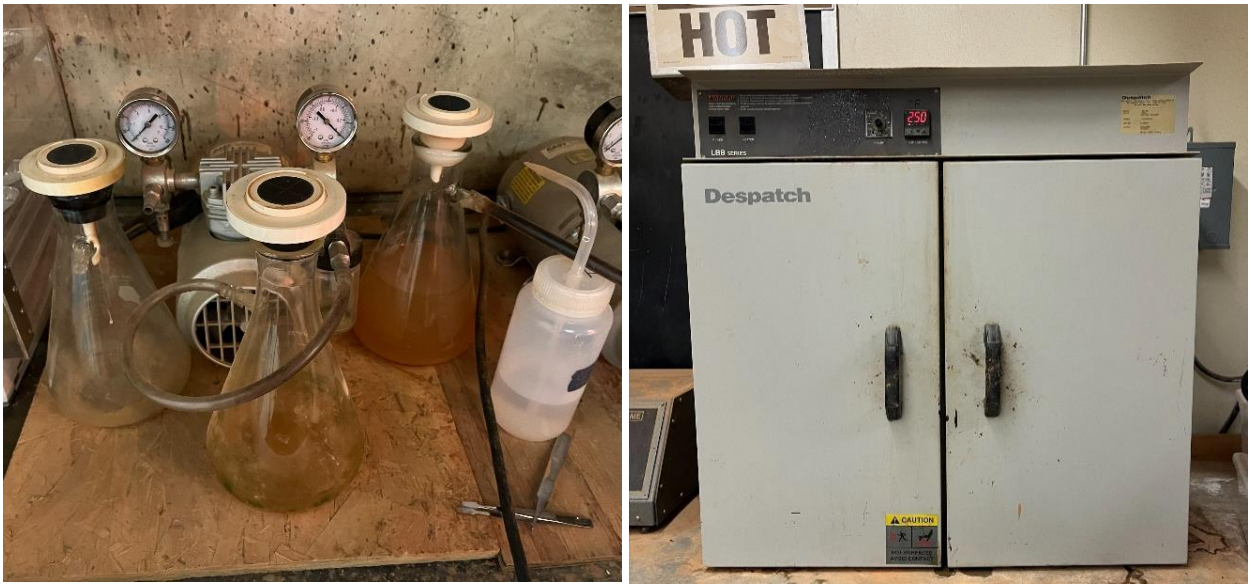

(a) TSS vacuum (b) drying oven

FIGURE 4.5: TSS Equipment.

4.2 INTENSITY CALIBRATION METHODS

Three tests for determining rainfall intensity on a large-scale rainfall simulator were examined in this work. The first method followed ASTM D6459-19 and used 20 rainfall gauges. The second method also used rainfall gauges and was used for verifying the results of the ASTM D6459-19 method during testing as shown in Figure 4.3; however, the difference from the first method was that only six rainfall gauges were used. This will be referred to as the 6-gauge, or 6-ga., method. The third method was the direct runoff collection method. This technique measured the volume of runoff that the rainfall simulator generated when the plot surface was impermeable and back-calculated to determine rainfall intensity.

The methods were compared statistically. First, ASTM D6459-19 intensity calibration test was performed for 15-min with target intensities of 2.0, 4.0, and 6.0 in./hr (51, 102, and 152 mm/hr). The gauges were leveled with an electronic level but were prone to becoming unleveled when filled, which was corrected on observation during the test. Finally, Christiansen uniformity was calculated following the procedure in ASTM6459-19 to verify that there was at least 80% uniformity.

The second method for determining intensity was the 6-ga. method. The 6-ga. method was performed in the same manner as the ASTM D6459-19 setup but lasted for 20 min and used suspended rainfall gauges. This method was for verifying intensity during testing and determining *R*-factor for the RUSLE equation when it was not reasonable to utilize 20 rainfall gauges. The gauges were suspended on rebar to not impede erosive processes during tests. They were spaced 2.0 ft (0.6 m) from the plot sides and 10, 20, and 30 ft (3.0, 6.1, and 9.1 m) from the top of the plot in two columns to be as similar to the ASTM D6459-19 placement as possible.

The third method was the runoff volume method, which included direct measurement of runoff volume on the plot of known size when the surface was impermeable. Testing intensity with this method included collecting all runoff with the plot covered by double-layered waterproof tarps and pumping it into a 300-gal. container. The research team checked that all runoff was collected in the tank by dropping water on the farthest reaches of the plot and observing that the path to reach the tank remained on the plot. The plot borders prevented flow from outside the plot from reaching the tank. Equivalent intensity was calculated similarly to the Rational method (Rossmiller, 1980).

$$i = \frac{Q}{C * A} \tag{4.2}$$

where,

i = calculated rainfall intensity, in./hr

Q = peak runoff, ft^3/s

C = runoff coefficient

A = tributary watershed area, ac.

When an impermeable tarp was placed on the plot, the runoff coefficient was equal to 1.0. Therefore, the equation became a mass balance where only intensity, i, was unknown and Q was average runoff instead of peak runoff. The area contributing to runoff was 320 ft^2 (29.7 m^2) as determined by the 8.0 by 40.0-ft (2.4 m by 12.2-m) plot area. To precisely measure the runoff volume, a relationship for the collection tank was established. Four rulers were attached to the corners of the tank, and water was added in 1.3-gal. (5-L) increments. The total volume was recorded along with height at each of the four rulers. Then, the heights of water in the tank were averaged for each increment of water volume, and a relationship was calculated that equated an average height in the tank with a volume, which streamlined the process of determining the runoff volume.

Both methods with rainfall gauges placed them uniformly; this meant that the distance of the gauges from the sprinklers was also uniform. The sprinklers had regions that were more intense in their distribution of raindrops, which was not accounted for in the Christiansen Uniformity calculation because the gauges are equal distances from the closest sprinklers. The runoff method determined the effectiveness of rainfall gauges for measuring the intensity.

To compare the 6-ga. method to the runoff method, tests were performed simultaneously to be statistically paired. During a paired test, runoff was collected for 20 min at each intensity and the height of the runoff in the tank was recorded while six suspended rainfall gauges were also prepared and recorded. Since the two tests were simultaneous, conditions were equivalent. The tank and an example 1.0 in^2 (6.5 cm^2) rainfall gauge are shown in Figure 4.6.

(a) tank for runoff collection (b) rainfall gauge

FIGURE 4.6: Rainfall Gauge and Runoff Method Measurement Containers.

The outcomes of the three methods for determining the intensity, including the ASTM D6459-19 method, the 6-ga. method, and the runoff collection method are compared in *Chapter 5: Results and Discussion*. To achieve stringent wind requirements of ASTM D6459-19, all tests were set up the day prior and performed early in the morning when local winds were calmest.

4.3 DROP SIZE CALIBRATION METHODS

Numerous methods for raindrop size calibration exist. Most notable practices are the flour pan method, the laser method, and the photographic method. The flour pan and photographic methods are examined in this research. While the flour pan method is well-established and is recommended by ASTM D6459-19, the photographic method presents opportunity for greater precision in measurement of raindrops.

4.3.1 Flour Pan Method

The flour pan method is the lowest-cost method for rainfall drop size calibration. The procedure for the test is detailed in *Chapter 2: Literature Review.* However, as stated by Tullis, the flour pan method can overrepresent drop size in comparison to more precise photography and laser methods. The notable steps of the procedure including preparing a flour pan, setting it uncovered on a plot during each intensity, sieving, and weighing and counting the pellets retained on each sieve size are documented in Figure 4.7.

(a) pan with flour

(b) raindrops in flour

(c) sieve stack

(d) precise scale

FIGURE 4.7: Flour Pan Method.

The results of this method are compared to the results of the photographic method in *Chapter 5: Results and Discussion.*

4.3.2 Photographic Method

The premise of using photography for the determination of raindrop size relies on several assumptions. Firstly, the method assumes that raindrops are perfectly round. This is because drop size can only be measured by the drop width since the height of the raindrop is captured by the camera during the time the camera lens is open while the raindrop is moving downward. This creates a "tail" for each raindrop.

The development of a method for capturing raindrop characteristics through photography is detailed in this section. First, a box, called the "raindrop box" in this work, was designed and constructed with the purpose of protecting a camera from rain while limiting the distance at which the camera would be able to observe rain. The design of the raindrop box is shown in Figure 4.8 with all dimensions in inches.

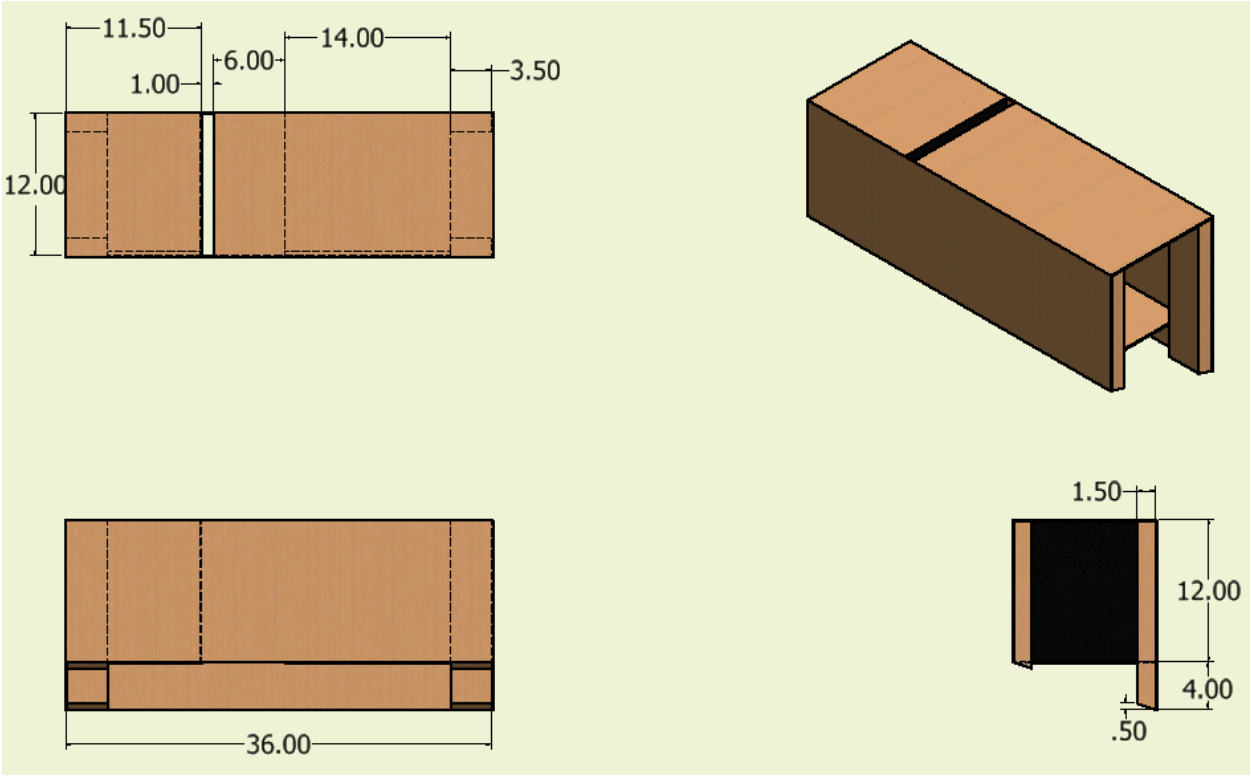

dimensions shown in inches (1 in. = 2.54 cm)

FIGURE 4.8: Raindrop Box Design.

The raindrop box was constructed identically to the design. One notable measurement of the first iteration of the design was that the width of the opening for raindrops was 1.0 in. (2.5 cm) wide.

FIGURE 4.9: Raindrop Box on Plot.

The initial attempt at utilizing the raindrop box was performed with an iPhone SE 2nd generation video camera. Grid paper was placed behind the raindrop region and distances were measured between the focal point of the camera to both the opening for raindrops, called the raindrop region, and the grid background. The concept of similar triangles was used to determine the size of the raindrops from the scale grid in the background. The x-axis represented the distance from the lens to each region and the y-axis represented the scale using the grid background.

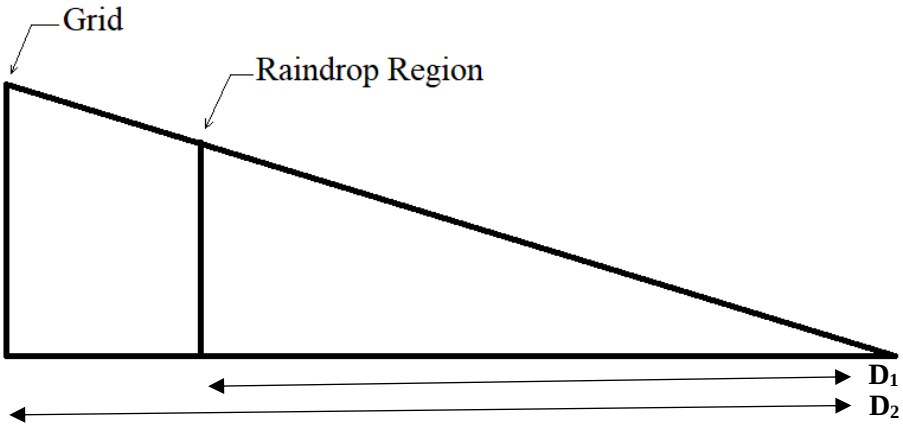

FIGURE 4.10: Raindrop Box Similar Triangles Diagram.

D_1 was equal to 14.75 in. (37.47 cm) and D_2 was equal to 17.50 in. (44.45 cm). Therefore, the conversion factor from the grid scale to the raindrop region scale was a range of 0.814 to 0.871. The range was present because the opening for raindrops introduced roughly ±3.4 percent error.

The width of each raindrop was measured in millimeters from the scale and similar triangles conversion. In photograph editing software, the raindrop width was measured in pixels and converted to millimeters. While this initial attempt yielded preliminary results proving that raindrops could be measured in some capacity by photography, several improvements could be made. An example photograph with the grid background is shown below in Figure 4.11 along with the four points used to measure the height and width of the raindrop. In addition to collecting the width of the raindrop for drop size, the height was used to determine velocity. Furthermore, the angle of each raindrop was calculated.

FIGURE 4.11: Raindrop on Grid Example.

The second attempt at utilizing photography to measure raindrop size improved on the first attempt immensely. These improvements included using a professional camera with flash. The professional camera, a Nikon D7200, was able to produce reliable shutter speeds. The shutter speed selected was 1/320 sec with other settings including 10,000 ISO for brightening the images of raindrops. Additionally, manual focus was used. Video capture was not necessary with the Nikon D7200.

The experiment was performed with a non-reflective black background. It was not necessary to utilize similar triangles to produce a conversion factor to the distance of the raindrops. Instead, a single calibration photograph was taken with a ruler with 1.0 mm precision placed in the center of the raindrop region. Thirty photos were collected during each target intensity using a remote, receiver, and flash trigger. The remote was an Aodelan Pebble Wireless Remote Shutter Release and the flash trigger was a Godox Studio Flash Trigger RT Series. The results and

comparison to the flour pan method for drop size are detailed in *Chapter 5: Results and Discussion*. The results of these photos were much clearer images of after processing as displayed in Figure 5.9.

4.4 DETERMINATION OF RAINDROP ENERGY

The purpose of determining raindrop size in ASTM D6459-19 is to determine the energy of the rainfall to be able to derive the *R*-factor in the RUSLE equation. However, if velocity was measured directly, potential sources of error including the measurement of raindrop size and the calculation of raindrop energy from raindrop size could be minimized. The traditional calculation of raindrop velocity by drop height and the direct measurement with photography are described in this section.

4.4.1 Drop Height Method

ASTM D6459-19 dictates that the fall height of the raindrops determines its velocity. Since the height of the sprinklers is 14 ft (4.3 m), raindrops theoretically reach terminal velocity before reaching the plot surface. The relationship is shown in Figure 4.12.

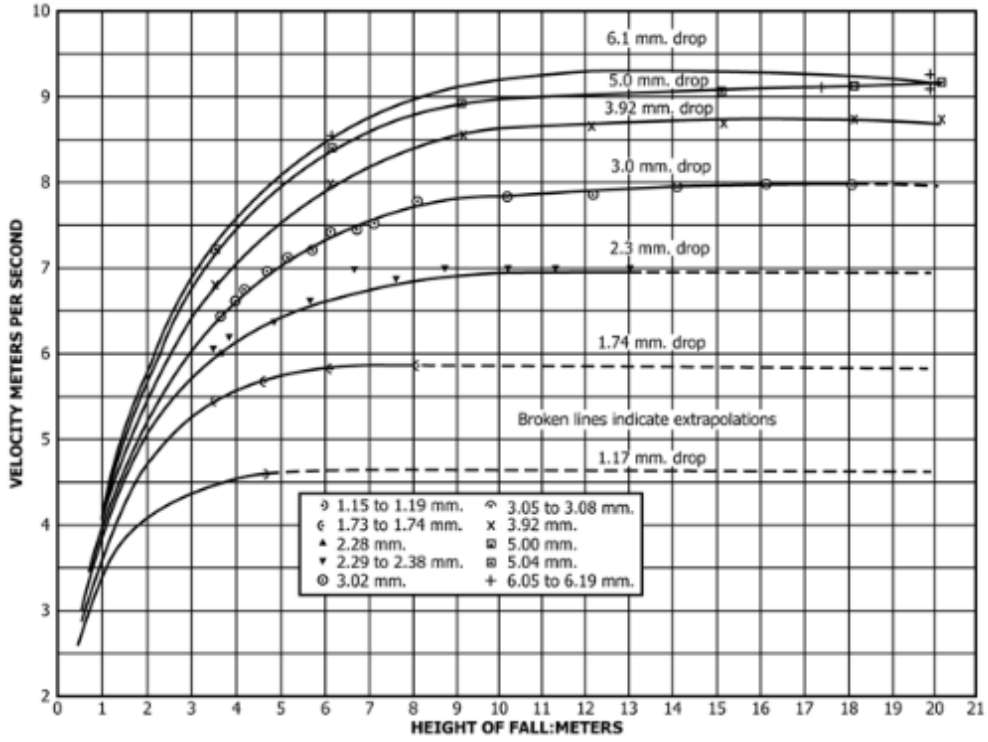

FIGURE 4.12: Theoretical Raindrop Velocity (ASTM 2019).

This method for determining raindrop velocity is straightforward since the only variable to determine velocity is drop size. However, errors in drop size determination create compounded error for the velocity. The effect of the error on the calculated raindrop energy, which is determined using Equation 2.3, is compounded even further since the equation for raindrop energy entails squaring the velocity. This presents a notable source of potential error for the *R*-factor of the RUSLE Equation, which linearly influences the soil erodibility that control tests determine using the rainfall erosivity and experimentally determined soil losses.

4.4.2 Photography for Experimental Determination of Raindrop Velocity

Photography presents an opportunity to experimentally determine the velocity by direct measurement. Cameras capture images over a period known as the shutter speed, which is the time that the camera lens is open and capturing light to form a photograph. When photographed by a camera with shutter speeds around 1/320 sec, a fast-moving raindrop will be observed to have a

non-spherical shape with the height being greater than the width like in Figures 4.12 and 5.9. Therefore, if raindrops are assumed as spherical, the distance traveled by the raindrop over the time of the shutter speed is equal to the height of the raindrop minus its width. Therefore, the speed of a raindrop as determined by a photograph can be represented by Equation 4.3.

$$S_{drop} = \frac{H_{drop} - W_{drop}}{t} \tag{4.3}$$

where,

S_{drop} = raindrop speed, mm/s

H_{drop} = apparent height of raindrop in photograph, mm

W_{drop} = apparent width of raindrop in photograph, mm

t = shutter speed of camera, s

Results of photographs included heights and widths of the raindrops in pixels. Calculations included height and width of the raindrop in millimeters, angle of velocity, speed, and drop size. The shutter speed used to capture the photographs in the first experiment was 1/480 sec. One additional assumption of the first experiment was that the shutter speed was not variable; however, the iPhone SE 2nd generation may have had variable shutter speed. In a spreadsheet, the raindrop heights and widths in each photograph were recorded and converted to the scale identically for the methods used for drop size. The data in the first experiment was not cleaned; velocities were calculated directly, and all visible raindrops were included.

The second experiment was performed with similar procedures. However, the precision of the experiment was increased by using a professional camera with reliable shutter speed and reducing the width of the raindrop region. Since a calibration photograph with a 1.0 mm precision ruler was taken at the same distance as the raindrops, there was no distance conversion factor for the second experiment. The error was equivalent to half the width of the raindrop region divided by the distance from the focal point of the camera to the center of the raindrop region. For the

second experiment, since the distance from the camera to the center of the raindrop region was 12.5 in. (31.8 cm) and the raindrop region width was reduced to 0.5 in. (1.3 cm) from 1.0 in. (2.5 cm) to minimize error, the percentage error was ±2%.

4.5 NEW APPARATUS CONTROL TEST METHOD

One goal for this report is to make large-scale rainfall simulation accessible to more researchers. Therefore, for an understanding of the process of performing a test on an ASTM D6459-19 rainfall simulator, the process is described. The procedure followed for testing on the new apparatuses was like the procedure on the original AU-SRF ASTM D6459-19 rainfall simulator; however, several facets of the experiment were updated including the compaction method, the 6.0 in./hr (152 mm/hr) target intensity flow collection technique, and the flashing system. This section describes the full testing process for continuity.

For a control test, no product was installed on the plot. The plot was tilled with a digging fork and compacted to 90 ± 3% compaction. On test day, a minimum of four personnel were required for the test. While the main operator operated the supply pump, monitored the sprinklers, and monitored the water pressure in the sprinkler trees, one worker collected sample bottle flow samples for turbidity and TSS every 180 sec. Another worker measured the flow rate every two min using a stopwatch and 1.0-gal. (3.8-L) container. Another worker operated the end valve of the supply pipe. This worker is necessary for both maintaining appropriate pressure in the system and operating as an emergency flow shutoff in case of electrical malfunction that closed the sprinkler valves. In general, this worker is only necessary at the start of the test to close the valve until the pressure in the sprinklers is appropriate.

Each intensity ran for 20 min. All runoff for the 2.0 in./hr test was collected in a barrel inside the catchment basin and pumped to a 300.0 gal. (1,147 L) tank. At twenty min, the test was paused, and a barrel was placed in the catch basin for the 4.0 in./hr (102 mm/hr) flow. The measurements for the six rainfall gauges were recorded before starting the next phase. The sump pump outlet was switched to a second trough and the pump was placed in a new barrel for runoff collection. Then, the second twenty-min portion of the test was performed at 4.0 in./hr (102 mm/hr) with two switches on. At forty min, the rainfall simulator was turned off again, the barrel was removed, and rainfall gauge depths were recorded. The procedure with a new barrel replacing the former was repeated for the 6.0 in./hr (152 mm/hr) target intensity, and the test was terminated at 60 min. The rainfall gauge depths were recorded once again and the sediment in each barrel was added to the tank corresponding to the target intensity that generated the sediment. Following the test, all containers were labeled and left undisturbed for 24 hr to allow settling. This process was like the procedure described in section 4.1.2; however, one difference is that runoff did not flow directly into the catchment basin for the 6.0 in./hr (152 mm/hr) flow. The catchment basins on the new plots were smaller and made of pre-formed plastic. Therefore, to avoid overflow or seepage of runoff outside the plot into the 6.0 in./hr (152 mm/hr) collection, a third tank was used. Furthermore, some soils may generate considerable sediment within the barrels and begin to bury the sump pump. To assuage this, a pipe system was constructed at the flashing of each plot. When a barrel was halfway full of sediment, the pipe was flipped to discharge into a second barrel and the sump pump was placed in the new barrel.

FIGURE 4.13: Flashing System.

Identical procedures for weighing sediment and laboratory analysis including turbidity and TSS can be found in sections 4.1.2 through 4.1.4. All data was compiled in a single spreadsheet to be used for RUSLE equation analysis. Importantly, the dry weight of the sediment eroded from the plot was equal to A, annual soil loss per acre. Using calibration data including raindrop energy and experimental rainfall intensity, the *R*-factor was determined for the test. Then, the *LS*-factor was calculated based on the slope length and steepness. For control testing, the *C*-factor was equal to 1.0. Then, with P also equal to 1.0 with the absence of any sediment control techniques, the equation was solved for *K*-factor. For a product test following control testing, The *C*-factor is not assumed to equal 1.0. The *K*-factor is used to calculate the *C*-factor for the product tested. Therefore, through back-calculation and experimental results, erosion control products can be fairly evaluated for different slopes and soils.

CHAPTER 5: RESULTS AND DISCUSSION

Results of this thesis include (1) a summary of construction of twelve ASTM D6459-19 rainfall simulators, (2) soil sieve analysis for determining a suitable source for ASTM sand for four of the rainfall simulator apparatuses, (3) statistical comparison of rainfall gauge and runoff rainfall intensity methods, (4) statistical and graphical comparisons of flour pan and photographic raindrop methods for determining raindrop characteristics, (5) results of the verification of the original ASTM D6459-19 large-scale rainfall simulator at the AU-SRF, and (6) findings of the initial control testing with the twelve new AU-SRF ASTM D6459-19 rainfall simulators.

5.1 CONSTRUCTION

The results of the construction portion of this thesis include twelve fully functional ASTM D6459-19 rainfall simulators. There are six different plot configurations, each of which is duplicated. The variation between the plots is only in soil installation and slope. Parameters including slope length, sprinklers used, and flow supply method. The testing method remains identical or similar for all twelve slopes. This continuity allows testing on the various slopes to be compared for differences from slope and soil. There are six 4H:1V plots and six 3H:1V plots with four plots for each soil type: sand, loam, and clay. These selected soils are representative for a large portion of the state of Alabama. Since each plot has an identical pair, one plot of the pair can be used for testing with topsoil while the other remains clean of any topsoil.

The methodology for constructing an ASTM D6459-19 plot has been sparsely documented. Furthermore, cost-saving techniques are rarely considered. The implementation of cost-saving techniques, such as wooden plot borders instead of concrete, a PVC manifold instead of

underground piping for each plot, and a plastic catchment basin instead of a concrete one, allowed more plots to be constructed. Rainfall simulation can be expensive and laborious; however, these measures increase accessibility for additional researchers, which increases the likelihood of more products being tested in various slope and soil conditions. Most important to the practice of rainfall simulation is standardization. While ASTM D6459-19 provides specific parameters for an apparatus, it does not specify how the apparatus should be constructed. Furthermore, sharing the methods for construction can lead to future improvements in the practice.

5.2 SOIL SIEVE ANALYSIS

The sand stockpile was exhausted following the completion of the construction of Plots 3 and 4. However, two more plots still had to be constructed with sand and the sand used for replacing the lost soil from tests still had to be procured. It was desirable that the same soil should be located and ordered; however, the source had to be verified as the same soil. Additionally, alternative sources with lower shipping cost that also fit ASTM D6459-19 soil requirements were considered. Table 2.1 has grain size requirements for ASTM D6459-19.

Numerous stockpiles at AU-SRF were also analyzed to determine potential future use. Using sieve test data following the procedure in Section 3.9 by Manning, which is known to be the same material as in Plots 3 and 4, it was confirmed that the source of the sand was Skipper's Trucking in Abbeville, AL (Manning, 2021). Figure 5.1 contains gradation curves for several samples of Skipper's Trucking's Dirt soil including Manning's results from when this soil was first obtained labeled as "CM Red Sand 1" and "CM Red Sand 2." Figure 5.1 also shows a sample from Plot 3 in red and a sample directly taken from Skipper's Trucking named "Skipper's Red Dirt" in orange.

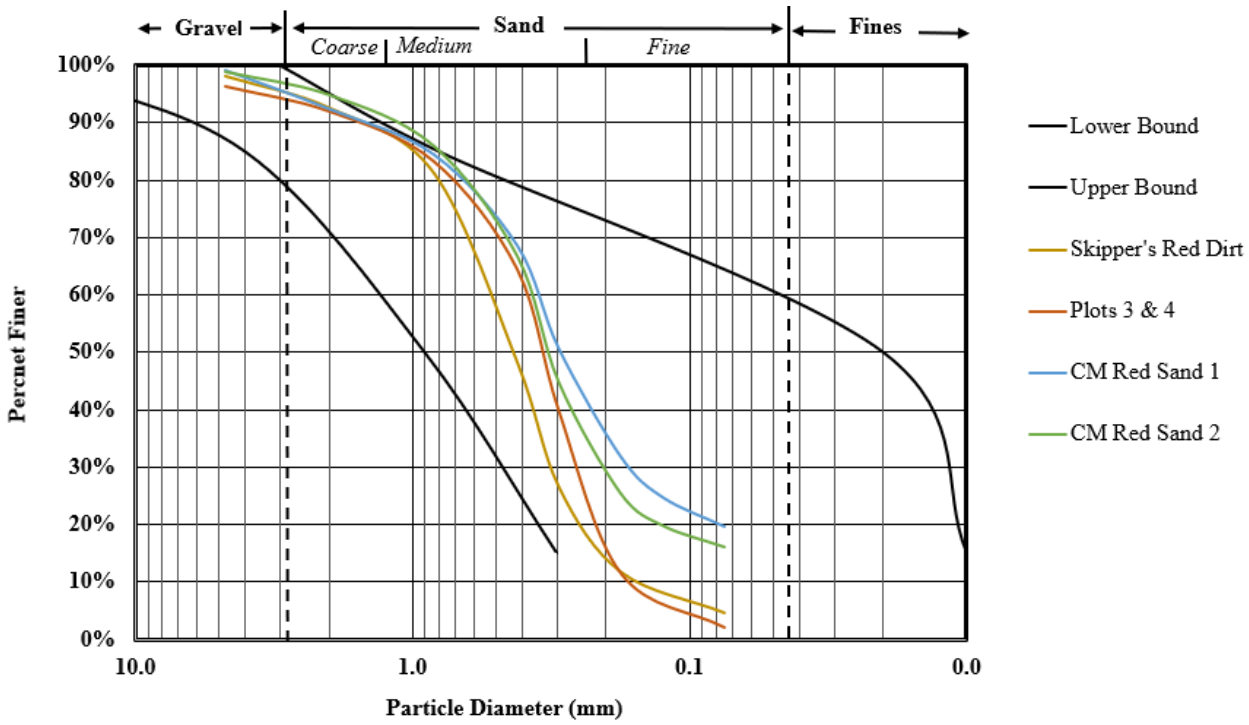

FIGURE 5.1: Verifying Plot 3 and 4 Soil Source.

The Plot 3 sample and Skipper's Red Dirt sample were observed to be nearly identical in gradation. Some differences were observed from 2021 sampling by Manning; however, this may have been from loss of fines from erosion in the two newer samples. Therefore, it was confirmed that Skipper's Trucking Dirt was the original soil source. However, numerous other soil sources were tested and considered as well, which are examined in Figure 5.2.

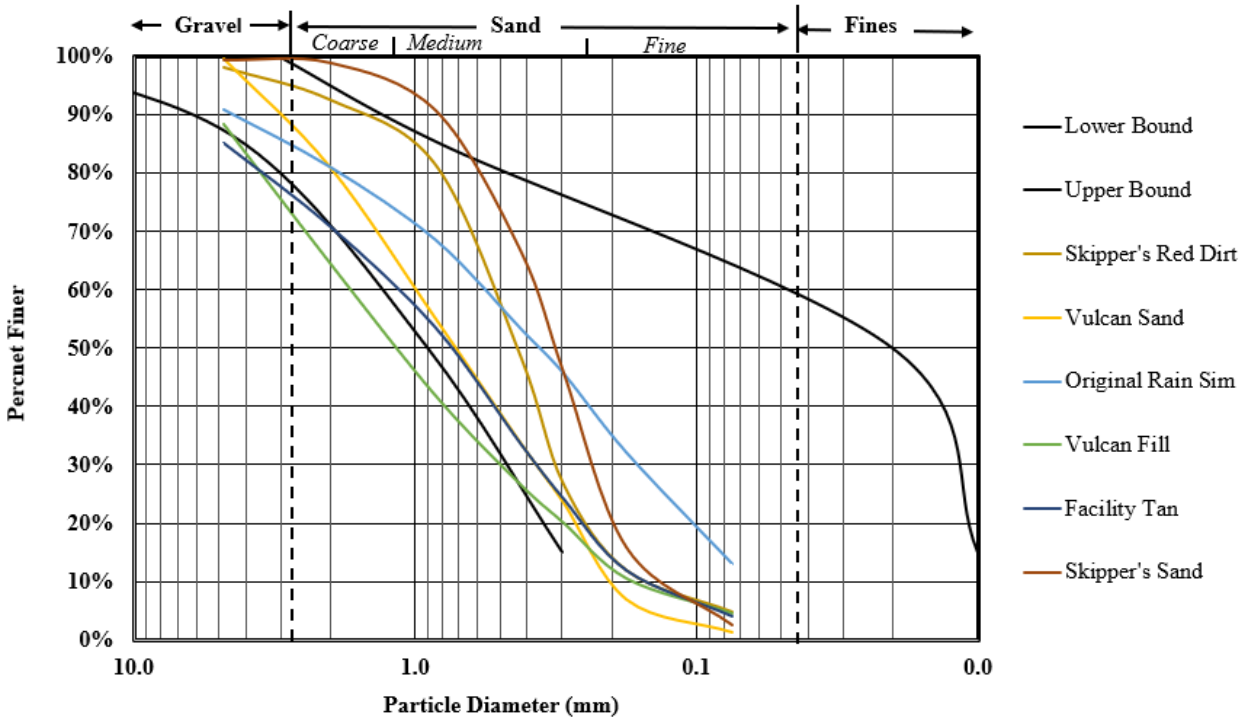

FIGURE 5.2: Grain Size Distribution for ASTM Sand Candidates.

Vulcan Materials Company's manufactured sand product met the required grain size distribution. However, Skipper's dirt had already been used for plots 3 and 4, and twice the material would need to be trucked in for the Vulcan sand. Additionally, the material cost of the manufactured sand from Vulcan was higher than the Skipper's Trucking source. Several other soils were tested for grain size distribution including the stockpile for the original AU-SRF rainfall simulator, another material available from Vulcan Materials Company called "Vulcan Fill," an unknown tan soil called "Facility Tan," and a second soil available from Skipper's Trucking named "Skipper's Sand." However, the older rainfall simulator stockpile's source was unknown, so it was not pursued. Additionally, "Vulcan Fill", the unknown tan soil, and Skipper's Sand each failed the ASTM requirements for upper and lower bound of grain size distribution for determining sand. Therefore, the remaining sand plots used sand from Skipper's Trucking, which had previously been confirmed to fit ASTM6459-19 soil requirements for both grain size distribution and plasticity (Manning, 2021).

This soil was ordered and trucked in for a total of 200 yd^3 (153 m^3) sand. The stockpile was surrounded by silt fence for sediment control.

FIGURE 5.3: ASTM Sand Delivery.

With the sand acquired, all three soils were obtained in large quantities. Following the completion of construction, including the installation of 18 yd^3 (14 m^3) of each soil per plot for a total of 71 yd^3 (54 m^3) of each soil, large stockpiles were still available. These stockpiles were intended for replacing soil lost from testing.

5.3 RAINFALL INTENSITY METHODS

Methods for measuring rainfall intensity on large-scale rainfall simulators were performed and statistically analyzed. Results included paired t-tests for statistical difference between the runoff volume and six rainfall gauge tests and unpaired t-tests for the 6-ga. test and the ASTM D6459-19 test.

5.3.1 Paired Runoff Volume and 6-Ga. Methods

Measurements collected in the paired intensity test include readings from the 6-ga. and runoff volume methods with nine 20-min tests for each target intensity, totaling 180 min of testing per target intensity. These measurements are used with static factors including the 20-min test length, 320 ft^2 (29.7 m^2) plot area, and tank calibration results to obtain two intensities per 20-min test: the average intensity measured from the rainfall gauges and the intensity calculated from the runoff volume. This is a statistically paired test because the same rainfall simulation is used to obtain both data series. Two significant figures are used. No data cleaning is required; however, the conditions required for the test are stringent since wind can affect rainfall gauge method results. The results are shown in Table 5.1.

TABLE 5.1: Runoff Method Versus 6-ga. Method for Intensity

Target Intensity, in./hr (mm/hr)	Method	Test 1	Test 2	Test 3	Test 4	Test 5	Test 6	Test 7	Test 8	Test 9
2.0 (51)	*6-ga.*	2.1 (53)	2.1 (53)	2.3 (58)	2.4 (61)	2.3 (58)	2.3 (58)	2.2 (56)	2.1 (53)	2.3 (58)
	Runoff	1.5 (38)	1.4 (36)	1.4 (36)	1.6 (41)	1.6 (41)	1.6 (41)	1.4 (36)	1.5 (38)	1.5 (38)
4.0 (102)	*6-ga.*	4.1 (104)	4.2 (107)	4.1 (104)	4.0 (102)	4.3 (109)	4.1 (104)	4.3 (109)	3.9 (99)	4.2 (107)
	Runoff	2.9 (74)	2.8 (71)	2.9 (74)	2.8 (71)	2.9 (74)	2.9 (74)	2.9 (74)	2.7 (67)	2.9 (74)
6.0 (152)	*6-ga.*	6.2 (157)	6.0 (152)	6.1 (155)	6.6 (168)	6.2 (157)	6.0 (152)	6.2 (157)	6.1 (155)	6.2 (157)
	Runoff	4.4 (112)	4.4 (112)	4.3 (109)	4.6 (117)	4.7 (119)	4.5 (114)	4.4 (112)	4.5 114)	4.3 (109)

There were nine data pairs collected for each target intensity. The pairing of tests seeks to offset any variable conditions such as unobserved wind gusts, clogging, and pump variability. The

paired t-test between the 6-ga. method and the runoff volume method was performed for each target intensity. The hypotheses are as follows:

$$H0: \mu_{6\text{-ga.}} = \mu_{runoff}$$

$$H1: \mu_{6\text{-ga.}} \neq \mu_{runoff}$$

where,

$\mu_{6\text{-ga.}}$ = mean intensity measured from 6 rainfall gauges, in./hr

μ_{runoff} = mean intensity measured from total runoff, in./hr

A 95% confidence level was used. The results of the statistical analysis are shown in Table 5.2.

TABLE 5.2: Runoff Method Versus 6-ga. Method for Intensity Statistical Analysis

Target Intensity, in./hr (mm/hr)	2.0 (51)	4.0 (102)	6.0 (152)
t-calc	-198.0	-355.0	-256.4
p-value	<0.001	<0.001	<0.001
Significant	Yes	Yes	Yes
Difference in Mean, %	32.8	30.9	27.8

The t-test indicated that the null hypothesis was rejected for all target intensities. The test yielded 95% confidence that the runoff volume method yielded a statistically different intensity than the 6-ga. method. The percentage differences demonstrated that the runoff volume intensities were lower than the rainfall gauge intensities.

A correlation equation was used to equate the two methods for the design used at AU-SRF. This equation and test can be used to verify the intensity calibration. The correlation equation is shown in Figure 5.4. The black line represents the expected 1:1 relationship between the two methods and the dashed blue trendline demonstrates that the runoff volume is less than the rainfall gauges predict.

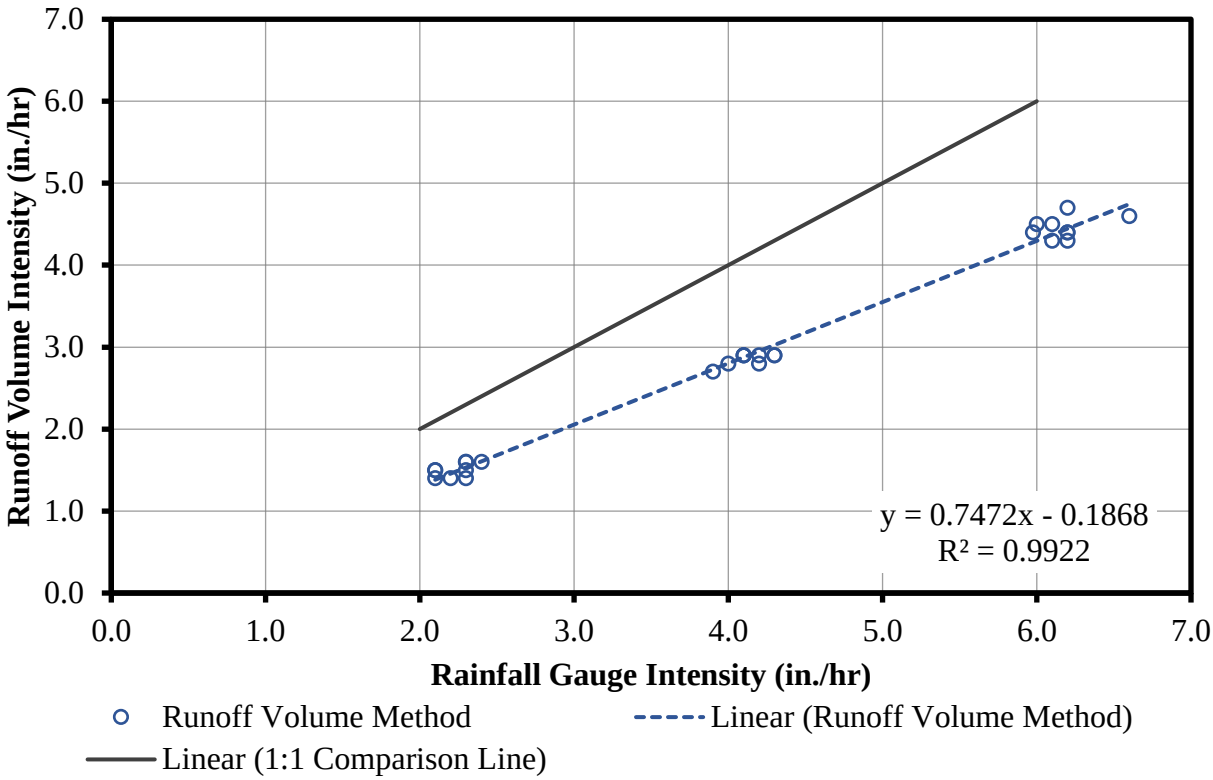

FIGURE 5.4: Correlation of Intensity Calibration Methods.

Using the linear regression equation, y = 0.7084x with R^2 = 0.99, the intensity from one method can be predicted from the results of using the other method. Thus, the runoff volume intensity test can be used as a check for the rainfall gauge intensity test. Alternatively, a rainfall simulator can be calibrated to runoff volume intensity results correlating to the target intensities. For target intensities of 2.0, 4.0, and 6.0 in./hr (51, 102, and 152 mm/hr), the correlating runoff volume method intensities were 1.4, 2.8, and 4.3 in./hr (36, 71, 109 mm/hr). The standard deviation for the runoff volume test was lower than the standard deviation for the 6-ga. test. The average sample standard deviation for the rainfall gauge tests was 0.14 in./hr (3.6 mm/hr) while the runoff volume test sample standard deviation was 0.10 in./hr (2.5 mm/hr).

Calibration is paramount to tests on the twelve new rainfall simulators at AU-SRF. Rainfall gauges can be troublesome to deal with, and the runoff volume method bypasses them. For instance, rainfall gauges can easily become unleveled as they fill and require greater iteration to confirm intensity than the runoff volume test because of greater deviation. While ASTM6459-19 calibration methods are still pertinent for promoting standardization in the field of large-scale rainfall simulation, the intensity should also be measured directly by measuring maximum runoff volume so that results can be more easily compared between different designs.

Implications of this runoff method are that rainfall gauges may overrepresent rainfall intensity. This overrepresentation can affect the rainfall erosivity calculation for usage in the RUSLE equation. When intensity is overrepresented in a bare soil test, the RUSLE equation yields a *K*-factor that is proportionally underrepresented. While cover factor calculations from product testing will not be affected by this situation, the misrepresentation of *K*-factor can lead to a lack of understanding regarding the correlation between rainfall intensity and soil erodibility. Therefore, more precise methods such as direct runoff measurement are desirable in large-scale rainfall simulation to provide the most accurate measurements for *K*-factor available.

5.3.2 ASTM D6459-19 Method and the 6-ga. Method

The ASTM6459-19 method for calibration was used to separately collect intensity information using twenty rainfall gauges. The rainfall simulator was originally designed using this method to target 2.0, 4.0, and 6.0 in./hr (51, 102, and 152 mm/hr) of rainfall. The results of this test are compared to the 6-ga. method in an unpaired t-test to confirm that the 6-ga. method can mimic ASTM D6459-19 calibration recommendations. Three iterations of the ASTM D6459-19 test were performed for a total test time of 45 min per intensity. The intensities from the ASTM

D6459-19 tests are shown in Table 5.3 with two significant figures along with average intensities from the nine 6-ga. method tests from Table 5.2.

TABLE 5.3: ASTM 20-Gauge Method Intensities

Target Intensity, in./hr (mm/hr)	Test Method	Test 1	Test 2	Test 3	Average
2.0 (51)	*ASTM*	2.3 (58)	2.5 (64)	1.8 (48)	2.2 (56)
	6-ga.	-	-	-	2.20 (56)
4.0 (102)	*ASTM*	4 (102)	4 (102)	3.8 (97)	3.9 (99)
	6-ga.	-	-	-	4.10 (104)
6.0 (152)	*ASTM*	6 (152)	6 (152)	6.1 (155)	6 (152)
	6-ga.	-	-	-	6.20 (157)

As anticipated, the ASTM method results adhered closely to target intensities because the apparatus was originally designed and calibrated with the ASTM D6459-19 method. To confirm that the 6-ga. method was representative of the ASTM D6459-19 method, an unpaired t-test was performed between sample series of both rainfall gauge arrangements. The methods were identical except that the 6-ga. method utilizes six rainfall gauges while the ASTM D6459-19 method utilizes twenty rainfall gauges. The hypotheses are as follows:

$$H_0: \mu_{6\text{-ga.}} = \mu_{ASTM}$$

$$H_1: \mu_{6\text{-ga.}} \neq \mu_{ASTM}$$

where,

$\mu_{6\text{-ga.}}$ = mean intensity measured from 6 rainfall gauges, in./hr

μ_{ASTM} = mean intensity measured from 20 rainfall gauges, in./hr

The results of the statistical analysis for each target intensity are shown in Table 5.4.

TABLE 5.4: ASTM D6459-19 Method Versus 6-ga. Method for Intensity Statistical Analysis

Target Intensity, in./hr (mm/hr)	*p-value*	*significant*	*percent difference*
2.0 (51)	0.98	No	0.30%
4.0 (102)	0.11	No	5.00%
6.0 (152)	0.14	No	1.95%

Therefore, for all three target intensities, the test fails to reject the null hypothesis. This means that there is not enough evidence to conclude that the six and twenty-gauge setups yield different intensities at 95% confidence, which supports the usage of only six suspended gauges to verify the *R*-Factor in bare soil and product testing.

5.4 RAINDROP CHARACTERISTICS WITH PHOTOGRAPHY

This section details results from two experiments. The first experiment used less advanced technology including an iPhone SE video camera with shutter speed around 1/480 sec. This experiment also used a grid paper background and tea lights to highlight raindrops. The first experiment proved that raindrops could be captured on camera for measurements but left notable room for improvement. The second experiment obtained more precise results with a Nikon D7200 camera. No backlight was used for this experiment; instead, the front flash of the camera was sufficient. This camera was capable of adjustable shutter speed, and 1/320 sec shutter speed was selected to obtain images with slightly longer raindrop lengths than the first experiment for more precise velocity observations. The first experiment's results are in section 5.4.1 and the second experiment's results are in sections 5.4.2 and 5.4.3. Both experiments utilized the Raindrop Box shown in Figure 4.6 with modifications specified in each section. For both experiments, a camera was secured at a set distance from an opening in the box for raindrops as described in *Chapter 4: Calibration and Testing Methodology*. Figure 5.5 shows the professional camera inside the box.

(a) Nikon D7200 in raindrop box (b) camera with cat

FIGURE 5.5: Camera Setup of Second Experiment.

5.4.1 First Experiment for Measuring Raindrop Characteristics with Videography

This experiment utilized an iPhone SE 2nd generation to obtain a video of raindrops falling through the gap in the raindrop box called the "raindrop region." A 2.0-mm grid was set in the box as the background of the video, and the principle of similar triangles was used to find the dimensions of the raindrops from the known 2.0-mm gridlines. Furthermore, tea lights were used to increase the visibility of raindrops. Each raindrop was measured at four points. The top, bottom, and two side points along the same section of the raindrop were recorded in cartesian coordinates with Microsoft Paint 3D.

TABLE 5.5: Example Raindrop Measurements from First Experiment

Raindrop Identification			Top (px)		Bottom (px)		Left (px)		Right (px)	
Frame No.	**Time (s)**	**Drop Number**	**X**	**Y**	**X**	**Y**	**X**	**Y**	**X**	**Y**
1	0.11	1	662	685	662	716	659	702	665	703
2	0.19	2	572	416	581	440	573	430	579	428
3	0.38	3	513	566	516	600	511	589	518	588
4	0.5	4	495	419	489	475	484	471	492	471
5	0.65	5	628	683	640	783	634	774	644	773

Using the distance formula, the height and width of each raindrop in pixels was calculated. Then, with the distance conversion factor from the background reference, the measurements were converted to millimeters. The distance from the camera lens to the center of the raindrop region was 14.75 in. (37.47 cm) and the distance from the camera to the grid background was 17.50 in. (44.45 cm). Therefore, the distance conversion factor was 0.843. This factor was multiplied by the pixel measurements and divided by the 2.0-mm grid measurement, which was 11.5 pixels, to obtain the conversion of 0.0735 mm per pixel in the center of the raindrop region. An example with the same example raindrops as Table 5.5 is shown in Table 5.6.

TABLE 5.6: Example Raindrop Characteristic Calculations

Drop Number	**Length (px)**	**Width (px)**	**Length (mm)**	**Width (mm)**	**Velocity (m/s)**
1	31.00	6.08	2.28	0.45	0.88
2	25.63	6.32	1.88	0.46	0.68
3	34.13	7.07	2.51	0.52	0.95
4	56.32	8.00	4.14	0.59	1.70
5	100.72	10.05	7.40	0.74	3.20

An example raindrop from the video is shown in Figure 5.6.

(a) raindrop with measurement points (b) height and width distances

FIGURE 5.6: Raindrop Example.

Several components of the experiment are visible in Figure 5.6. The tea light is present in the top left of the video frame while the grid is visible on the right side. The raindrop is shown with a circle demonstrating the two-dimensional section of the assumed spherical raindrop at the last moment of the camera shutter being open for this video frame. This circle represents the locations of the bottom, left, and right points. The top point is also visible in red with a line connecting the top and bottom points. This distance minus the drop size represents the travel distance of the raindrop, which will be referred to as the "tail" of the raindrop.

The sample size of the experiment was 60 raindrops. Since the goal of the first experiment was to determine whether raindrops could be measured with a camera in the raindrop box, this sample size was sufficient. No data cleaning was performed; however, in future experiments, the removal of outliers that were drips from the top of the raindrop box was accomplished. One min

of rainfall video with intensities increasing from 2.0 in./hr (51 mm/hr) to 4.0 in./hr (102 mm/hr) to 6.0 in./hr (152 mm/hr) every 20 sec. However, only 16 sec of video footage was used to reach 60 raindrops. The results yielded the drop size distribution in Figure 5.7 which contains results from all three target intensities.

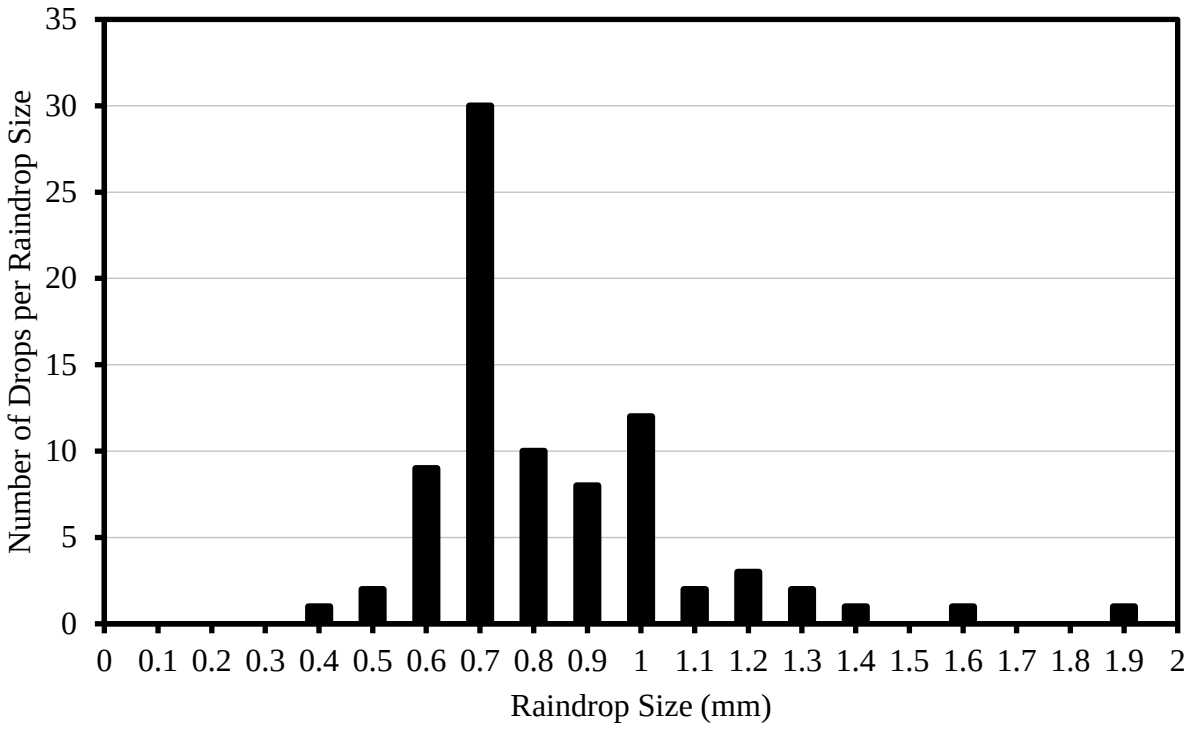

FIGURE 5.7: First Experiment Combined Raindrop Size Distribution.

Since the sample size was small, the raindrops from the three intensities were combined. The result was a drop size distribution with a notable portion of the raindrops in the 0.6 to 1 mm diameter range. These raindrops comprise of the smallest raindrop groupings in the flour pan method that is suggested by ASTM D6459-19. However, in the flour pan test, the drop count also increases as drop size decreases. Some raindrops were even smaller than those measurable by the flour pan method, which discards pellets smaller than 0.59 mm. This experiment produced measurements for raindrops ranging from 0.4 mm to 1.9 mm diameter; although, notable improvements for the experiment were needed for precise measurements. While these results were

not used in analysis versus other methods, this first experiment proved that raindrop size could be measured by camera methods.

One of the greatest reasons for investigating the camera method is that it may be capable of directly measuring raindrop velocity when the shutter speed of the camera is known. This principle was applied to the same raindrop sample as drop size distribution analysis. Since the raindrop region was 1.0-in. (2.5 cm) wide, the distance from the raindrops to the camera lens was not the same for every raindrop. This introduced error. Maximum and minimum values for drop size and velocity based on the variable distance were found, with the conversion factor from the grid to the raindrop region ranging from 0.814 to 0.871. This represented around ±3.5% error in the experiment from the size of the raindrop region. Therefore, in Figure 5.8, this error is represented in error bars for both the raindrop diameter and velocity. The line represents theoretical velocity based on drop size and fall height as predicted by Laws and Parsons (Laws, 1941).

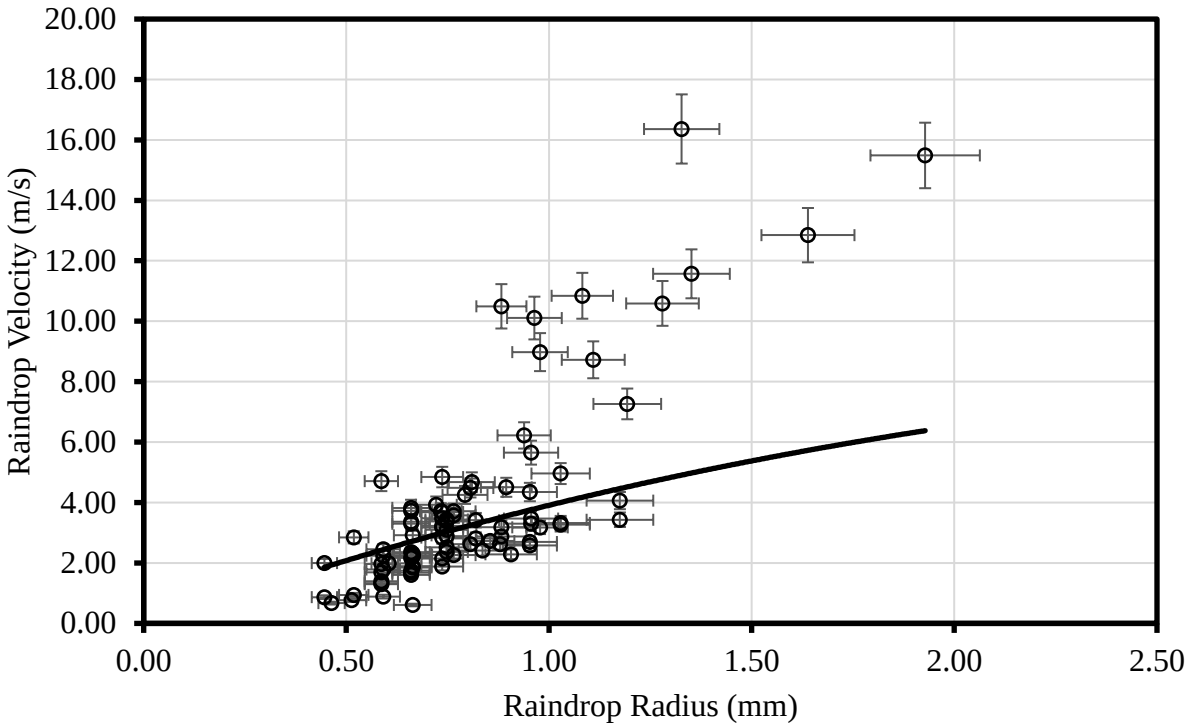

FIGURE 5.8: Experimental Raindrop Velocity Versus Laws and Parsons Theoretical Velocity.

The data points are experimental findings of the first experiment with each point representing a raindrop. Experimental velocity was greater than anticipated for most drops greater than 1.3 mm diameter in this experiment. This error in the experiment may be due to variable shutter speed of the iPhone SE 2nd generation camera. Additional limitations of this first experiment are that the 1.0-in. (2.5 cm) opening for raindrops to enter may reduce the likelihood of larger raindrops entering the raindrop box. A larger opening size would allow larger drops to be viewed per image; however, it would also increase the error from uncertainty of the distance of the raindrop from the camera lens. Similarly, the method could have bias towards smaller raindrops because the larger drops are more likely to be cut off near the top and bottom of the frame.

Interestingly, the angle of the raindrops was highly variable. While the median angle was zero, the sample standard deviation of the absolute value of the impact angles of the 60 drops was

9.6 degrees. One explanation for this phenomenon could be that raindrops with greater angles travel from more distant sprinklers while raindrops closer to perpendicular to the ground disperse from closer sprinklers.

However, the first attempt successfully measured raindrop velocities. Improvements identified for this method included increasing the quality of the camera and the background. Additionally, video capture was not necessary. Instead, photographs taken by a professional camera of known shutter speed with manual focus set to the center of the raindrop region would suffice.

5.4.2 Rainfall Drop Size Measurement

5.4.2.1 Data Cleaning

For the second experiment, the same raindrop box as the preliminary test was utilized with a Nikon D7200 camera. The camera was manually focused to the distance of the center of the raindrop region by placing a ruler at this location. The ruler picture functioned as the calibration for conversion from pixel to millimeter units as well. Figure 5.9 shows the reference photograph. This image was taken immediately prior to the rainfall simulator being operated and the camera was not moved. The conversion between pixels and inches for a photograph can vary by numerous parameters including the distance from the raindrop region, lens zoom, and photograph resolution. The red square demonstrates the usage of the shape tool in Adobe Photoshop Version 24.2.1 to measure distance in pixels. Along with the free transform function to rotate the shape, the shape tool was used to obtain the conversion between pixels and inches for the experiment.

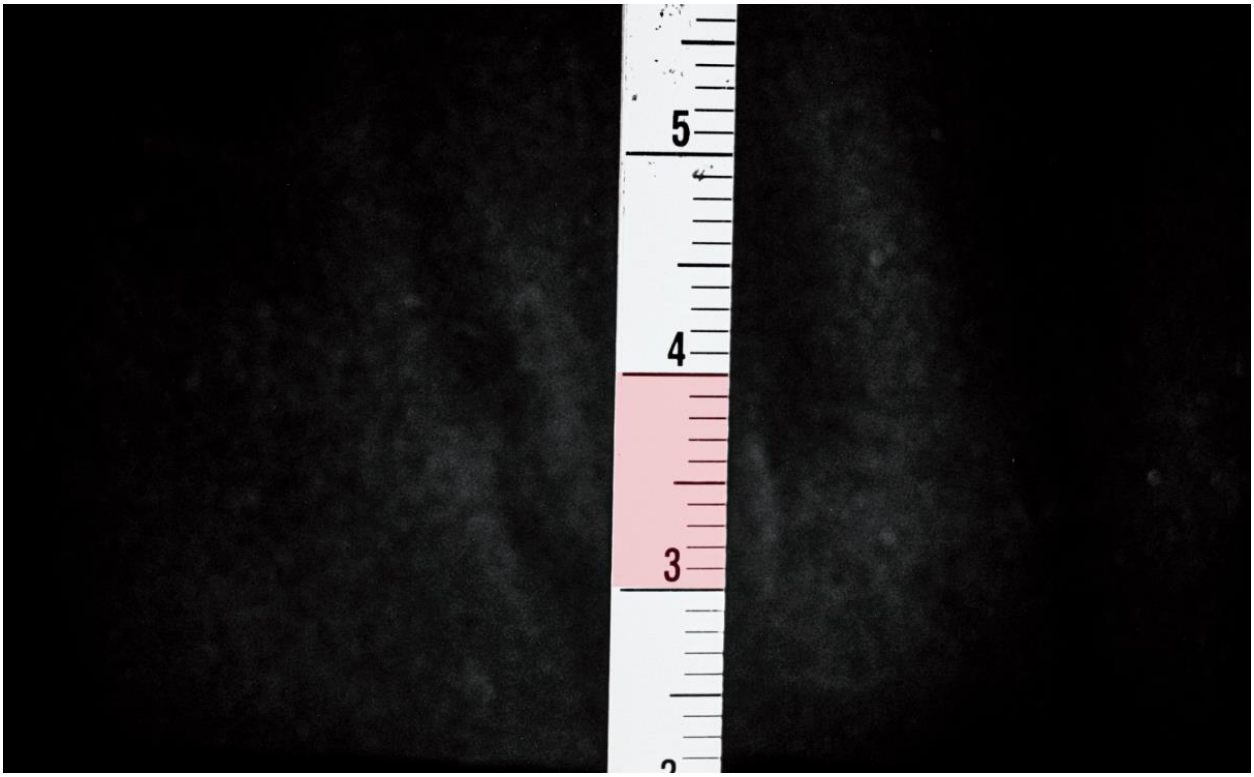

FIGURE 5.9: Raindrop Region Reference Photograph.

The background was a non-reflective black fabric. This created contrast between the raindrops and the background with the camera flash. The rainfall simulator was operated, and ten photographs were captured for 2.0, 4.0, and 6.0 in./hr (51, 102, and 152 mm/hr) intensities with the camera in the raindrop box 12.5 in. (31.8 cm) from the center of the raindrop region. Furthermore, the width of the raindrop region was reduced from 1.0 in. (2.5 cm) to 0.5 in. (1.3 cm) to reduce error.

The photographs required data processing. The photographs were edited in Adobe Lightroom Classic Version 12.2 to improve contrast between the raindrops and the background. Figure 5.10 shows an example raw photograph and a photograph after Lightroom adjustments.

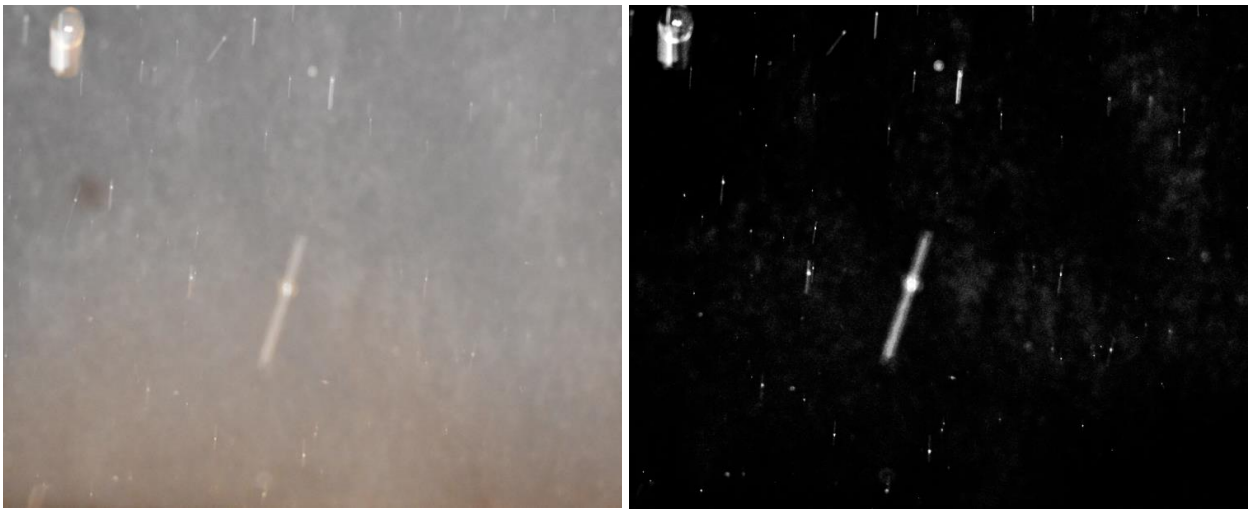

before Adobe Lightroom adjustments after Adobe Lightroom adjustments

FIGURE 5.10: Example Raindrop Photograph.

Notable Lightroom adjustments include reducing exposure, increasing contrast, and changing color to black and white. Figure 5.11 demonstrates the settings and histogram of the final photograph in monochrome. ISO refers to the camera sensitivity to light. Therefore, these photographs were adjusted to be highly sensitive to light with ISO of 10,000. Figure 5.11(b) displays the high percentage of the adjusted photograph that is black while the right side of the histogram shows the portion of the photograph area occupied by raindrops, which are white from the camera flash.

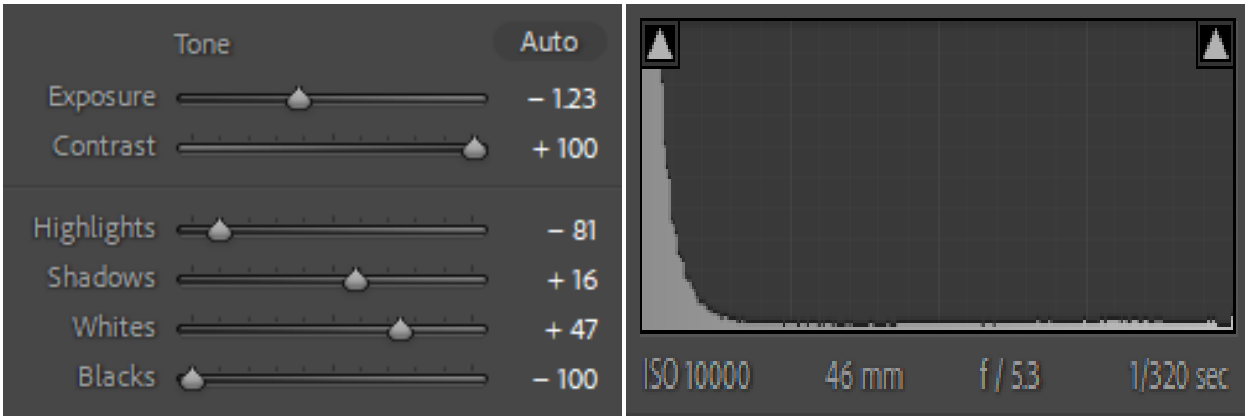

(a) Adobe Lightroom photo adjustment (b) histogram of color in Figure 5.9b

FIGURE 5.11 Adobe Lightroom Classic Adjustments.

The resulting photographs were exported to Adobe Photoshop with Lightroom adjustments rendered. Raindrops were measured by creating a rectangle and adjusting its shape and angle to fit the visible height and width of each raindrop. Each shape was placed in a unique layer with a name corresponding to the number of the raindrop in the spreadsheet, and the height and width of each rectangle was measured in pixels. Figure 5.12 demonstrates the measurement technique.

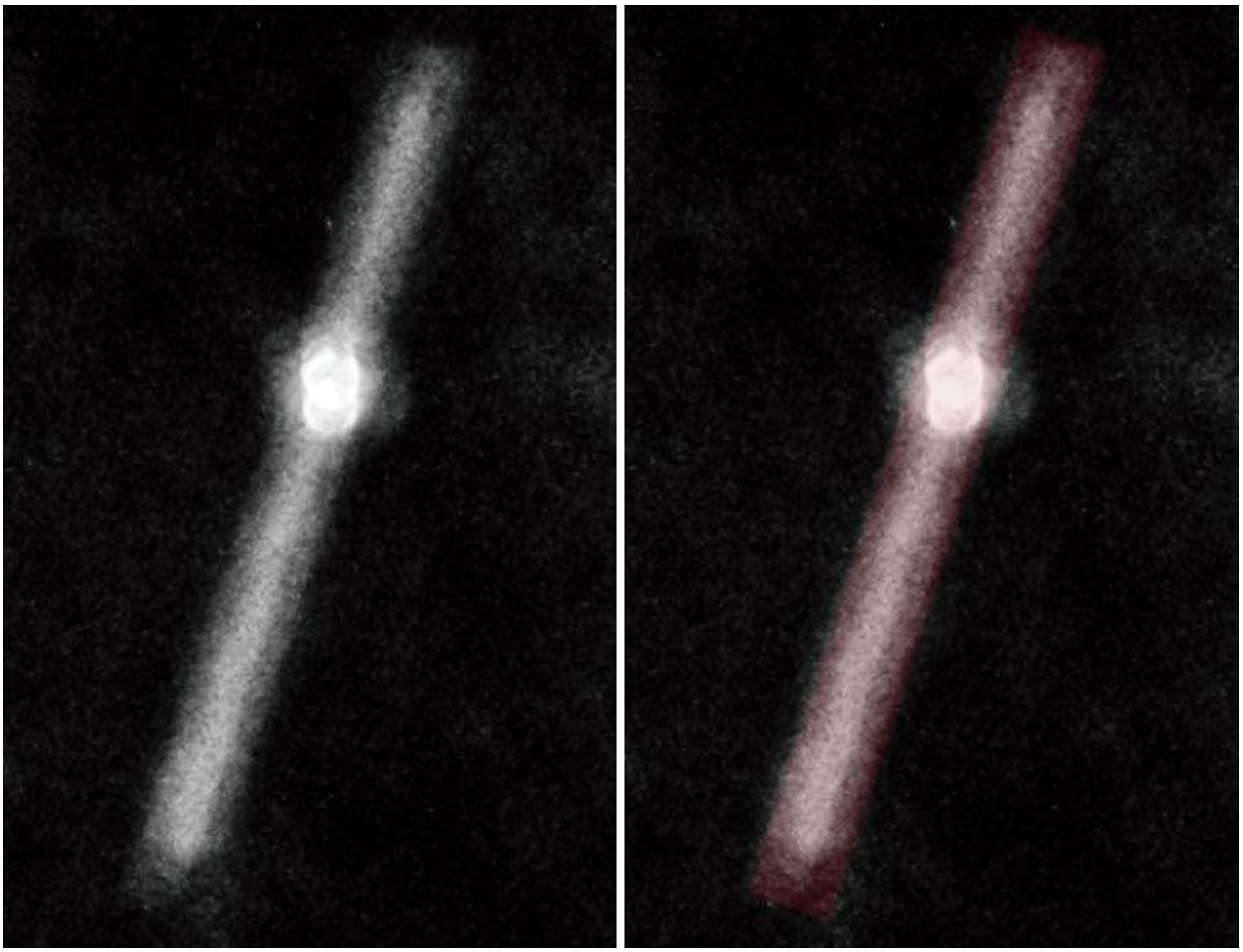

(a) raindrop before measurement (b) raindrop after measurement

FIGURE 5.12: Raindrop Photography Measurement Technique with Shape Tool.

Raindrops less than 0.59 mm were not measured because they have negligible energy. In the first photograph, all raindrops, regardless of diameter, were examined. These results are in Table 5.7, which demonstrates that, despite accounting for a high number of raindrops, drops less than 0.59 mm diameter account for very little of the total rainfall energy.

TABLE 5.7: Energy Distribution for First Photograph

Drop Size (mm)	Count	Mass (kg)	Energy (J)	% energy
4.76<	0	0	0	0.0%
4.76-2.38	1	9.5E-05	0.0026	94.6%
2.38-2.0	0	0	0	0.0%
2.0-1.41	0	0	0	0.0%
1.41-0.841	5	1.9E-05	0.00010	3.8%
0.841-0.59	11	1.6E-05	4.2E-05	1.5%
<0.59	21	6.0E-06	2.4E-06	0.09%
Sum	38	0.00016	0.0027	100.0%

Since the raindrops with less than 0.59 mm diameter accounted for less than 0.1% of the total raindrop energy for this sample despite accounting for 21 of the 38 raindrops, these droplets were not measured for remaining photographs.

The process in Figure 5.12 was performed for 10 photographs from the 2.0 in./hr (51 mm/hr) target intensity, 10 photographs from the 4.0 in./hr (102 mm/hr) target intensity, and 4 photographs from the 6.0 in./hr (152 mm/hr) target intensity. At least 50 raindrops from each intensity were measured. Next, the measurements were converted from pixel units to inches and then millimeters utilizing the calibration photograph in Figure 5.9. One inch was equal to 1041 pixels and one millimeter was equal to 41 pixels. Velocity calculations were performed identically to the first raindrop box experiment where the distance traveled was equal to the raindrop tail, which was the raindrop height minus raindrop width. Shutter speed was set to 1/320 sec with the Nikon D7200. This shutter speed was selected to capture raindrop tails several times the raindrop width.

However, data processing was not complete. Outliers were examined. The drop size versus drop velocity was plotted on a scatter plot with the x-axis representing measured drop diameter and the y-axis representing measured velocity, as shown in Figure 5.13. Then, Laws and Parsons

theoretical velocities by drop size for a fall height of 4.7 meters were plotted on a line (Laws, 1941). Upper and lower bounds 50% variable from Laws and Parsons theoretical velocity were created for determining the difference between the expected and experimentally determined velocities. Drops beyond 50% variable from the theoretical velocity were re-examined in Adobe Photoshop to determine the existence of error in the drop measurement process.

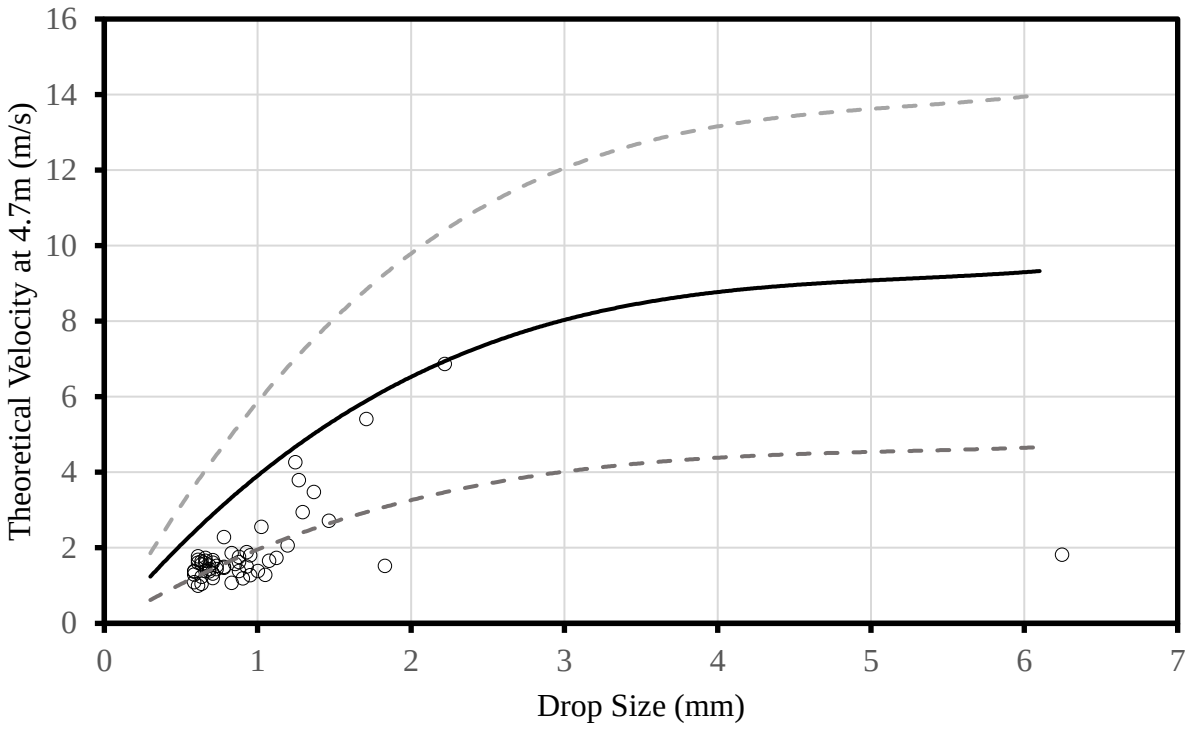

FIGURE 5.13: Velocity Predicted by Fall Height and Drop Size.

Six out of 156 drops were determined to be in error. Some drops were theorized to be drips from the top of the raindrop box rather than raindrops. These drops had very low velocity relative to their size; this may have been because their fall height was less than 1.0 ft (0.3 m) from the top of the raindrop box. Figure 5.14(a) shows an example suspected drip from the top of the box. Additionally, two drops were determined to be not fully shown in the photograph such as in Figure 5.14(b)

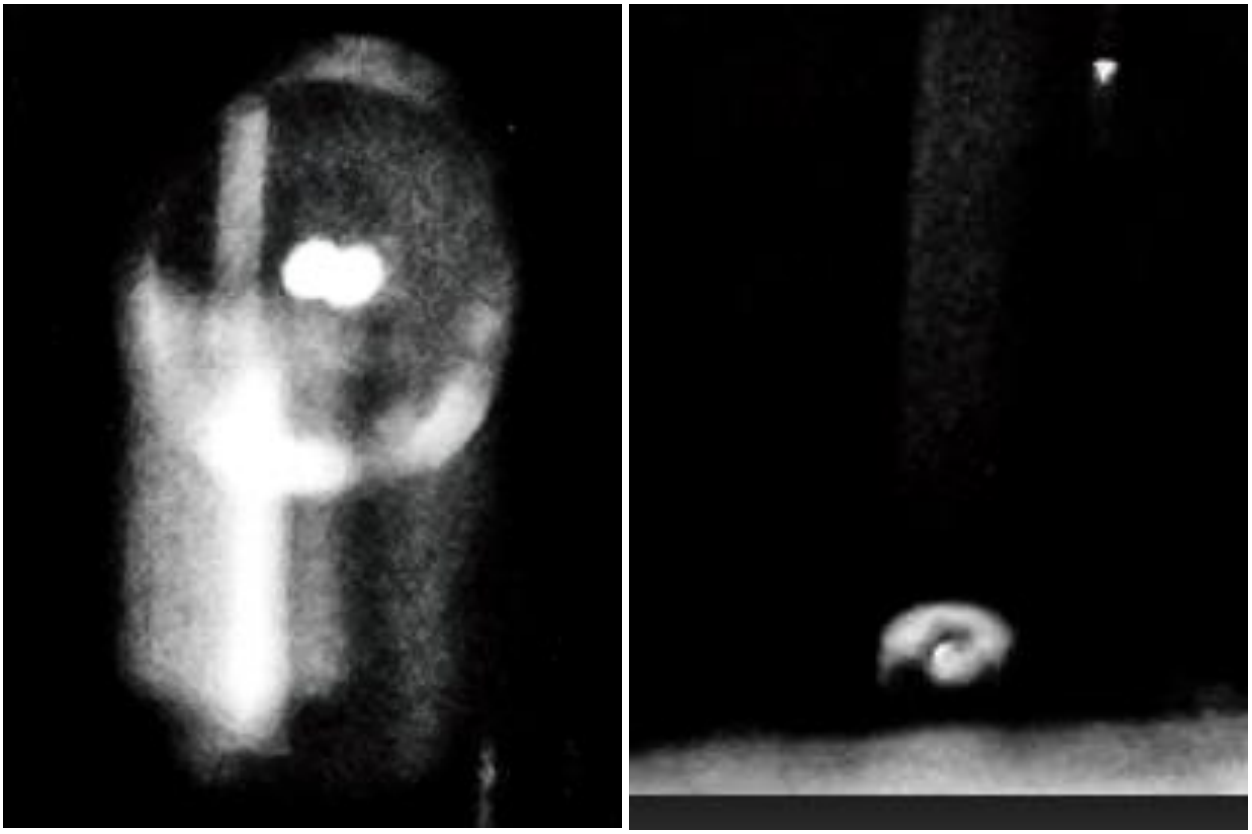

(a) suspected drip from top of box (b) drop not fully visible

FIGURE 5.14: Erroneous Drops.

Once these erroneous drops were culled from the dataset, 152 drops remained. The remaining drops were organized into bins identical to the flour pan test from ASTM D6459-19 that is described in *Chapter 3: Construction Methodology* of this work. The flour pan was performed simultaneously with the photograph collection in the same location on the raindrop simulator plot, the center. The flour pan test also used data cleaning techniques. Once drop size weight and count were collected for each sieve size, mass ratio adjustment was performed according to the Laws and Parsons method in Figure 5.15.

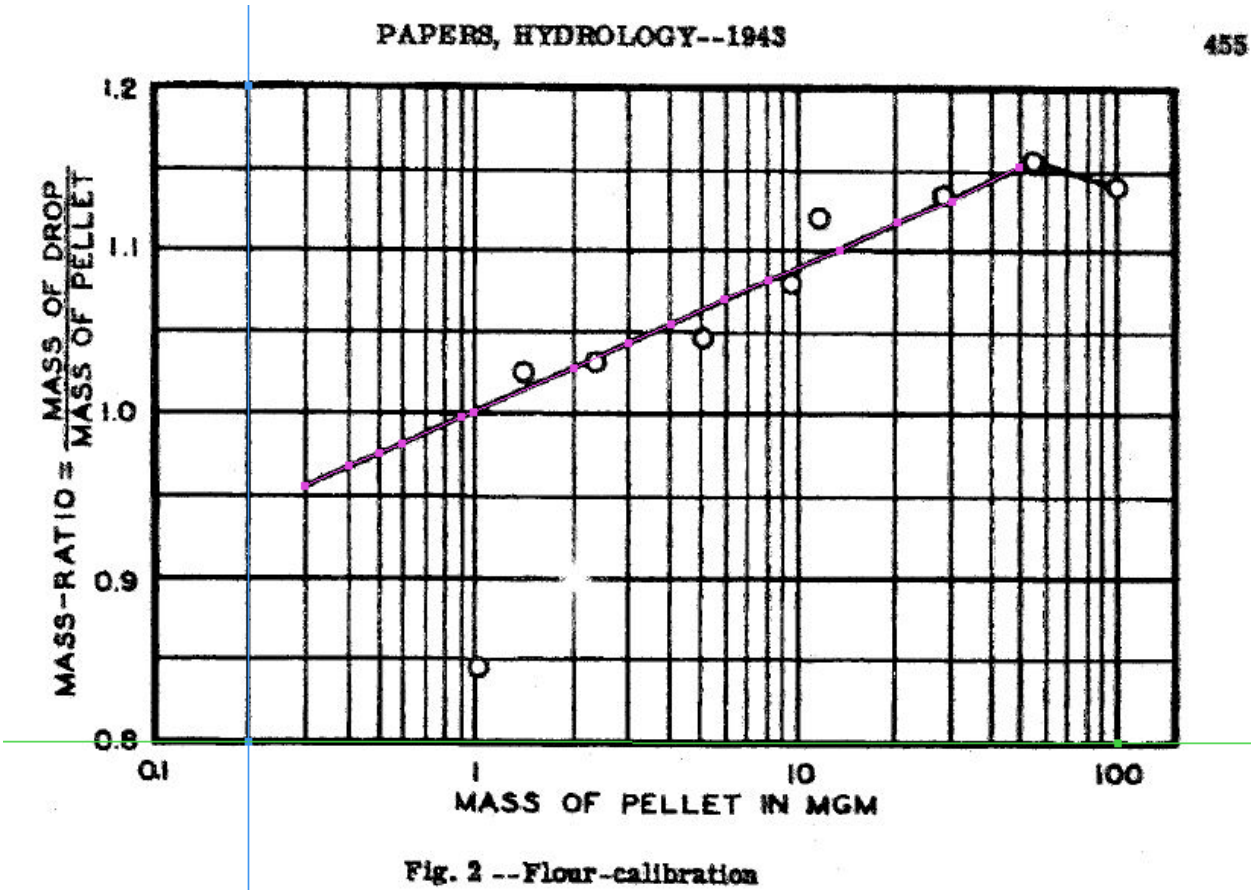

FIGURE 5.15: Mass Ratio Adjustment by Average Pellet Size per Bin (Laws, 1941).

Equation 5.1 represents the mass ratio adjustment for flour pellets. The adjustment had a minimum value of 1. The mass ratio was multiplied by the average drop size per bin and the adjusted mass distribution by drop size bin was calculated.

$$Mass\ Ratio = 0.037 * \ln(D) + 1 \tag{5.1}$$

where,

D = drop diameter (mm)

Finally, the flour pan and photography results were both used to calculate mass percentage by raindrop bin size. A summary of the results of each test is shown in Table 5.8. The sample size of the photography method ranged from 49 to 52 drops per intensity while the sample size of the flour pan method ranged from 1711 to 2626 per intensity. The samples were taken at identical times and locations on a plot calibrated to ASTM D6459-19 standards.

TABLE 5.8: Summary of Mass Distribution Results for Photography and Flour Pan Methods

	2.0 in./hr (51 mm/hr) Mass Percentage		4.0 in./hr (102 mm/hr) Mass Percentage		6.0 in./hr (152 mm/hr) Mass Percentage	
Drop Size (mm)	*Photography*	*Flour Pan*	*Photography*	*Flour Pan*	*Photography*	*Flour Pan*
2.38 to 4.76	37.3%	54.9%	0.0%	58.2%	0.0%	22.6%
2 to 2.38	0.0%	22.5%	0.0%	20.8%	21.7%	57.8%
1.68 to 2	12.2%	13.8%	0.0%	11.6%	9.9%	12.6%
1.19 to 1.68	11.2%	5.0%	43.1%	6.7%	26.8%	4.9%
0.841 to 1.19	19.3%	2.9%	33.8%	2.1%	22.6%	1.5%
0.595 to 0.841	20.0%	1.0%	23.0%	0.7%	19.0%	0.7%

5.4.2.2 Raindrop Size Comparative Analysis with Photography and Flour Pan Methods

The mass distribution graphs are shown side by side in Figure 5.16 for each intensity and the combined data. The black bars represent the adjusted flour pan mass percentage of the flour pellets while the white bars represent the mass percentage of the raindrops captured by the photography method.

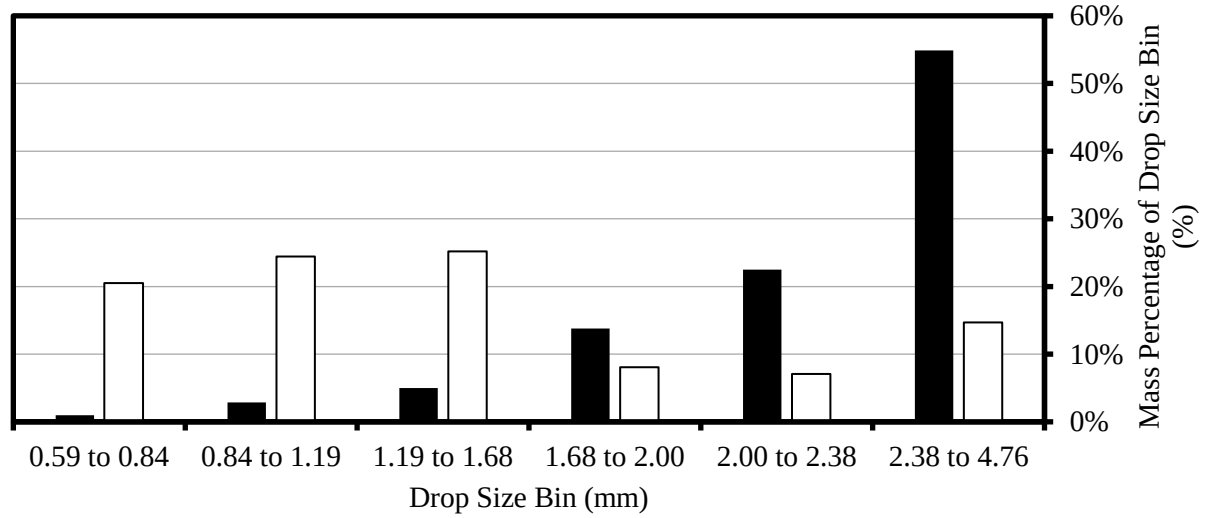

FIGURE 5.16: Mass Distributions of Combined Intensities.

The photography method represented the mass of small raindrops, defined in this work as raindrops less than 1.68 mm diameter, as a higher percentage of the total mass of the rainfall than the flour pan method. However, the sample sizes for the methods were unequal. The effect of small sample size on the mass distribution can be observed in Figure 5.17b. There are only 5 raindrops greater than 1.68 mm with the photography method out of the 152 total raindrops measured. Meanwhile, for the combined intensities, the flour pan method identified 611 out of 6501 drops with diameter greater than 1.68 mm. Therefore, drop size percentage is examined instead of mass percentage. Figure 5.17 illustrates the difference in drop size distribution between the two methods.

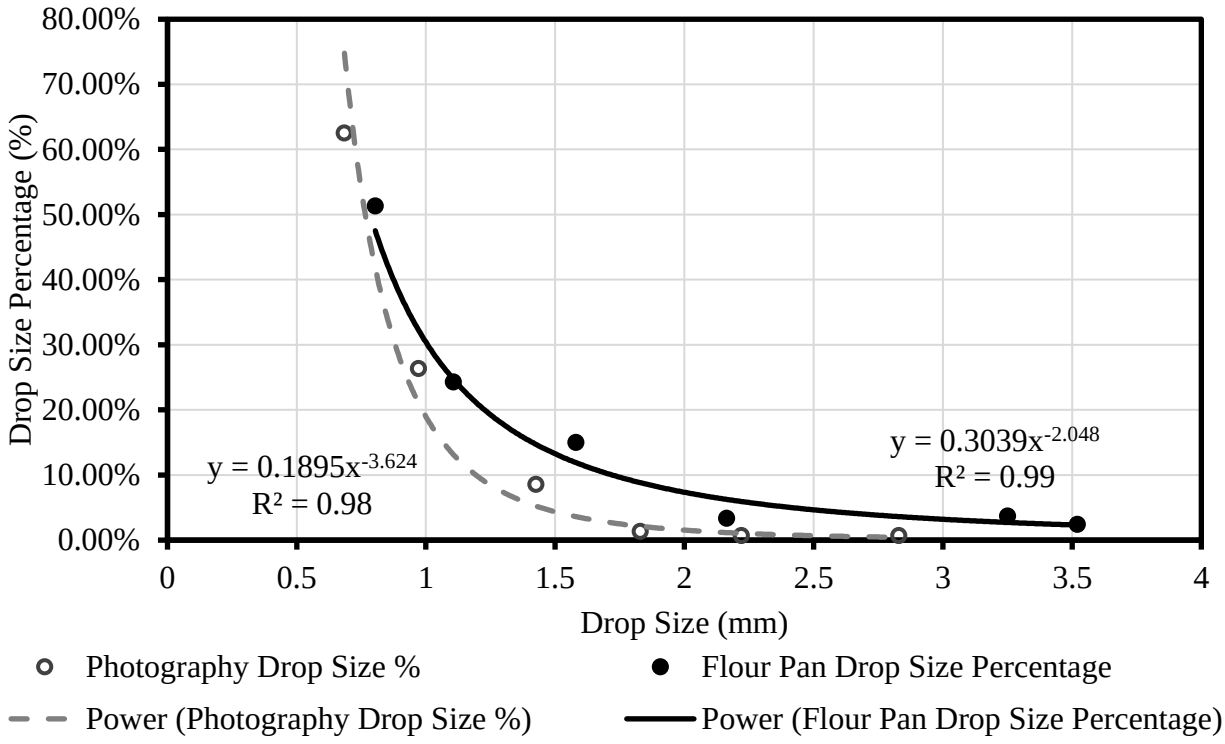

FIGURE 5.17: Comparison of Drop Size Distribution Between Two Methods.

The best fit power equation for the flour pan drop size percentage is to the power of -2.048 while the photography drop size percentage relationship is to the power of -3.624. These best-fit

equations demonstrate that the photographic method captures exponentially more small raindrops than the flour pan. For both methods, a large portion of the drops captured were in the smallest drop categories. While the photography method was capable of measuring drops even smaller than the smallest drop size bin of 0.59 mm diameter and exceled at measuring small drops, measuring smaller raindrops gives diminishing returns for calculating total raindrop energy because tiny raindrops have negligible energy as illustrated in Table 5.8.

The photography method results suggest that one method is misrepresenting drop size distribution. Tullis found that drop size was overrepresented by 41% by the flour pan method compared to his application of a photography method for measuring raindrop size (2016). However, his test used highly controlled conditions including a single drop sprinkler. This is not applicable to large-scale rainfall simulation because countless drops are sprayed on the plot at a given instant. However, Figure 5.17 suggests that the flour pan method may overrepresent drop size more for larger raindrops as a function of raindrop impact area because the drop sizes were increasingly different between the methods as raindrop size increases. The two methods also appear to converge near the smallest drop sizes, which also supports this idea. Therefore, the percentage that the flour pan overrepresents the raindrop energy due to overrepresenting drop size is dependent on the drop size distribution of the sample, which will vary by sprinkler system.

The focus of this research is improving the accuracy and precision of rainfall simulation. Therefore, the implications of overrepresented drop size are examined. The effect of raindrop size distribution on *R*-factor in the RUSLE equation was examined in Table 5.9 for the center of the plot.

TABLE 5.9: Raindrop Mass Distribution R-Factors

Drop Size Method	R-Factor
Flour Pan	163.2
Photography Method	109.7

The mass distributions from Table 5.9 were used in conjunction with target intensities to calculate *R*-factor for usage in the RUSLE equation. The percent difference in *R*-factor between the flour pan test performed in conjunction with the photography test and the photography test was 32.8%. The overrepresentation of the *R*-factor can lead to control tests which calculate a *K*-factor that is underrepresented. This is because, in the RUSLE equation, $K = A / (R * LS)$ when *C* and *P* = 1.0. In a product test the equation becomes $C = A / (R * LS * K)$. If the photography results are assumed to be accurate, the *K*-factor would be underrepresented while the *R*-factor would be overrepresented. However, the same real *R*-factor would be present for the product test as the bare soil test when the same sprinkler apparatus is used. The effect on the cover factor would cancel out. Therefore, if rainfall simulation is consistent, the method used to find drop size distribution is irrelevant to the determined cover factor and previous rainfall simulation tests using the RUSLE equation to find erosion control product runoffs are unaffected by this revelation.

However, overrepresented drop sizes by the flour pan method can affect *K*-factors which are used in field applications for theoretical soil loss calculations. Experiments used to determine K-factor for usage in theoretical field calculation may be providing underestimated *K*-factors when the flour pan method is used to determine drop size via the RUSLE equation. Tullis found that a disdrometer slightly underrepresented raindrop size (2016). Laser-optical equipment may have a similar problem for determining raindrop size distribution as the flour pan method, which requires further investigation.

5.4.3 Rainfall Velocity Measurement with Photography

The velocity of each raindrop was examined. Methodology for this process was identical to the first experiment; however, the camera upgrade to the Nikon D7200 and non-reflective black background provided much clearer images of the raindrop tails such as in Figure 5.12.

The photographically determined drop velocity was compared to the theoretical drop velocity based on Laws and Parsons theoretical calculations. Two-tailed, paired t-tests were performed with 95% significance for the drops found in each intensity and for all three target intensities combined. The null and alternate hypotheses are:

$$H_0: \mu_{\text{Photography Drop Size Distribution}} = \mu_{\text{Flour Pan Drop Size Distribution}}$$

$$H_1: \mu_{\text{Photography Drop Size Distribution}} \neq \mu_{\text{Flour Pan Drop Size Distribution}}$$

where,

$\mu_{\text{Photography Drop Size Distribution}}$ = Drop size distribution obtained by photography method

$\mu_{\text{Flour Pan Drop Size Distribution}}$ = Drop size distribution obtained by flour pan method

Measurements were grouped into drop size bins. The 4.0 in./hr (102 mm/hr) test did not have any drops greater than 1.68 mm width; therefore, only 2 degrees of freedom were available for that intensity. For the remaining t-tests, 4 and 5 degrees of freedom were used. The statistical analysis results are displayed in Table 5.10.

TABLE 5:10: Experimental Versus Theoretical Raindrop Velocity t-tests

Target Intensity, in./hr (mm/hr)	2.0 (51)	4.0 (102)	6.0 (152)	Combined
t-calc	6.589	4.676	2.996	3.452
p-value	0.0027	0.0428	0.0401	0.0182
Degrees of Freedom	4	2	4	5
Significant	Yes	Yes	Yes	Yes
Percent Difference of Means	25.5%	50.8%	29.2%	25.8%

The statistical analysis indicated that the photographic method and Laws and Parsons theoretical velocity are statistically different for all three target intensities and for the combined data. The photography method measured velocity less than predicted by Laws and Parsons for all drop size bins at each intensity by 25.5 to 50.8 percent. For the combined data, the velocity was 25.8 percent less using the photography method. One explanation for this phenomenon is that the sprinkler-formed raindrops are not actually spherical as assumed in calculation of measured velocity. This explanation was investigated further with Figure 5.18.

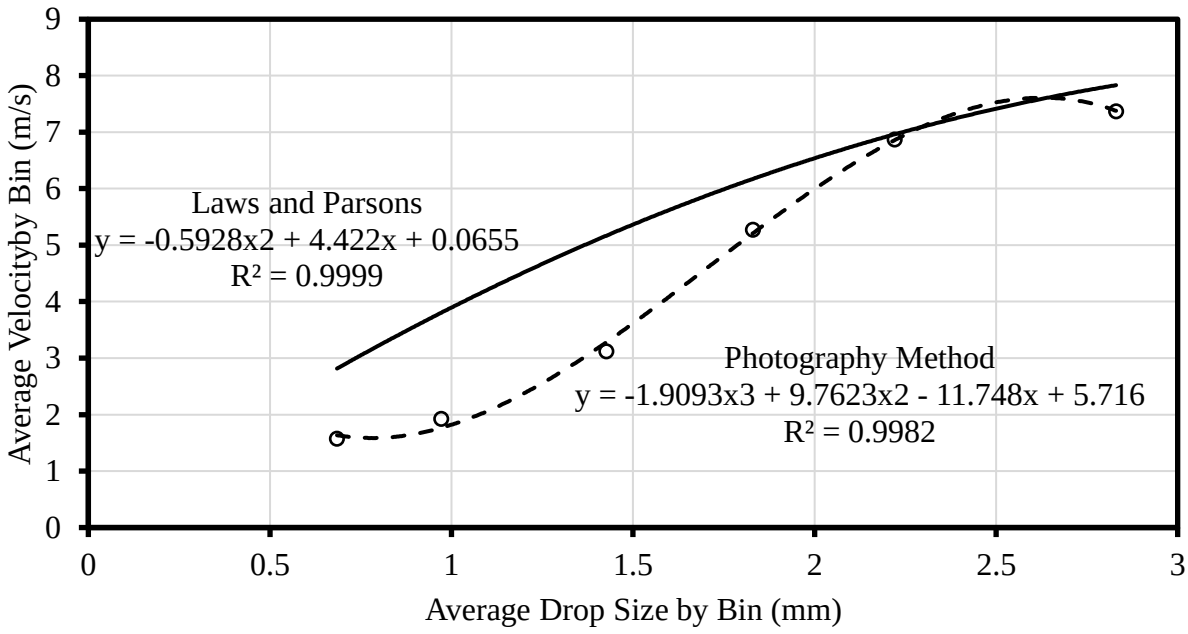

FIGURE 5.18: Combined Target Intensity Velocity Measurement Techniques.

As drop size increased, the difference between methods decreased. The techniques may converge at larger drop sizes. However, a larger sample size for large drops using the photography method would be required to confirm this. As drop size increases, the ratio between the raindrop tail and the observed width of the raindrop increases because velocity increases exponentially with drop size. Therefore, error caused by non-spherical drop size would dampen as drop size increased.

The photography method represents velocity consistently lower than Laws and Parsons as demonstrated in Figure 5.19.

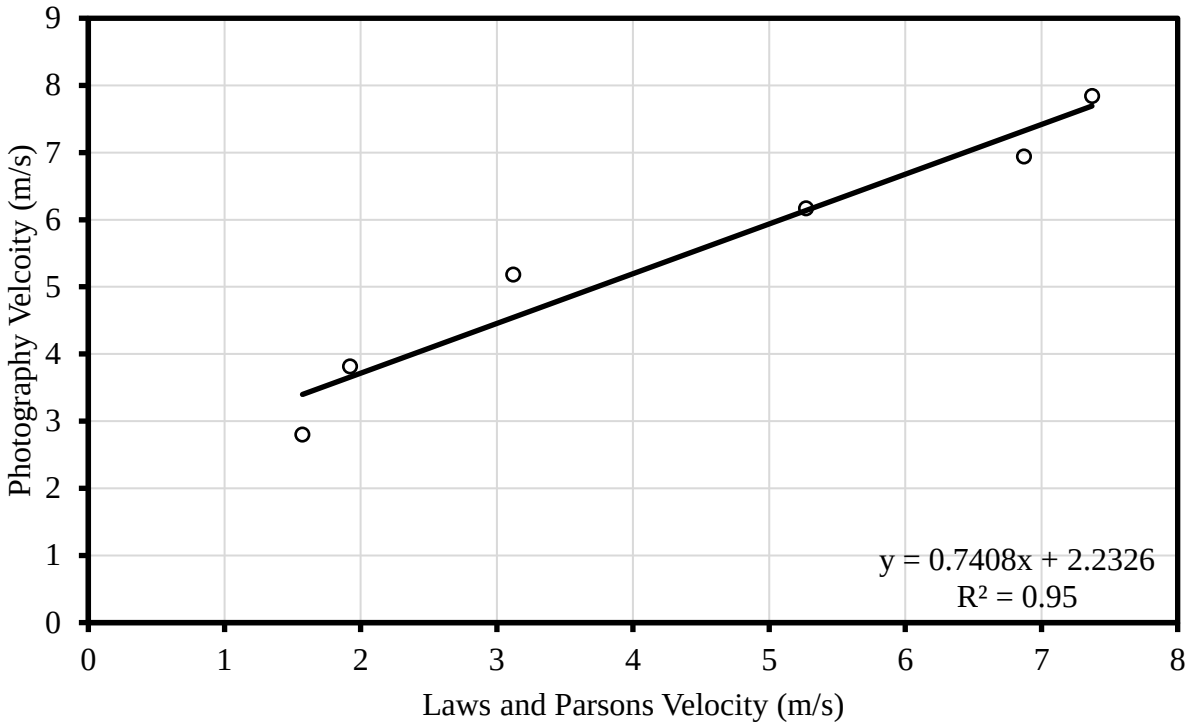

FIGURE 5.19: Photography Measured Velocity Versus Predicted Velocity.

While the photography method yielded significantly lower velocity than Laws and Parsons theoretical calculation, the relationship was near linear. The best-fit equation in Figure 5.19 has an R^2 value of 0.95, indicating that the equation represents 95% of the relationship for this raindrop sample.

5.5 CALIBRATION

This section describes results from applying calibration techniques on both the original rainfall simulator and the twelve new rainfall simulators. While the apparatuses differ slightly in water delivery method and slope, the methods utilized to verify intensity and drop size are identical. These methods follow ASTM D6459-19 guidelines and used rainfall gauges for determining rainfall intensity and the flour pan method for determining raindrop mass distribution.

5.5.1 Original Rainfall Simulator Intensity Verification

The original rainfall simulator was verified before control testing to ensure that it was still outputting near the target intensities. Following the methodology for repairing and ensuring that the correct switch order was used described in *Chapter 4: Calibration and Testing Methodology*, the final results with ASTM D6459-19 calibration techniques for the intensity and Christiansen uniformity calibration, Cu, were obtained on July 22, 2022, with wind less than 1.0 mi/hr (1.6 km/hr).

TABLE 5.11: Original AU-SRF Rainfall Simulator Calibration

Target Intensity, in./hr (mm/hr)	**2.0 (51)**	**4.0 (102)**	**6.0 (152)**
Measured Intensity, in./hr (mm/hr)	2.05 (52)	3.98 (101)	5.99 (152)
Cu (%)	82.20	84.97	80.47

The measured intensities were very close to the target intensities, which was expected since the initial design of the sprinklers was to meet ASTM D6459-19 parameters. Therefore, with the intensity verified and using previously obtained flour pan results, control testing for rainfall simulator verification proceeded.

5.5.2 Calibration on Twelve New Rainfall Simulators

The twelve new ASTM D6459-19 rainfall simulators used the same sprinkler design as the original rainfall simulators. However, the water delivery method was modified. The new method involved using a PVC manifold as described in *Chapter 3: Construction Methodology*. The effect of the manifold on the pressure in each sprinkler was unknown, and it was desired to determine whether the pressure changes affected rainfall simulator calibration results despite that other parameters of the rainfall simulators were identical including sprinkler components, plot dimensions, and raindrop gauge placement pattern.

Two methods for determining rainfall intensity were performed, which were ASTM D6459-19 calibration with 20 rainfall gauges and runoff volume measurement. Intensity findings are in Table 5.12. For the runoff volume test, the previously determined equation for converting between runoff volume method and rainfall gauge method intensity was used.

TABLE 5.12: Intensity Calibration for New Rainfall Simulator Plots

Target Intensity, in./hr (mm/hr)	2.0 (51)	4.0 (102)	6.0 (152)
ASTM D6459-19 20-Rainfall Gauge Test	2.1 (54)	4.2 (106)	6.3 (160)
Runoff Volume Test with Conversion	1.8 (47)	3.82 (97)	5.75 (146)
Christiansen Uniformity (%)	82.24%	83.35%	81.1%
ASTM D6459-19 Method Percent Error from Target Intensity (%)	7.0%	4.5%	4.7%
Runoff Method Percent Error from Target Intensity (%)	-14.2%	-8.5%	-8.4%

Christiansen uniformity was greater than 80 percent for all intensities. Additionally, the rainfall gauge method yielded intensities within 7.0% of the target intensity while the runoff method yielded intensities within -14.2% of the target intensity. Therefore, while the sprinklers were designed on a 3H:1V plot, the target intensities were still nearly met on the 4H:1V slope rainfall simulators. For both methods, the 2.0 in./hr (51 mm/hr) rainfall presented the greatest percent difference from the target intensity.

Next, drop size calibration commenced for the new rainfall simulators. Utilizing the flour pan method, nine flour pan tests were completed. Each target intensity had three flour pan tests

with flour pans at quarter points along the length of the plot. The mass distributions were averaged by target intensity. The final mass distributions of the pellets are shown in Table 5.13.

TABLE 5.13: Average Mass Distributions by Target Intensity

Bin Size (mm)	2.0 in./hr (51 mm/hr)	4.0 in./hr (102 mm/hr)	6.0 in./hr (152 mm/hr)
2.38 to 4.76	0.00%	1.92%	4.52%
2 to 2.38	38.39%	35.70%	27.95%
1.68 to 2	12.22%	13.32%	31.77%
1.19 to 1.68	21.50%	21.45%	16.09%
0.841 to 1.19	19.27%	18.19%	11.98%
0.595 to 0.841	8.63%	9.42%	7.69%

The mass distributions yielded an *R*-factor of 148.5. The *R*-factor was applied in RUSLE equation calculations in control testing.

5.5 CONTROL TESTING

This section contains results from bare soil testing at AU-SRF. In 2022, bare soil testing was conducted on the original rainfall simulator for verification that it was operating to the ASTM D6459-19 standard. Following calibration, two total bare soil tests were performed on this slope. The first bare soil test was not sufficient for confirming the plot's viability because of errors in soil preparation. Therefore, a second test was conducted, and the results were similar to previous successful bare soil testing on this slope.

5.5.1 Original AU-SRF Rainfall Simulator ASTM D6459-19 Verification

The results of the first bare soil test include the intensities, sediment loss, average turbidity per intensity, and average total suspended solids by turbidity in Table 5.14.

TABLE 5.14: Original Rainfall Simulator Verification Attempt 1

Target Intensity, in./hr (mm/hr)	2.0 (51)	4.0 (102)	6.0 (152)
Intensity, in/hr (mm/hr)	1.75 (44)	3.65 (93)	6.18 (157)
Sediment, lb (kg)	182.7 (82.9)	370.1 (167.9)	470.7 (213.5)
Runoff, gal. (L)	113.0 (428.0)	262.3 (992.9)	555.6 (2103.2)
Average turbidity (NTU)	50,630	61,130	49,470
Average TSS (mg/L)	64,510	73,770	53,880

The first verification test yielded unsatisfactory results because the soil was unexpectedly gravelly and had higher compaction than previous testing. The compaction method used was the plate compactor while the previous compaction method for this plot had been the roller compactor. The average compaction using Proctor density was 87.7% with 19.2% moisture content. Figure 5.20 shows images following each intensity.

(a) after 2.0 in./hr (51 mm/hr) (b) after 4.0 in./hr (102 mm/hr) (c) after 6.0 in./hr (152 mm/hr)

FIGURE 5.20: Original Rainfall Simulator Verification Attempt 1.

The plot was visually lacking in rills typically present after previous ASTM D6459-19 testing on this soil. Therefore, the test was redone with the exact parameters in place for previous testing.

For the second test, two changes in preparation were made. A digging fork was used to till, which was very effective for loosening the soil. Additionally, the roller compactor was used in compaction instead of the plate compactor. The 4.0-ft (1.2-m) wide roller compactor was brought to the top of the plot, filled with water, and rolled slowly down the left side, right side, and middle of the plot. This achieved lower compaction of 82.9% with moisture content of 17.3%, which was like past Proctor density test results.

TABLE 5.15: Original Rainfall Simulator Verification Attempt 2

Target Intensity, in./hr (mm/hr)	**2.0 (51)**	**4.0 (102)**	**6.0 (152)**
Intensity, in/hr (mm/hr)	2.1 (52)	3.8 (97)	5.3 (133)
Sediment, lb (kg)	204.7 (92.9)	416.5 (188.9)	850.3 (385.7)
Runoff, gal. (L)	84.9 (321.4)	131.4 (497.4)	377.1 (1427.5)
Average turbidity. NTU)	60,520	51,960	55,070
Average TSS, mg/L	71,930	92,520	90,550

The sediment loss increases from the first to second test were 12.1%, 12.5%, and 60.7% for 2.0, 4.0, and 6.0 in./hr (51, 102, 152 mm/hr) target intensities, respectively. The results of bare soil test two aligned with testing from previous years despite that the compaction was still slightly higher than some previous control tests. Therefore, these methods should also be used in future

testing for this soil for continuity with previous testing. Figure 5.21 demonstrates erosive processes during and after the second test.

(a) during 2.0 in./hr (51 mm/hr) (b) during 4.0 in./hr (102 mm/hr) (c) after 6.0 in./hr (152 mm/hr)

FIGURE 5.21: Original Rainfall Simulator Verification Attempt 2.

In the second test, rills began formation during the 2.0 in./hr (51 mm/hr) intensity, which was anticipated because of previous testing results. This test was satisfactory for providing renewed verification of the effective operation of this rainfall simulator. Continuity with compaction methods ensures that soil erodibility is consistent for all testing.

5.5.2 First Tests on Twelve New Rainfall Simulators

Three control tests were performed on the new rainfall simulator plots in partial fulfillment of the "Evaluation of ALDOT Erosion Control Products Using Rainfall Simulation on Various Soil Types and Slope Gradients" project. Each test was performed on a different soil and on 4H:1V slopes. The three soils were the ASTM clay, sand, and loam. In this section, the results of the first tests on these new rainfall simulators are provided. Additionally, the difference between soils in soil erodibility in the RUSLE equation is examined.

5.5.2.1 Sand

The first test was performed on Plot 3 with a sand soil from Abbeville, AL. With the procedure for bare soil testing described in Section 4.5, an ASTM D6459-19 rainfall simulator test was performed. The average Proctor compaction was 88.2% with 14.8% moisture content.

Several notable observations were made during this test. This soil was highly erodible and tended to fill the runoff collection barrels with solid material. Therefore, the flashing system in Figure 4.13 was developed based on observations during this experiment. Rills formed beginning around 10 ft (3 m) from the toe of the slope. The manifold successfully distributed flow to all sprinklers.

(a) rainfall simulator operation (b) filled runoff collection tank

FIGURE 5.22: First Bare Soil Test on New ASTM D6459-19 Rainfall Simulators.

The test was successful. A summary of the results is in Table 5.16.

TABLE 5.16: Sand Bare Soil Test Results

Target Intensity, in./hr (mm/hr)	2.0 (51)	4.0 (102)	6.0 (152)
Intensity, in/hr (mm/hr)	2.3 (57)	4.3 (110)	6.1 (155)
Sediment, lb (kg)	136.4 (61.9)	268.1 (121.6)	620.5 (281.5)
Runoff, gal. (L)	96.9 (366.8)	234.1 (866.2)	446.5 (1690.2)
Average turbidity (NTU)	50,290	52,490	104,520
Average TSS (mg/L)	40,210	63,870	185,160

5.5.2.2 Loam

The loam ASTM D6459-19 test was performed on plot 5 on the 4H:1V slope. The Proctor compaction was 87.7% with 18.8% moisture content. Observations from this test include that the runoff collection barrels did not fill with soil. Therefore, the improved flashing system was not necessary for this plot. The results of the loam test are in Table 5.17.

TABLE 5.17: Loam Bare Soil Test Results

Target Intensity, in./hr (mm/hr)	2.0 (51)	4.0 (102)	6.0 (152)
Intensity, in/hr (mm/hr)	2.25 (57)	4.00 (102)	5.85 (148.6)
Sediment, lb (kg)	18.9 (8.6)	82.9 (37.6)	193.1 (87.6)
Runoff, gal. (L)	59.5 (225.2)	239.9 (908.1)	391.5 (1482.0)
Average turbidity, NTU	21,410	22,500	13,810
Average TSS, mg/L	11,540	15,100	10,610

5.5.2.3 Clay

The clay ASTM D6459-19 test was performed on Plot 1 with a 4H:1V slope. The Proctor compaction was 92.2% with 22% moisture content. This compaction was higher than both the sand and loam soils despite that the method of using the plate compactor to pass over all areas of the plot one time was identical. The first attempt to conduct this test was stopped due to excessive wind conditions. However, the second attempt proceeded with suitable wind conditions meeting ASTM D6459-19 criteria. Like the loam test, the barrels did not fill with soil during the test, and the improved flashing system was not necessary. The results of the clay test are displayed in Table 5.18.

TABLE 5.18: Clay Bare Soil Test Results

Target Intensity, in./hr (mm/hr)	**2.0 (51)**	**4.0 (102)**	**6.0 (152)**
Intensity, in/hr (mm/hr)	2.7 (69)	4.5 (114)	7.3 (187)
Sediment, lb (kg)	4.3 (2.0)	50.1 (22.7)	123.4 (56.0)
Runoff, gal. (L)	23.9 (90.4)	178.1 (674.2)	284.1 (1075.4)
Average turbidity, NTU	9,450	17,850	23,550
Average TSS. mg/L	7,490	16,510	18,960

5.5.2.4 Comparison of Results

With one test on each soil completed, the *K*-factors were compared. Using the flour pan method drop size calibration results from Table 5.13, *R*-factors for rainfall were determined for each test based on previous flour pan test results and the recorded intensity during the test. *K*-factors, were calculated with the RUSLE equation with factors in Table 5.19.

TABLE 5.19: First Test RUSLE Factors on New Rainfall Simulators

RUSLE Factor	Sand	Loam	Clay
***A*, ton/ac/yr**	60.91	19.18	7.73
Theoretical *R*	148.5	148.5	148.5
LS	2.23	2.23	2.23
C	1	1	1
P	1	1	1
K	0.18	0.06	0.02

As expected, the sand had the highest *K*-factor while the clay had the lowest *K*-factor. These *K*-factors are unique to the plot preparation; ASTM D6459-19 requires compaction 90 ± 3% of maximum compaction, which affects the soil erodibility. Continued testing will refine these results.

CHAPTER 6: CONCLUSION

6.1 INTRODUCTION

The objective of this research was to construct, calibrate, and test on twelve large-scale ASTM D6459-19 rainfall simulators and to investigate alternative calibration techniques. Five tasks were completed to accomplish these goals. The first task was to construct twelve new rainfall simulators with ASTM D6459-19 parameters. These rainfall simulators were built with two types of slopes and three different soils. The soils represented sand, clay, and loam common in the state of Alabama. Grain size distribution testing on several soils determined an appropriate source for ASTM sand. Numerous efficient construction techniques were implemented and improved through the construction. The second task completed in this work was the verification of the original ASTM D6459-19 rainfall simulator at AU-SRF, which included rainfall intensity calibration and control testing. The third task was to investigate novel calibration techniques for rainfall intensity, rainfall drop size distribution, and rainfall velocity and compare them to standard practices in ASTM D6459-19. The fourth task was to calibrate the new rainfall simulators for rainfall intensity and drop size distribution using ASTM D6459-19 methods. The fifth and final task included initial testing on bare soil on the new rainfall simulators to experimentally determine *K*-factors of the three new soils for later use in evaluating erosion control products on various slopes and soils. Procedures for test plot preparation, testing, and data collection on the new plots were developed.

6.2 CONSTRUCTION

The rainfall simulators plots were designed to accommodate ASTM D6459-19 requirements including plot dimensions of 40.0 ft (12.2 m) by 8.0 ft (2.4 m) and 4H:1V or 3H:1V slopes. With three soils and two slopes, six types of plots were constructed with two of each combination of slope and soil. The plots were constructed along a road embankment in pairs. The first steps of construction were land clearing, rough grading, and creating a survey digital terrain model with a Total Station for the top elevations of the plots. Then, the plot corners were marked before beginning individual plot construction.

The procedure for constructing plots was: (1) Excavate for a plot using a terrace in the center of the slope for parking the excavator while digging the upper reaches of the plot, (2) Perform fine grading with three workers including an excavator operator, a surveyor, and a raker, (3) Add the first 6.0 in. (15 cm) lift of soil with a skid steer, (4) Construct and install plot borders, (5) Add and compact two additional soil lifts, (6) Construct and install drainage features including catchment basins, channels, and culverts, (7) Design and install a water supply system including a water distribution manifold, in-line filter, and floating dock, (8) Ensure proper runoff collection for each plot, and (9) Design and build an electrical system with a controller box with switches for 2.0 in./hr (51 mm/hr), 4.0 in./hr (102 mm/hr), and 6.0 in./hr (152 mm/hr) target intensities. Additional grading was performed below the 3H:1V plots to improve drainage. Soil testing was performed to identify a source for ASTM sand and to ensure ASTM D6459-19 compliance for grain size distribution. Each soil was stockpiled with quantities viable for long term testing.

The construction process used cost-effective methods. Recommended practices for design and construction methods include creating survey data to streamline precise construction, using pre-made tanks to reduce cost for a catchment basin, and sharing sprinkler systems between

multiple plots. Additional strategies include 2.0-in. (5.1-cm) thick lumber for plot borders, utilizing terracing for safer grading on slopes with heavy equipment, and anchoring for protecting retention tanks from flood damage. Furthermore, flow delivery, flow distribution, and drainage systems are absent from ASTM D6459-19 and should be considered. Techniques described in this work for proper planning, construction, and calibration methods intend to complement ASTM D6459-19 to facilitate the process of creating large-scale simulators.

6.3 EVALUATION OF NOVEL CALIBRATION METHODS

Two alternative methods for rainfall simulator calibration were examined. The first method was for determining rainfall intensity. While ASTM D6459-19 requires rainfall gauges to determine intensity, the effects of imperfect uniformity may skew results from the actual runoff produced on the plot. Therefore, using paired statistical analyses, a method for determining rainfall intensity from direct measurement of runoff was compared to traditional rainfall gauge setups. The two methods were statistically different for three target intensities in a paired test with 95% confidence and percent differences in mean ranging from 27.8% to 32.8%. The runoff was less than the rainfall gauges predicted. The two methods were strongly correlated with a linear regression with R^2 greater than 0.99. The runoff method is a precise measurement of the actual runoff produced by the plot and can be used in conjunction with the ASTM D6459-19 rainfall gauge recommendation to precisely measure rainfall intensity. Additionally, the usage of six suspended rainfall gauges during a control or product test to verify intensity was statistically compared to the ASTM D6459-19 recommendation of twenty rainfall gauges during calibration. The results indicate with 95% confidence that there is not enough evidence to conclude that the six suspended rainfall gauges and twenty rainfall gauges arrangements yield different intensities.

Raindrop characteristics were examined first with videography and then with photography. The videography experiment was to determine whether raindrops could be measured for drop size and velocity using video frames. The results of this initial test indicated that the method was viable with some improvement. The second experiment utilized a professional camera, improved lighting, and improved background. This test yielded results which were compared to the ASTM D6459-19 standard flour pan test for determining drop size distribution of rainfall. The results indicated that the photography method represented exponentially more small raindrops than the flour pan method. The photography method produced an *R*-factor 32.8% lower than the flour pan test. The percentage that the flour pan overrepresents raindrop energy compared to the photography method may be dependent on the drop size distribution of the sample, which varies by sprinkler system.

The velocities of individual raindrops were measured using the distance that each raindrop traveled while the camera was capturing the photograph. The velocities were compared to theoretical predictions that are used in ASTM D6459-19 rainfall energy calculations using a paired t-test and the drop sizes measured photographically. The results indicated that the photography method yielded statistically significantly different velocity for raindrops with 95% certainty. As drop size increased, the difference between the methods for determining velocity decreased. A linear correlation was plotted between the experimental and theoretical velocities, and a best-fit linear equation with R^2 of 0.95 was obtained; however, the relationship may be more complex and require larger sampling of raindrops greater than 1.68 mm diameter.

Implications of these findings include that the *R*-factor in the RUSLE equation, which is obtained by the flour pan method, may be overrepresented because the flour pan test represented a greater percentage of larger raindrops than the photography method sample demonstrated. The

R-factors obtained by each method were 109.7 and 163.2 for the photography and flour pan methods in the center of the plot, respectively. If the *R*-factor, is less than the flour pan method obtained, the *K*-factor, obtained through bare soil testing will be overrepresented. However, if product testing to evaluate cover factor used the same method as the control testing to determine *R*-factor, the overrepresented *R*-factor does not affect the calculation of cover factor. Therefore, previous testing is not affected by this finding. However, *K*-factors are used for practical RUSLE calculations in the construction industry, and researchers attempting to determine or compile *K*-factors should consider that the method used to determine drop size distribution can affect the result.

6.4 CALIBRATION

Calibration testing was performed on the original rainfall simulator for renewal of accreditation and on a representative plot for the new rainfall simulators. ASTM D6459-19 procedures for calibration were followed for both rainfall intensity and raindrop size distribution. Together, the results indicated that all thirteen rainfall simulators at AU-SRF are operational and capable of 2.0 in./hr, 4.0 in./hr, and 6.0 in./hr (51, 102, and 152 mm/hr) target rainfall intensities. The theoretical *R*-factor for target intensities based on the results of the flour pan test drop size calibration for the new rainfall simulators was 148.5. Continued renewal of accreditation for ASTM D6459-19 testing through the Geosynthetic Accreditation Institute is vital to future erosion control product testing.

6.5 TESTING

This work established procedures for ASTM D6459-19 testing on the new rainfall simulators. Improvements to the procedure on the original large-scale rainfall simulator procedure include collecting all three target intensities in tubs to avoid run-on into the catchment basin

affecting 6.0 in./hr (152 mm/hr) test results, incorporating the suspension of rainfall gauges to prevent the gauges from affecting rill formation, and utilizing a portable manifold to distribute flow to sprinklers shared by all plots. Initial control testing yielded *K*-factors of 0.18, 0.06, and 0.02 for sand, loam, and clay, respectively. As anticipated, the sand was the most erodible soil, and the clay was the least erodible soil. Future testing will refine these factors. These *K*-factors are unique to the sprinkler design at AU-SRF and may be influenced by raindrop size distribution; however, identical rainfall characteristics will be present during product testing to determine cover factors of erosion controls. Therefore, these control tests represent the maximum soil losses for calculating cover factor during future erosion control product testing.

6.6 SUMMARY

The five tasks were successfully completed, which are described as follows:

1. Twelve new ASTM D6459-19 rainfall simulators were constructed on three soils and two slopes in pairs with each soil stockpiled for long term testing. The rainfall simulators utilized a portable sprinkler system with a flow distribution manifold and supply pipe across the length of the top of the slopes. Additionally, they were constructed with cost-effective techniques including wooden plot borders and anchored plastic catchment basin tubs.

2. The original AU-SRF ASTM D6459-19 rainfall simulator was verified for renewal of Geosynthetic Accreditation Institute accreditation. This accreditation is critical to ensuring AU-SRF adherence to ASTM D6459-19 testing parameters. The test procedures used in this verification were the basis for the testing procedure on the new rainfall simulators.

3. Novel calibration techniques including runoff to calculate rainfall intensity and photography to directly measure rainfall characteristics were investigated. Results suggested that photography for determining drop size distribution could be a viable alternative to the flour pan test. The photography method results indicated that raindrops less than 1.68 mm diameter represent a greater portion of the total rainfall than the flour pan method could identify. Additionally, the runoff method for determining intensity is more precise than rainfall gauges and can be used in conjunction with ASTM D6459-19 calibration methods.

4. The twelve new rainfall simulators were calibrated by performing ASTM D6459-19 calibration techniques on a representative apparatus. The flour pan results yielded a theoretical *R*-factor assuming target intensities of 148.5. Additionally, intensity calibration indicated sufficient Christiansen uniformity and intensities near the target intensities. Therefore, the new rainfall simulators were determined to be ready for control testing with bare soil.

5. Initial testing was performed on the new rainfall simulators. One test was performed on each soil for the 4H:1V slope plots. The sand had the greatest soil erodibility, which was followed by the loam, and the clay had the lowest *K*-factor. Continued testing will refine these results and provide a basis for finding cover factors of erosion control products.

6.7 RECOMMENDATIONS FOR FUTURE RESEARCH

The twelve new ASTM D6459-19 rainfall simulators will be used in Phase II of the AU-SRF rainfall simulator project, “Evaluation of ALDOT Erosion Control Products Using Rainfall Simulation on Various Soil Types and Slope Gradients.” This project will include more control testing and testing of numerous erosion control practices on each soil type and slope. This project will yield results which produce recommendations for erosion control based on soil type and slope

to increase the effectiveness of erosion control in Alabama. Additionally, this work produced auxiliary methods for experimentally determining rainfall intensity, raindrop size distribution, and raindrop velocity. These methods should be further developed into standard procedures. The runoff method for rainfall intensity was immediately implemented to verify rainfall intensity on the new apparatuses.

Based on findings from construction, calibration, and testing with ASTM D6459-19 and experimentation with alternative methods for intensity and rainfall characteristics, several recommendations can be made to improve future large-scale rainfall simulation testing:

1. Rainfall erosivity factor, *R*, should be more carefully examined. The photography method sample size of raindrops greater than 1.68 mm diameter in this study was small, and the flour pan method suggested that these raindrops account for the majority of the rainfall energy. Laser-optical technology such as a disdrometer should be applied on the rainfall simulator and compared to flour pan and photography methods. Additionally, the raindrop method should be improved for experimental determination of the raindrop velocity by determining the true shape of raindrops. This research assumed that the raindrops from the sprinklers were perfectly spherical while their shapes may be more complex and related to size. This could be accomplished by performing a similar experiment as this work except with the shortest possible shutter speed.

2. Future researchers can reduce potential for testing delays by constructing replacement rainfall trees. In the case of a broken or malfunctioning rainfall tree, a replacement could be installed from reserve to immediately become operational. Additionally, a second full set of sprinklers with a second manifold could reduce the need to move the sprinkler systems.

3. The capacity for testing should be increased by implementing wind-blocking structures at the top of the slopes. ASTM D6459-19 has stringent wind requirements for testing, which means that ideal days and times for testing where wind speed is less than 1.0 mi/hr (1.6 km/hr) can be infrequent. While the original AU-SRF ASTM D6459-19 utilized wind curtains to block the wind, this system was difficult to use because of the pulley system. Future research would benefit greatly by increasing the times that tests could be performed by designing and implementing a simple-to-use wind reducing or blocking system.

REFERENCES

Aksoy, H., N. Erdem Unal, S. Cokgor, and A. Gedikli. 2012. “A Rainfall Simulator for Laboratory-Scale Assessment of Rainfall-Runoff-Sediment Transport Processes Over a Two-Dimensional Flume.” *Catena*, 98, 63–72.

American Excelsior Company Earth Science Division. 2022. “ErosionLab.” https://americanexcelsior.com/erosion-control/erosionlab/, accessed April 2022.

ASTM (2008). “Standard Test Method for Determination of Water (Moisture) Content of Soil by Microwave Oven Heating.” West Conshohocken, PA, 1-7.

ASTM (2010). “Standard Test Method for Density of Soil in Place by the Drive-Cylinder Method.” West Conshohocken, PA, 1-7.

ASTM (2014). “Standard Test Method for Sieve Analysis of Fine and Coarse Aggregates.” West Conshohocken, PA, 1-5.

ASTM (2019). “Standard Test Method of Rolled Erosion Control Product (RECPs) Performance in Protecting Hillslopes from Rainfall Induced Erosion.” West Conshohocken, PA, 1-10.

ASTM (2021), “Standard Test Methods for Laboratory Compaction Characteristics of Soil Using Standard Effort (12,400 ft-lbf/ft3 (600 kN-m/m3)).” West Conshohocken, PA, 1-13.

ASTM (2022), “Standard Test Method for Determination of Erosion Control Products (ECP) Performance in Protecting Slopes from Sequential Rainfall-Induced Erosion Using a Tilted Bed Slope.” West Conshohocken, PA, 1-15.

ASTM (2020) “Determination of Erosion Control Products (ECP) Performance in Protecting Slopes from Continuous Rainfall-Induced Erosion Using a Tilted Bed Slope.” West Conshohocken, PA, 1-15.

Barkley, T. 2004. “Erosion Control with Recycled Materials.” *U.S. Department of Transportation*, 65 (5).

City of Springfield Environmental Services. 2008. “Erosion Control Blankets.” https://www.springfieldmo.gov/DocumentCenter/View/3466/Erosion-Prevention-and-Sediment-Control-Guidelines-PDF?bidId, accessed May 2022.

Cottenot, L., Courtemanche, P., Nouhou-Bako, A., and Darboux, F. 2021. “A Rainfall Simulator Using Porous Pipes as Drop Former.” Catena, 200.

Erosion Control Technology Council. 2017. “Installation Guide for Rolled Erosion Control Products (RECPs) Including Mulch Control Nettings (MCNs), Open Weave Textiles (OWTs), Erosion Control Blankets (ECBs), and Turf Reinforcement Mats (TRMs).”

Faulkner, B. 2020. “Evaluation of Erosion Control Practices Under Large-Scale Rainfall Simulation Following ASTM D6459 Standard Test Methods.” M.S. Thesis, Auburn University, Auburn, AL.

Fay, L., M. Akin, and X. Shi. 2012. “Cost-Effective and Sustainable Road Slope Stabilization and Erosion Control.” National Academy of Sciences, Transportation Research Board National Research Council.

Gantzer, C., S. Anderson, and R. Miles. 2018. “The Centennial of the First Erosion Plots.” Journal of Soil and Water Conservation, 72 (3), 57A-59A.

Hagman, B. B., and F. W. Madison. 1979. “Methods for Controlling Erosion and Sedimentation from Residual Construction Activities.” *National Conference on Urban Erosion and Sediment Control*, St. Paul, MN.

Han, J., and Guo, J. 2017. “Geosynthetics Used to Stabilize Vegetated Surfaces for Environmental Sustainability in Civil Engineering.” *Frontiers of Structural and Civil Engineering*, 11(1).

Hanrahan, P. 2015. “The Evolution of Erosion Control Technology.” Maine Water Utilities Association.

Horne, M.A. 2017. “Design and Construction of a Rainfall Simulator for Large-Scale Testing of Erosion Control Practices and Products.” M.S. Thesis, Auburn University, Auburn, AL.

Hubbert, K.R., Wohlgemuth, P.M., and Beyers, J.L. 2012. “Effects of Hydromulch on Post-fire Erosion and Plant Recovery in Chaparral Shrublands of Southern California.” *International Journal of Wildland Fire*, 21 (2): 155–167.

Kaszynski, W. 2000. “The History and Culture of Roads in the United States.” *McFarland Publishing.*

Kelsey, K. 2014. “40 Years of Slope Surface Stabilization Evolution.” *Land and Water*, 2014 Volume (Sept/Oct), 7-14.

Kumarasinghe, U. 2021. “A review on new technologies in soil erosion management.” *Journal of Research Technology and Engineering*, 2 (1).

Laws, J. O. 1941. “Measurements of the fall-velocity of water -drops and raindrops.” *Eos Trans. AGU*, 22(3), 709– 721.

Manning, C. 2021. “Rainfall Simulator Construction and Evaluation of Erosion Control Practices.” M.S. Thesis, Auburn University, Auburn, AL.

McFalls, J., Ming-Han, L., Young-Jae, Y., and Landphair, H. 2007. “Cost Performance Index of Temporary Erosion Control Products.” Texas Transportation Institute, College Station, TX.

Ming-Han, L. 2014. “Evaluating Erosion Control Performance of Crimped Straw Mulch in Comparison with RECPs on Simulated Highway Roadsides.” *International Journal of Geotechnical Engineering*, 307-314.

Minnesota Pollution Control Agency. 2012. “Erosion prevention practices - Erosion Control Blankets and Anchoring Devices.” https://stormwater.pca.state.mn.us/index.php/Erosion_prevention_practices_-_erosion_control_blankets_and_anchoring_devices, accessed April 2022.

Prunty, T., Johnson, W.E., and Johnson, J.W. 1997. “Erosion control blanket and method of manufacture.” U.S. Patent No. 5,735,982A.

Ricks, M.D.., Fang, X., Zech, W.C., Donald, W.N., and Perez, M.A.. 2020. “Comparative Analysis of Soil Erosion Using Large-, Intermediate-, and Small-Scale Test Plots of Bare Soil and Different Hydromulch Products under Large-Scale Rainfall Simulator.” M.S. Thesis, Auburn University, Auburn, AL.

Rossmiller, R. L. .1980. “Rational Formula Revisited.” *International Symposium on Urban Storm Runoff*, University of Kentucky, Lexington, KY.

Sawasky, L., Dick, W., Cooper, D., and Keys, M. 1996. “Design of a Rainfall Simulator to Measure Erosion of Reclaimed Surfaces.” *20th Annual British Colombia Mine Reclamation Symposium*. Kamloops, BC.

Schussler, J., Perez, M.A., and Donald, W.N. 2022. “Decade of Research in Review at the Auburn University Stormwater Research Facility.” *Journal of the Transportation Research Board, 2676 (5).*

Shoemaker, A. L., Zech, W. C., and Clement, T. P. 2012. "Laboratory-Scale Evaluation of Anionic Polyacrylamide as an Erosion and Sediment Control Measure on Steep-Sloped Construction Sites." *Transactions of the American Society of Agricultural and Biological Engineers*, 55(3), 809-820.

Tullis, B. P. 2016. “Comparing Raindrop Size and Velocity Measurement Accuracy Using Shadowgraphy, Disdrometery, and Pie Pan Measurement Techniques.” *Journal of Testing and Evaluation*, 44 (6).

United States Soil Conservation Service, Alabama Cooperative Extension Service, and U.S. National Cartographic Center. *Soil Areas of Alabama.* Fort Worth, TX: USDA-SCS-National Cartographic Center ; Auburn, ALA.: State Conservationist, distributor, 1986. Map. https://www.loc.gov/item/90684181/, accessed November 2021.

USDA. 2016. “USLE History.” National Soil Erosion Research: West Lafayette, IN. https://www.ars.usda.gov/midwest-area/west-lafayette-in/national-soil-erosion-research/docs/usle-database/usle-history/, accessed May 2022.

Wilson, Christopher. 2021. “Performance Based Testing for Erosion Prevention and Sediment Control (EPSC) Devices.” National Transportation Library.

Wilson, W.T., Zech, W.C., Clement, P., Crowley, L.G. 2010. “Evaluation of Hydromulches as an Erosion Control Measure Using Intermediate-Scale Experiments.” M.S. Thesis, Auburn University, Auburn, AL.

APPENDICES

Appendix A: Manufacturer Specifications for Select Rainfall Simulator Components

Appendix B: Standard Operating Procedures for Control Testing on New Rainfall Simulators

Appendix C: Experimental Data

APPENDIX A

MANUFACTURER SPECIFICATIONS FOR SELECT RAINFALL SIMULATOR COMPONENTS

HAYWARD

YS Series
Y-Strainers

1/2" - 2" PVC, CLEAR PVC AND CPVC
2-1/2" - 4" PVC AND CPVC

KEY FEATURES

- Available in PVC, CPVC and Clear PVC
- Horizontal or Vertical Installation
- FPM O-Ring Seals
- 2:1 Open Area Ratio
- Hex Cap for Easy Access to Screen
- Standard Screen has 1/32" Perforation

OPTIONS

- Stainless Steel Perforated or Mesh Strainer Screens Available in Various Sizes and Alloy Materials

MATERIALS

- PVC Cell Class 12454 per ASTM D1784
- Clear PVC Cell Class 12454 per ASTM D1784
- CPVC Cell Class 23447 per ASTM D1784
- FPM and EPDM O-Ring Seals

TECHNICAL INFORMATION

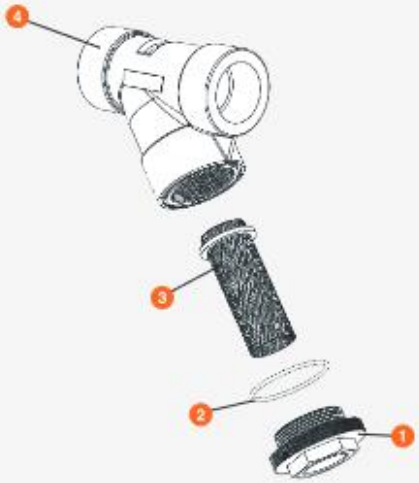

SELECTION CHART

SIZE	MATERIAL	END CONNECTION	SEALS	PRESSURE RATING
1/2" – 1" (DN15 – DN25)	PVC, CPVC or Clear PVC	Socket or Threaded	FPM and EPDM	150 PSI @ 70°F 10 Bar @ 21°C Non-Shock
1–1/4" (DN32)	PVC and Clear PVC			
1–1/2" (DN40)	PVC, CPVC or Clear PVC			
2" (DN50)				
2–1/2" (DN65)	PVC	Socket, Threaded or Flanged		
3–4" (DN80-DN100)	PVC and CPVC			

* PVC and CPVC socket ends available to ISO 727-1 and threaded ends to BS21. Flanged ends available in DIN / EN PN10.

YS Series
Y-Strainers

1/2" - 2" PVC, CLEAR PVC AND CPVC
2-1/2" - 4" PVC AND CPVC

TECHNICAL INFORMATION, *CONTINUED*

PARTS LIST

1. Cap
2. O-Ring Seal
3. Screen
4. Body

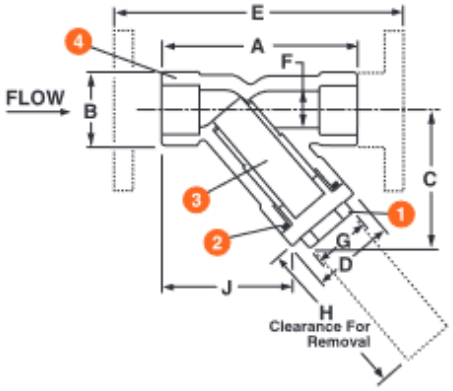

SCREEN OPTIONS

PERFORATION SIZES	MESH SIZES	SCREEN MATERIAL
1/32"	20	SSTL, Hastelloy, Monel and Titanium
1/16"	40	
1/8"	60	
5/32"	80	
3/16"	100	
1/4"	200	
3/8"	325	
1/32"	N/A	PVC and CPVC
1/16"		
1/8"		
3/16"		

DIMENSIONS

SIZE in / DN	A in / mm	B in / mm	C in / mm	D in / mm	E in / mm	F in / mm	G in / mm	H in / mm	J in / mm	WEIGHT lbs / kg SOC / THD	WEIGHT lbs / kg FLANGED
1/2 / 15	3.38 / 86	1.38 / 35	2.25 / 57	1.50 / 38	N/A	.56 / 14	1.00 / 25	2.13 / 54	2.50 / 64	.25 / .11	N/A
3/4 / 20	4.18 / 106	1.69 / 43	2.88 / 73	2.00 / 51	N/A	.81 / 21	1.25 / 32	2.75 / 70	3.00 / 76	.63 / .29	N/A
1 / 25	5.19 / 132	2.00 / 51	3.63 / 92	2.16 / 55	N/A	1.00 / 25	1.50 / 38	3.30 / 84	3.32 / 84	.88 / .40	N/A
1-1/4 / 32	6.63 / 168	2.63 / 67	4.50 / 114	2.94 / 75	N/A	1.25 / 32	2.00 / 51	4.50 / 114	4.45 / 113	1.75 / .79	N/A
1-1/2 / 40	6.63 / 168	2.63 / 67	4.50 / 114	2.94 / 75	N/A	1.56 / 40	2.00 / 51	4.50 / 114	4.45 / 113	1.63 / .74	N/A
2 / 50	7.63 / 194	3.38 / 86	5.38 / 137	3.75 / 95	11.00 / 279	2.00 / 51	2.38 / 60	5.06 / 129	4.88 / 124	3.00 / 1.36	5.00 / 2.27
2-1/2 / 65	10.31 / 262	4.69 / 119	7.25 / 184	5.25 / 133	N/A	2.90 / 74	3.50 / 89	6.60 / 168	6.54 / 166	7.75 / 3.52	N/A
3 / 80	10.31 / 262	4.69 / 119	7.25 / 184	5.50 / 140	14.37 / 365	2.90 / 74	3.50 / 89	6.60 / 168	6.54 / 166	7.50 / 3.40	12.25 / 5.56
4 / 100	12.81 / 325	5.75 / 146	8.88 / 226	6.18 / 157	17.73 / 450	3.78 / 96	4.25 / 108	8.00 / 203	8.58 / 218	9.50 / 4.30	17.50 / 7.94

Dimensions are subject to change without notice – consult factory for installation information

Cv VALUES*

SIZE in / DN	Cv VALUES	SIZE in / DN	Cv VALUES
1/2 / 15	4.0	2 / 50	28
3/4 / 20	6.8	2-1/2 / 65	40
1 / 25	9.0	3 / 80	65
1-1/4 / 32	12	4 / 100	100
1-1/2 / 40	28		

* With 1 / 32" plastic screen

PRESSURE LOSS CALCULATION FORMULA

$$\Delta P = \left[\frac{Q}{Cv}\right]^2$$

ΔP = Pressure Drop
Q = Flow in GPM
Cv = Flow Coefficient

OPERATING TEMPERATURE/PRESSURE

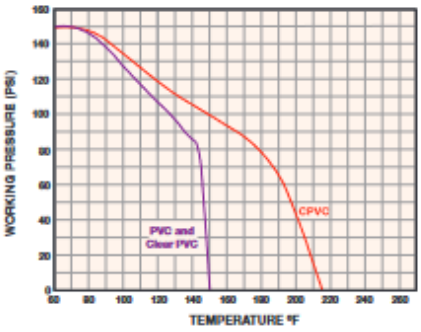

USA: 1.888.429.4635 • Fax: 1.888.778.8410 • One Hayward Industrial Drive • Clemmons, NC 27012 • Email: hfcsales@hayward.com
Canada: 1.888.238.7665 • Fax: 1.905.829.3636 • 2880 Plymouth Drive • Oakville, ON L6H 5R4 • Email: hflowcanada@hayward.com
Visit us at: haywardflowcontrol.com

CHARLOTTE PIPE AND FOUNDRY COMPANY

SUBMITTAL FOR CHARLOTTE PIPE®
PVC SCHEDULE 40 PRESSURE PIPE AND FITTING SYSTEM

Date: _____

Job Name: _____ Location: _____

Engineer: _____ Contractor: _____

Scope:
This specification covers PVC Schedule 40 pipe and fittings for pressure applications. This system is intended for pressure applications where the operating temperature will not exceed 140° F.

Specification:
Pipe and fittings shall be manufactured from virgin rigid PVC (polyvinyl chloride) vinyl compounds with a cell class of 12454 as identified in ASTM D 1784.

PVC Schedule 40 pipe shall be Iron Pipe Size (IPS) conforming to ASTM D 1785. Injection molded PVC Schedule 40 fittings shall conform to ASTM D 2466. Pipe and fittings shall be manufactured as a system and be the product of one manufacturer. All pipe and fittings shall be manufactured in the United States. Pipe and fittings shall conform to NSF International Standard 61 and the health-effects portion of NSF Standard 14.

Installation:
Installation shall comply with the latest installation instructions published by Charlotte Pipe and Foundry and shall conform to all applicable plumbing, fire, and building code requirements. Buried pipe shall be installed in accordance with ASTM F 1668. Solvent cement joints shall be made in a two-step process with primer conforming to ASTM F 656 and solvent cement conforming to ASTM D 2564. The system shall be protected from chemical agents, fire-stopping materials, thread sealant, plasticized-vinyl products or other aggressive chemical agents not compatible with PVC compounds. The system shall be hydrostatically tested after installation. **WARNING!** Never test with or transport/store compressed air or gas in PVC pipe or fittings. Doing so can result in explosive failures and cause severe injury or death.

Referenced Standards:

ASTM D 1784: Rigid Vinyl Compounds
ASTM D 1785: PVC Plastic Pipe, Schedule 40
ASTM D 2466: PVC Plastic Fittings, Schedule 40
ASTM D 2564: Solvent Cements for PVC Pipe and Fittings
ASTM F 1668: Procedures for Buried Plastic Pipe
NSF Standard 14: Plastic Piping Components & Related Materials
NSF Standard 61: Drinking Water System Components – Health Effects

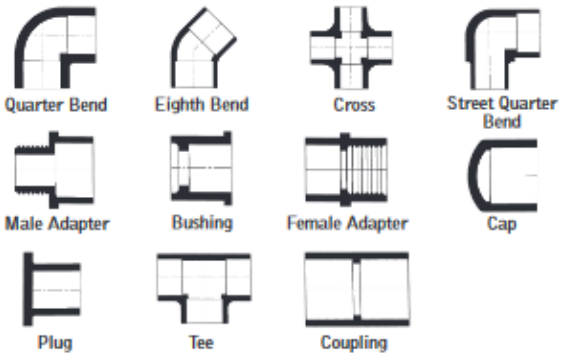

Not all fitting patterns shown

Schedule 40 Tapered Socket Dimensions

PVC SCHEDULE 40 - ASTM D 2466

Nominal Size	Schedule 80 and Schedule 40 Socket Diameter: Entrance A	Bottom B	Tolerance	Schedule 80 Socket Length C (Minimum)	Schedule 40 Socket Length C (Minimum)
½	0.848	0.836	±0.004	0.875	0.688
¾	1.058	1.046	±0.004	1.000	0.719
1	1.325	1.310	±0.005	1.125	0.875
1¼	1.670	1.655	±0.005	1.250	0.938
1½	1.912	1.894	±0.006	1.375	1.094
2	2.387	2.369	±0.006	1.500	1.156
2½	2.889	2.868	±0.007	1.750	1.750
3	3.516	3.492	±0.008	1.875	1.875
4	4.518	4.491	±0.009	2.250	2.000
6	6.647	6.614	±0.011	3.000	3.000
8	8.655	8.610	±0.015	4.000	4.000
10	10.780	10.735	±0.015	5.000	5.000
12	12.780	12.735	±0.015	6.000	6.000

PIPE REFERENCE GUIDE

Product	Sizes Available														
	½	¾	1	1¼	1½	2	2½	3	4	5	6	8	10	12	14	16
PVC Schedule 40	•	•	•	•	•	•	•	•	•	•	•	•	•	•	•	•

Charlotte Pipe and Foundry Company • P.O. Box 35430 Charlotte, NC 28235 • (800) 438-6091 • www.charlottepipe.com

FO-SUB-PVC-40 (5-30-19)

PVC Schedule 40 Pipe - Bell End*

PVC SCHEDULE 40 (WHITE)		BELL END		PVC 1120		ASTM D 1785	
PART NO.	NOM. SIZE	UPC # 611942-	AVG. OD (IN.)	MIN. WALL (IN.)	MAX WORK PRESSURE AT 23° C OR 73° F	BELL DEPTH (IN.)	WT. PER 100 FT. (LBS.)
PVC 4005B**	½" x 10'	04986	.840	.109	600 PSI	2.00	15.9
PVC 4005B**	½" x 20'	03923	.840	.109	600 PSI	2.00	15.9
PVC 4007B**	¾" x 10'	04987	1.050	.113	480 PSI	2.25	21.1
PVC 4007B**	¾" x 20'	03926	1.050	.113	480 PSI	2.25	21.1
PVC 4010B**	1" x 10'	04988	1.315	.133	450 PSI	2.50	31.3
PVC 4010B**	1" x 20'	03929	1.315	.133	450 PSI	2.50	31.1
PVC 4012B§	1¼" x 10'	04989	1.660	.140	370 PSI	2.75	42.4
PVC 4012B§	1¼" x 20'	03930	1.660	.140	370 PSI	2.75	42.4
PVC 4015B§	1½" x 10'	04990	1.900	.145	330 PSI	3.00	51.8
PVC 4015B§	1½" x 20'	03931	1.900	.145	330 PSI	3.00	51.8
PVC 4020B†	2" x 10'	04991	2.375	.154	280 PSI	4.00	69.5
PVC 4020B†	2" x 20'	03932	2.375	.154	280 PSI	4.00	69.5
PVC 4025B‡	2½" x 20'	04206	2.875	.203	300 PSI	4.00	110.0
PVC 7300B§	3" x 10'	04853	3.500	.216	260 PSI	4.00	147.6
PVC 4030B†	3" x 20'	03933	3.500	.216	260 PSI	4.00	144.2
PVC 7400B§	4" x 10'	04835	4.500	.237	220 PSI	4.00	212.3
PVC 9400B†	4" x 20'	03964	4.500	.237	220 PSI	5.00	210.6
PVC 7600B§	6" x 10'	04850	6.625	.280	180 PSI	6.50	379.3
PVC 9600B†	6" x 20'	03965	6.625	.280	180 PSI	6.50	373.2
PVC 7800B†	8" x 10'	09903	8.625	.322	160 PSI	7.00	556.9
PVC 9800B†	8" x 20'	03967	8.625	.322	160 PSI	7.00	564.0
PVC 7910B†	10" x 20'	03960	10.750	.365	140 PSI	9.00	781.4
PVC 7912B†	12" x 20'	03962	12.750	.406	130 PSI	10.00	1033.2
PVC 7914B†	14" x 20'	04863	14.000	.437	130 PSI	10.00	1221.8
PVC 7916B†	16" x 20'	04929	16.000	.500	130 PSI	10.00	1594.5

* Bell dimensions meet either ASTM D 2672 or ASTM F 480, depending upon pipe diameter
** ASTM D 1785
‡ Dual Marked ASTM D 1785 & ASTM F 480
§ Dual Marked ASTM D 1785 & ASTM D 2665
† Triple Marked ASTM D 1785 & ASTM D 2665 & ASTM F 480

MADE IN U.S.A.

⚠ WARNING

Testing with or use of compressed air or gas in PVC / ABS / CPVC pipe or fittings can result in explosive failures and cause severe injury or death.

- NEVER test with or transport/store compressed air or gas in PVC / ABS / CPVC pipe or fittings.
- NEVER test PVC / ABS / CPVC pipe or fittings with compressed air or gas, or air over water boosters.
- ONLY use PVC / ABS / CPVC pipe or fittings for water or approved chemicals.
- Refer to warnings on PPFA's website and ASTM D 1785.

POLY-TANK CONTAINMENT UNIT/275™

For the widely-used 275-gallon obround tank, PolyTank Containment Unit/275™ helps protect against hazardous and costly spills. PolyTank 275 is designed to save space and provide easy access to the tank and pump preventing harmful spills from contaminating your yard. Optional fitted tarp (Part #: 5275-TARP) and trickle filter (Bazooka).

(see Tarp on page 13)

POLY-TANK CONTAINMENT UNIT/275™

Part #	Description	Ext. Dimension L x W x H in. (cm)	Int. Top Dimension in. (cm)	Int. Bottom Dimension (cm)	Weight lb. (kg)	Spill Cap. gal. (L)
5275-BK 5275-BK-D	Poly-Tank (w/drain)	82 x 45 x 35.38 (208 x 114 x 90)	77 x 39.5 (196 x 188)	66 x 29 (168 x 74)	98 (44.5)	275 (1,041)
5275-TARP	Tarp	82.25 x 45 x 45.5 (208.9 x 114 x 115.5)			10 (4.5)	

Regulations: EPA 40 CFR 264.175, SPCC, NPDES and UFC

POLY-TANK CONTAINMENT UNIT/550™

KEEP HAZARDOUS LIQUID STORED SAFELY ABOVE THE GROUND.

Designed for the 550-gallon skid tank, (and 150-gallon, 300-gallon skid elevated tanks) this unit safely protects against hazardous liquid discharge into the ground. Large interior leaves space for hoses and related equipment. Ideal for construction sites, marine, and farm use. Optional fitted tarp (Part #: 5550-TARP), drain (5551), and trickle filter (Bazooka).

POLY-TANK CONTAINMENT UNIT/550™

Part #	Description	Dimensions L x W x H in. (cm)	Weight lb. (kg)	Spill Cap. gal. (L)
5550-BK 5550-BK-D	Forkliftable (w/drain)	113 x 71 x 32 (287 x 180 x 81)	190 (86.2)	750 (2,082)
5550-TARP	Tarp	115 x 75 x 50.5 (292 x 190.5 x 128)	12 (5.5)	

EPA 40 CFR 264.175, SPCC, NPDES and UFC

(see Tarp on page 13)

BULKHEAD FITTINGS™

Optional bulkhead fittings make pumping and draining fast and easy. (For Part # 5275-BK and 5550-BK)

BULKHEAD FITTING

Part #	Dimensions Ext. Dia in. (cm)	Connection Dimensions in. (cm)	Weight lb. (kg)
5276	3 (8)	.75 (2)	1 (.5)

(See Bazooka on page 25.)

ELECTRICAL SYSTEM PART LIST

- Mil. Spec. Signal/Power Connector Receptacle, External Thread, 4 Poles, MS3102R14S-2S8903T43
- Mil. Spec. Signal/Power Connector Plug, Internal Thread, 4 Poles, MS3106F14S-2P Trade No. 8903T13
- Wet-Location Toggle Switch 2 Position, Rounded, NEMA 4, Maintained, SPST-NO, with Quick-Disconnect 8002K71
- Communication and Security System Cable Riser-Rated, Four 16-Gauge Wires, 250 Ft Long 8280T42
- Mil. Spec. Signal/Power Connector Cap with 7/8"-20 UNEF Internal Threads 8903T84
- Mil. Spec. Signal/Power Connector Cap with 7/8"-20 UNEF External Threads 8903T83
- 10Gauge Low-Voltage Cable, 10 ft. length 9697T5
- Plastic Submersible Cord Grip NPT Threads, for 0.24"-0.47" Cord OD, 1/2 Knockout Size 69915K53
- Phillips Rounded Head Screws for Sheet Metal 18-8 Stainless Steel, Number 4 Size, 5/8" Long 92470A112
- Solder-Loaded Heat-Shrink Ring Terminals for 12-10 Wire Gauge and 1/4" Screw Size 9983K27
- Solder-Loaded Heat-Shrink Ring Terminals for 16-14 Wire Gauge and Number 8 Screw Size 9983K18
- Abrasion-Resistant Stranded Wire with FEP Insulation, 600V AC, 12 Wire Gauge, Red, 10 ft. length 6276T18
- Abrasion-Resistant Stranded Wire with FEP Insulation, 600V AC, 12 Wire Gauge, Black, 10 ft. length 6276T18

  Solder-Loaded Heat-Shrink Quick-Disconnect Terminals Fully Insulated, for 12-10 Wire Gauge 9397K18
- Submersible Enclosure with Hinged Cover Quick-Release Latch, 11-3/4" x 9-1/2" x 4-1/4", Gray 7740K141

APPENDIX B

STANDARD OPERATING PROCEDURE FOR CONTROL TESTING ON NEW RAINFALL SIMULATORS

1. Prepare the plot
    a. Till existing plot to 6.0 in. (15 cm) with digging fork
    b. Rake plot to be level with top of wooden plot borders.
    c. If necessary, add soil from top of slope and rake down
    d. Compact plot with plate compactor by passing over all areas of the plot once. Perform Proctor compaction test at three random points on the plot. Re-compact if necessary.
    e. For an erosion control product test, install a product. For a control test, skip this step
2. Prepare a test
    a. On test day, connect hoses, connect electrical box, connect the car battery, and ensure that the valves are functioning properly by toggling the switches and listening for a "click"
    b. Remove the tarp from the plot
    c. Prepare four 300 gal. (1136 L) runoff collection tanks
    d. Set up two sump pumps. Place one pump in a barrel for plot runoff to go into and be pumped into a collection tank. Place the second pump in the bottom of the catchment basin
    e. Connect the generator to both pumps and ensure their function
    f. Set up the tent or lean-to above the catchment basin
    g. Place or suspend 6 rainfall gauges in rows of 2 at quarter points on the plot and 2 ft (0.6 m) from the side borders. Check that they are level
    h. Assign workers, including:
        i. One worker to collect runoff data by taking the time to fill a container of known size every 2 min
        ii. One worker to collect turbidity samples every 3 min
        iii. One worker to start and stop the pump
        iv. One worker to operate the end valve to control pressure
        v. One worker to oversee the proper operation of the rainfall simulator and ensure that runoff is being collected separately for each intensity
        vi. Place GoPro on adjacent plot's bottom post, facing the test plot and start when ready to begin test

3. Begin a test with 2.0 in./hr (51 mm/hr) target intensity
    a. Begin the test with the end valve open and the 2.0 in./hr (51 mm/hr) switch on. Check that the 2.0 in./hr switch is on to hear the click of the valves
    b. Start the supply pump
    c. When flow reaches the end valve, allow discharge for 30 sec to ensure air pockets are not present
    d. Slowly turn the end valve until all sprinklers are functioning. The rainfall tree pressure gauges halfway up the slope should read 25 to 40 PSI (172 to 276 kPA)
    e. When all sprinklers are operating, begin the test timer
    f. For the sand plots, use the flashing pipe to switch barrels when they reach half capacity. Make sure that the pump does not get buried
    g. At 20 min, open the end valve and turn off the pump
    h. Record rainfall gauge measurements for 2.0 in./hr (51 mm/hr) target intensity
4. Continue a test with 4.0 in./hr (102 mm/hr) target intensity
    a. Switch the outlet of the sump pump inside the barrel to the 4.0 in./hr (102 mm/hr) collection tank
    b. If necessary, clean the in-line filter at the inlet of the supply pipe
    c. Turn on the 4.0 in./hr (102 mm/hr) switch on the electrical controller and listen for the “click”
    d. Re-start the rainfall simulator by turning on the pump and controlling pressure with the end valve
    e. At 40 min, open the end valve and turn off the pump
    f. Record rainfall gauge measurements for 4.0 in./hr (102 mm/hr) target intensity
5. Finish a test with 6.0 in./hr (152 mm/hr) target intensity
    a. Switch the outlet of the sump pump inside the barrel to the 6.0 in./hr (152 mm/hr) collection tank
    b. Turn on the 6.0 in./hr (152 mm/hr) switch on the electrical controller and listen for the “click”
    c. If necessary, clean the in-line filter at the inlet of the supply pipe
    d. Re-start the rainfall simulator by turning on the pump and controlling pressure with the end valve
    e. During the 6.0 in./hr (152 mm/hr) intensity, two runoff collection tanks may be necessary. Switch the hose outlet when required
    f. At 60 min, open the end valve and turn off the pump
    g. Record rainfall gauge measurements for 6.0 in./hr (152 mm/hr) target intensity

h. If necessary, clean the in-line filter at the inlet of the supply pipe

6. Clean up after testing
    a. Collect GoPro
    b. Cover collection tanks with tarp for 24 hr or more for settling
    c. Clean up materials and make sure that the electrical control box is not left outside
7. Measure sediment from runoff
    a. After at least 24 hr, uncover the runoff collection tanks
    b. Collect sediment in 5-gal. (19-L) buckets and separate by strata or apparent moisture content
    c. Weigh all buckets and record weights by strata or apparent moisture content
    d. Find representative moisture contents for each strata or apparent soil moisture group by weighing 100 g of wet sediment, microwaving for 6 min or until dry, and then weighing dry sample. The weight difference between the samples divided by the wet weight is the moisture content
    e. Clean collection tanks and buckets

APPENDIX C

EXPERIMENTAL DATA

TABLE C.0.1: Original AU-SRF Rainfall Simulator Rainfall Intensity Verification Data

Rain Gauge Number	2 in./hr	4 in./hr	6 in./hr
1	0.4	0.85	1.2
2	0.35	0.8	1.4
3	0.5	0.8	1.4
4	0.65	1.15	1.6
5	0.45	1	1.6
6	0.45	0.8	1.5
7	0.65	1.25	1.9
8	0.7	1.2	2.1
9	0.5	0.9	1.4
10	0.65	0.8	1.3
11	0.5	1.15	1.75
12	0.55	1.05	1.85
13	0.7	1.4	2.2
14	0.6	0.8	0.1
15	0.4	0.95	1.55
16	0.5	0.9	1.45
17	0.45	1	1.4
18	0.5	1.25	1.85
19	0.4	0.95	1.3
20	0.35	0.9	1.1

	Results			
	2 in./hr	**4 in./hr**	**6 in./hr**	
Number of Observations	20	20	20	
Total Rainfall Depth	10.25	19.9	29.95	*in*
Avg. Rainfall Depth	0.51	1.00	1.50	*in*
$\sum$|V*i*-VA*vg*| (cm)	3.04	2.99	5.85	*in*
Coefficient of Uniformity (Cu)	82.20	84.97	80.47	*%*
Avg. Rainfall Intensity	5.21	10.11	15.21	*cm/hr*
Avg. Rainfall Intensity	2.05	3.98	5.99	*in./hr*
Standard Deviation	0.11	0.18	0.44	*in./hr*

TABLE C.0.2: Original AU-SRF Rainfall Simulator 2 in./hr Switch Selection Data

Rain Gauge Number	Top	Middle	Bottom
1	0.45	0.35	0.45
2	0.5	0.3	0.50
3	0.5	0.3	0.60
4	0.75	0.65	0.50
5	0.55	0.4	0.55
6	0.5	0.4	0.60
7	0.6	0.65	0.75
8	0.75	0.6	0.75
9	0.5	0.6	0.60
10	0.45	0.5	0.45
11	0.7	0.45	0.55
12	0.75	0.45	0.65
13	0.75	0.65	0.95
14	0.85	0.5	0.15
15	0.5	0.4	0.50
16	0.55	0.35	0.50
17	0.55	0.4	0.65
18	0.8	0.5	0.60
19	0.7	0.45	0.40
20	0.4	0.3	0.50

Results

	Top	Middle	Bottom	
Number of Observations	20	20	20	
Total Rainfall Depth	12.10	9.20	11.2	*in*
Avg. Rainfall Depth	0.61	0.46	0.56	*in*
$\sum$|V*i*-VA*vg*| (cm)	2.42	1.94	2.22	*in*
Coefficient of Uniformity (Cu)	80.00	78.91	80.18	*%*
Avg. Rainfall Intensity	6.15	4.67	5.69	*cm/hr*
Avg. Rainfall Intensity	2.42	1.84	2.24	*in./hr*
Standard Deviation	0.14	0.12	0.16	*in./hr*

TABLE C.0.3: 2 in./hr Rainfall Gauge Versus Runoff Volume Intensity Method Comparison

Rain Gauge Number	Test 1	Test 2	Test 3	Test 4	Test 5	Test 6	Test 7	Test 8	Test 9
1	0.8	0.7	0.8	0.7	0.7	0.7	0.8	0.7	0.7
2	1	0.9	0.9	0.8	0.7	0.9	0.6	0.8	0.7
3	0.8	0.7	0.8	0.6	0.6	0.7	0.7	0.7	0.8
4	0.8	0.9	0.8	0.8	0.6	0.9	0.8	0.6	0.8
5	0.7	0.70	0.7	0.7	0.80	0.7	0.6	0.70	0.8
6	0.6	0.60	0.6	0.8	0.80	0.7	0.7	0.70	0.7
Runoff Depth in Tank, in.	8.5	8.6	8.4	7.7	7.8	7.9	7.8	7.7	7.7

Results		
Number of Observations per Test	6	
Avg. Rainfall Gauge Intensity	2.20	*in/hr*
Rainfall Gauge Standard Deviation	0.11	*in./hr*
Average Runoff Volume	100	*gal.*
Average Runoff Intensity Conversion	1.5	*in./hr*
Runoff Volume Intensity Standard Deviation	0.09	*in./hr*

TABLE C.0.4: 4 in./hr Rainfall Gauge Versus Runoff Volume Intensity Method Comparison

Rain Gauge Number	Test 1	Test 2	Test 3	Test 4	Test 5	Test 6	Test 7	Test 8	Test 9
1	1.4	1.8	1.5	1.4	1.2	1.4	1.3	1.5	1.3
2	1.50	1.4	1.6	1.50	1.4	1.6	1.30	1.4	1.3
3	1.4	1.3	1.5	1.3	1.3	1.3	1.4	1.2	1.5
4	1.4	1.3	1.4	1.5	1.4	1.4	1.5	1.5	1.4
5	1.1	1.4	1.3	1.4	1.2	1.3	1.2	1.4	1.3
6	1.1	1.3	0.9	1.4	1.3	1.4	1.4	1.3	1.3
Runoff Depth in Tank, in.	14.8	15.2	15.4	15.4	14.4	15.1	15.2	14.9	15.1

Results		
Number of Observations per Test	6	
Avg. Rainfall Gauge Intensity	4.10	*in/hr*
Rainfall Gauge Standard Deviation	0.13	*in./hr*
Average Runoff Volume	190.3	*gal.*
Average Runoff Intensity Conversion	2.9	*in./hr*
Runoff Volume Intensity Standard Deviation	0.07	*in./hr*

TABLE C.0.5: 6 in./hr Rainfall Gauge Versus Runoff Volume Intensity Method Comparison on Original AU-SRF Rainfall Simulator

Rain Gauge Number	Test 1	Test 2	Test 3	Test 4	Test 5	Test 6	Test 7	Test 8	Test 9
1	2.7	1.8	2.2	2	1.8	1.9	1.9	2	1.8
2	2.2	2.7	2.2	2.1	2.1	2.2	2	2	2
3	1.7	2.2	2	2	2	2	2.1	2	2.1
4	1.8	2.1	1.8	2	1.8	1.8	2.1	1.8	1.9
5	2.40	1.7	1.9	1.90	2.3	2.3	2.10	2.2	2.2
6	2.40	1.8	1.8	2.30	2.1	2.1	2.20	2	2.1
Runoff Depth, in.	24.0	24.4	23.8	23.0	23.3	22.6	23.3	22.9	22.7

Results		
Number of Observations per Test	6	
Avg. Rainfall Gauge Intensity	6.2	*in/hr*
Rainfall Gauge Standard Deviation	0.18	*in./hr*
Average Runoff Volume	296.41	*gal.*
Average Runoff Intensity Conversion	4.5	*in./hr*
Runoff Volume Intensity Standard Deviation	0.13	*in./hr*

TABLE C.0.6: New Rainfall Simulators Rainfall Intensity Verification Data on Plot 3

Rain Gauge Number	2 in./hr	4 in./hr	6 in./hr
1	0.6	1.3	2.2
2	0.6	1.2	1.9
3	0.6	1.2	2.3
4	0.7	1	1.7
5	0.6	1.5	1.9
6	0.5	1	1.4
7	0.6	1.3	1.2
8	0.3	0.9	1.5
9	0.6	1	1.8
10	0.6	1.4	1.3
11	0.5	1.1	1
12	0.5	1	1.3
13	0.5	0.9	1.5
14	0.6	0.8	2
15	0.8	0.9	1.3
16	0.5	1.1	1.7
17	0.4	0.9	1.1
18	0.4	0.7	1.6
19	0.4	1	1.3
20	0.4	0.7	1.4

	Results			
	2 in./hr	**4 in./hr**	**6 in./hr**	
Number of Observations	20	20	20	
Total Rainfall Depth	10.7	20.9	31.4	*in*
Avg. Rainfall Depth	0.54	4.18	6.28	*in*
∑|V*i*-VA*vg*| (cm)	1.90	3.48	5.85	*in*
Coefficient of Uniformity (Cu)	82.24	83.35	81.08	*%*
Avg. Rainfall Intensity	5.44	10.62	15.95	*cm/hr*
Avg. Rainfall Intensity	2.14	4.18	6.28	*in./hr*

TABLE C.0.7: Calibration with Runoff Volume on New Rainfall Simulators, Plot 3

Rain Gauge Number	2 in./hr	4 in./hr	6 in./hr
1	0.7	1.7	2.4
2	0.6	1.4	1.1
3	0.9	2.1	2.6
4	0.8	1.3	2
5	0.7	1.7	2.1
6	0.6	1.4	2.5
Average Runoff Depth, in.	6.58	14.29	21.78

	Results			
	2 in./hr	**4 in./hr**	**6 in./hr**	
Number of Rainfall Gauge Observations per Test	6	6	6	
Avg. Rainfall Gauge Intensity	2.15	4.80	6.35	*in/hr*
Runoff Volume	81.97	180.69	276.53	*gal.*
Runoff Intensity Without Conversion	1.23	2.72	4.16	*in./hr*
Runoff Intensity With Conversion	1.83	3.82	5.75	*in./hr*

TABLE C.0.8: New AU-SRF Rainfall Simulators 2 in./hr Flour Pan Method Data

Sieve Size	Pellet Weight (g)	Number of Pellets
#4 (4.76 mm)	0	0
#8 (2.38 mm)	0.458	27
#10 (2.0 mm)	0.19	33
#14 (1.41 mm)	0.2323	69
#20 (0.841 mm)	0.205	336
#30 (0.595 mm)	0.1042	536
Total	1.1895	1001

Sieve Size	Pellet Weight (g)	Number of Pellets
#4 (4.76 mm)	0	0
#8 (2.38 mm)	1.0257	60
#10 (2.0 mm)	0.3607	58
#14 (1.41 mm)	0.62815	271
#20 (0.841 mm)	0.6361	493
#30 (0.595 mm)	0.2813	837
Total	2.93195	1719

Sieve Size	Pellet Weight (g)	Number of Pellets
#4 (4.76 mm)	0	0
#8 (2.38 mm)	0.5407	27
#10 (2.0 mm)	0.1183	20
#14 (1.41 mm)	0.3627	239
#20 (0.841 mm)	0.2862	332
#30 (0.595 mm)	0.1191	567
Total	1.427	1185

TABLE C.0.9: New AU-SRF Rainfall Simulators 4 in./hr Flour Pan Method Data

Sieve Size	Pellet Weight (g)	Number of Pellets
#4 (4.76 mm)	0	0
#8 (2.38 mm)	0.3422	23
#10 (2.0 mm)	0.2511	27
#14 (1.41 mm)	0.6595	265
#20 (0.841 mm)	0.3843	627
#30 (0.595 mm)	0.3078	1391
Total	1.9449	2333

Sieve Size	Pellet Weight (g)	Number of Pellets
#4 (4.76 mm)	0	0
#8 (2.38 mm)	1.4516	74
#10 (2.0 mm)	0.5151	71
#14 (1.41 mm)	0.7516	242
#20 (0.841 mm)	0.8673	811
#30 (0.595 mm)	0.361	1428
Total	3.9466	2626

Sieve Size	Pellet Weight (g)	Number of Pellets
#4 (4.76 mm)	0.136	1
#8 (2.38 mm)	0.8987	39
#10 (2.0 mm)	0.2704	32
#14 (1.41 mm)	0.3217	108
#20 (0.841 mm)	0.2756	388
#30 (0.595 mm)	0.122	594
Total	2.0244	1162

TABLE C.0.10: New AU-SRF Rainfall Simulators 6 in./hr Flour Pan Method Data

Sieve Size	Pellet Weight (g)	Number of Pellets
#4 (4.76 mm)	0	0
#8 (2.38 mm)	0.9864	52
#10 (2.0 mm)	0.1458	19
#14 (1.41 mm)	0.4948	184
#20 (0.841 mm)	0.2396	231
#30 (0.595 mm)	0.2694	942
Total	2.136	1428

Sieve Size	Pellet Weight (g)	Number of Pellets
#4 (4.76 mm)	0.1475	1
#8 (2.38 mm)	0.1604	21
#10 (2.0 mm)	2.2094	117
#14 (1.41 mm)	0.4896	194
#20 (0.841 mm)	0.5717	761
#30 (0.595 mm)	0.2703	1071
Total	3.8489	2165

Sieve Size	Pellet Weight (g)	Number of Pellets
#4 (4.76 mm)	0.1923	2
#8 (2.38 mm)	1.0918	57
#10 (2.0 mm)	0.1953	23
#14 (1.41 mm)	0.3891	102
#20 (0.841 mm)	0.2518	254
#30 (0.595 mm)	0.1429	671
Total	2.2632	1109

TABLE C.0.11: Photography 2 in./hr Drop Size Data

Photo	Drop	Width (px)	Height (px)	Angle (deg)	Width (mm)	Height (mm)	Distance (mm)
2.1	1	116	1060	3	2.83	25.86	23.03
	4	39	390	1.1	0.95	9.52	8.56
	5	43	488	23.2	1.05	11.91	10.86
	6	32	437	22	0.78	10.66	9.88
	8	28	121	2.1	0.68	2.95	2.27
	10	24	158	2.9	0.59	3.86	3.27
	11	24	152	1.1	0.59	3.71	3.12
	12	26	149	1.7	0.63	3.64	3.00
	13	31	340	3.9	0.76	8.30	7.54
	14	41	479	10	1.00	11.69	10.69
	15	30	362	7.4	0.73	8.83	8.10
	16	38	526	11	0.93	12.83	11.91
	18	36	400	7.9	0.88	9.76	8.88
	20	28	271	0.6	0.68	6.61	5.93
	22	24	166	2.9	0.59	4.05	3.46
	24	34	432	4.2	0.83	10.54	9.71
	27	29	352	5.9	0.71	8.59	7.88
2.3	1	32	220	0.8	0.78	5.37	4.59
	2	32	200	0.7	0.78	4.88	4.10
	3	48	308	5.2	1.17	7.52	6.34
	4	26	161	4.8	0.63	3.93	3.29
	5	35	264	6.7	0.85	6.44	5.59
	6	26	177	3.6	0.63	4.32	3.68
2.4	1	33	239	5.1	0.81	5.83	5.03
	2	32	213	11.4	0.78	5.20	4.42
	3	28	260	6	0.68	6.34	5.66
	4	30	235	3.2	0.73	5.73	5.00
	5	43	251	0	1.05	6.12	5.08
	6	80	737	17.3	1.95	17.98	16.03
	7	64	590	20	1.56	14.40	12.83
2.10	1	37	336	4.3	0.90	8.20	7.30
	2	38	334	-19.5	0.93	8.15	7.22

	3	24	136	1.2	0.59	3.32	2.73
2.5	5	31	217	3.7	0.76	5.29	4.54
	6	24	221	11.6	0.59	5.39	4.81
	8	33	416	22.2	0.81	10.15	9.35
	9	31	213	0	0.76	5.20	4.44
	10	59	542	16.1	1.44	13.22	11.79
2.6	1	36	411	8	0.88	10.03	9.15
	2	25	253	7.3	0.61	6.17	5.56
	4	28	228	5.5	0.68	5.56	4.88
2.7	1	24	219	4.7	0.59	5.34	4.76
	2	26	229	3.7	0.63	5.59	4.95
2.9	1	26	213	4.8	0.63	5.20	4.56
2.8	1	24	118	1.3	0.59	2.88	2.29
	2	48	194	4.5	1.17	4.73	3.56
	3	25	193	2.5	0.61	4.71	4.10
	4	31	259	2.5	0.76	6.32	5.56
	5	32	322	12.4	0.78	7.86	7.08
	6	29	315	9.1	0.71	7.69	6.98
	7	27	240	8.3	0.66	5.86	5.20
2.2	1	25	261	11.6	0.61	6.37	5.76

TABLE C.0.12: Photography 4 in./hr Drop Size Data

Photo	Drop	Width (px)	Height (px)	Angle (deg)	Width (mm)	Height (mm)	Distance (mm)
4.1	1	31	156	4.8	0.76	3.81	3.05
	2	27	185	8.2	0.66	4.51	3.86
	3	38	219	2.2	0.93	5.34	4.42
	4	25	156	-8.8	0.61	3.81	3.20
	5	29	206	-7.4	0.71	5.03	4.32
	6	25	192	9.3	0.61	4.68	4.07
	7	24	165	8.4	0.59	4.03	3.44
4.2	1	61	328	-12.5	1.49	8.00	6.51
	2	64	340	-23.3	1.56	8.30	6.73
	3	48	271	13.5	1.17	6.61	5.44
	4	39	304	-20.1	0.95	7.42	6.47
	5	56	330	6.8	1.37	8.05	6.69
4.3	1	29	261	1.5	0.71	6.37	5.66
	2	28	212	1.8	0.68	5.17	4.49
4.4	1	67	524	1.3	1.63	12.79	11.15
4.5	1	31	216	6.7	0.76	5.27	4.51
	2	29	224	3	0.71	5.47	4.76
	3	27	468	13.5	0.66	11.42	10.76
	4	26	193	1.7	0.63	4.71	4.07
	5	34	242	4.5	0.83	5.90	5.08
	6	32	214	5.1	0.78	5.22	4.44
4.6	1	45	290	15	1.10	7.08	5.98
	2	36	208	6	0.88	5.08	4.20
	3	39	310	7.2	0.95	7.56	6.61
	4	46	302	12.1	1.12	7.37	6.25
4.7	1	35	232	9.2	0.85	5.66	4.81
	2	24	177	-10.9	0.59	4.32	3.73
	3	24	175	6.3	0.59	4.27	3.68
	5	26	130	0.5	0.63	3.17	2.54
	7	31	265	-9.1	0.76	6.47	5.71
	8	32	220	0.8	0.78	5.37	4.59
	9	44	272	9.5	1.07	6.64	5.56

	10	26	205	0	0.63	5.00	4.37
4.8	1	30	257	7.3	0.73	6.27	5.54
	2	39	254	3.4	0.95	6.20	5.25
	3	33	246	3.2	0.81	6.00	5.20
	4	24	247	11	0.59	6.03	5.44
	5	24	222	2.8	0.59	5.42	4.83
	6	40	273	2.6	0.98	6.66	5.69
	7	26	247	2.5	0.63	6.03	5.39
	8	32	473	4.3	0.78	11.54	10.76
4.9	1	33	220	15.6	0.81	5.37	4.56
	2	68	515	3.8	1.66	12.57	10.91
	3	24	210	0	0.59	5.12	4.54
	4	38	216	5.1	0.93	5.27	4.34
4.10	1	41	231	-5	1.00	5.64	4.64
	2	40	220	11.5	0.98	5.37	4.39
	3	36	212	10.9	0.88	5.17	4.29
	4	34	211	8	0.83	5.15	4.32

TABLE C.0.13: Photography 6 in./hr Drop Size Data

Photo	Drop	Width (px)	Height (px)	Angle (deg)	Width (mm)	Height (mm)	Distance (mm)
6.1	1	52	538	4.8	1.27	13.13	11.86
	2	38	280	9	0.93	6.83	5.90
	3	29	243	6.3	0.71	5.93	5.22
	4	24	190	0	0.59	4.64	4.05
	5	38	231	0	0.93	5.64	4.71
	6	56	502	5.4	1.37	12.25	10.88
	7	30	225	10	0.73	5.49	4.76
	8	28	212	5	0.68	5.17	4.49
	9	37	190	2.1	0.90	4.64	3.73
	10	51	597	15.2	1.24	14.57	13.32
	11	28	204	0	0.68	4.98	4.29
	12	25	252	11.5	0.61	6.15	5.54
	13	26	236	-13.7	0.63	5.76	5.12
6.2	2	42	369	6	1.02	9.00	7.98
	3	91	971	16.9	2.22	23.69	21.47
	4	28	224	6.2	0.68	5.47	4.78
	5	26	184	3	0.63	4.49	3.86
	6	24	199	1.5	0.59	4.86	4.27
	7	27	205	14.4	0.66	5.00	4.34
	8	25	231	39.6	0.61	5.64	5.03
	1	53	430	0	1.29	10.49	9.20
6.3	2	25	240	3	0.61	5.86	5.25
	3	39	202	2.6	0.95	4.93	3.98
	4	39	270	0.9	0.95	6.59	5.64
	5	34	272	5.8	0.83	6.64	5.81
	6	49	313	0	1.20	7.64	6.44
	7	32	220	1.1	0.78	5.37	4.59
	8	29	183	12.8	0.71	4.47	3.76
	10	27	249	14.8	0.66	6.08	5.42
	11	32	224	-2.3	0.78	5.47	4.68
	12	41	219	3.8	1.00	5.34	4.34
	13	44	256	-4	1.07	6.25	5.17

	14	36	261	6.9	0.88	6.37	5.49
	15	30	214	6.5	0.73	5.22	4.49
	16	46	268	17.7	1.12	6.54	5.42
	17	70	763	-2.4	1.71	18.62	16.91
	18	27	230	0	0.66	5.61	4.95
	19	60	408	-41.8	1.46	9.96	8.49
6.4	1	32	325	1.1	0.78	7.93	7.15
	2	24	202	-2.2	0.59	4.93	4.34
	3	29	235	6.3	0.71	5.73	5.03
	5	27	239	9.4	0.66	5.83	5.17
	6	34	171	9.7	0.83	4.17	3.34
	7	36	214	10.6	0.88	5.22	4.34
	8	29	198	5.9	0.71	4.83	4.12
	9	24	163	3.8	0.59	3.98	3.39
	10	35	236	0	0.85	5.76	4.90
	11	36	244	-8.2	0.88	5.95	5.08
	12	26	160	0	0.63	3.90	3.27
	13	26	226	11.7	0.63	5.51	4.88
	14	25	153	6.6	0.61	3.73	3.12

TABLE C.0.14: Photography 2 in./hr Drop Size Analysis

Sieve Equivalent	Bin Size	Total Weight	Count	Average Drop Weight	Average Drop Diameter (mm)	Mass Percentage
8	2.38 to 4.76	9.49755E-05	1	9.49755E-05	2.83	37.3%
10	2 to 2.38	0	0			0.0%
12	1.68 to 2	3.11535E-05	1	3.11535E-05	1.95	12.2%
16	1.19 to 1.68	2.84473E-05	2	1.42236E-05	1.50	11.2%
20	0.841 to 1.19	4.8983E-05	12	4.08192E-06	0.98	19.3%
30	0.595 to 0.841	5.08663E-05	36	1.41295E-06	0.69	20.0%
Sum		0.000254426	52			100.0%

TABLE C.0.15: Photography 4 in./hr Drop Size Analysis

Sieve Equivalent	Bin Size	Total Weight	Count	Average Drop Weight	Average Drop Diameter (mm)	Mass Percentage
8	2.38 to 4.76	0	0			0.0%
10	2 to 2.38	0	0			0.0%
12	1.68 to 2	0	0			0.0%
16	1.19 to 1.68	7.788E-05	5	1.5576E-05	1.54	43.1%
20	0.841 to 1.19	6.11538E-05	15	4.07692E-06	0.98	33.8%
30	0.595 to 0.841	4.16278E-05	29	1.43544E-06	0.69	23.0%
Sum		0.000180662	49			100.0%

TABLE C.0.16: Photography 6 in./hr Drop Size Analysis

Sieve Equivalent	Bin Size	Total Weight	Count	Average Drop Weight	Average Drop Diameter (mm)	Mass Percentage
8	2.38 to 4.76	0	0			0.0%
10	2 to 2.38	4.58524E-05	1	4.58524E-05	2.22	21.7%
12	1.68 to 2	2.08704E-05	1	2.08704E-05	1.71	9.9%
16	1.19 to 1.68	5.66727E-05	6	9.44546E-06	1.31	26.8%
20	0.841 to 1.19	4.79112E-05	13	3.68548E-06	0.95	22.6%
30	0.595 to 0.841	4.02292E-05	30	1.34097E-06	0.68	19.0%
Sum		0.000211536	51			100.0%

TABLE C.0.17: Photography Combined Intensity Drop Size Analysis

Sieve Equivalent	Bin Size	Total Weight	Count	Average Drop Weight	Average Drop Diameter (mm)	Mass Percentage
8	2.38 to 4.76	9.49755E-05	1	9.49755E-05	2.83	14.7%
10	2 to 2.38	4.58524E-05	1	4.58524E-05	2.22	7.1%
12	1.68 to 2	5.2024E-05	2	2.6012E-05	1.83	8.0%
16	1.19 to 1.68	0.000163	13	1.25385E-05	1.43	25.2%
20	0.841 to 1.19	0.000158048	40	3.9512E-06	0.97	24.4%
30	0.595 to 0.841	0.000132723	95	1.39709E-06	0.68	20.5%
Sum		0.000646623	152			

TABLE C.0.18: Original AU-SRF Rainfall Simulator Verification Bare Soil Test 1

Date:	5/31/2022		**Weather**		
Operator:	JE		**Temperature:**	84	F
Operating Pressure:	35	psi	**Wind Speed:**	1	mi/hr
Test Total Intensity:	3.86	In./hr	**Wind Direction:**	ESE	
Test Start Time:	9:30	AM	**Humidity**	73	%
Test Finish Time:	11:00	AM			

Drive Cylinder Compaction Data

Cylinder Number	**1**	**2**	**3**
Test Location Number	9	31	17
Depth of Soil Sample (in)	3.4	3	2.8
Volume of Soil in Drive Cylinder (in^3)	40.10	35.38	33.02
Weight of Drive Cylinder Soil (g)	1062	974	825
Wet Weight of Soil (g)	99	125.0	154.0
Dry Weight of Soil (g)	82	98.0	125.0
Water Content (%)	17.2	21.6	18.8
Wet Density (lb/ft^3)	100.90	104.88	95.18
Dry Density (lb/ft^3)	86.11	86.25	80.10
Maximum Dry Density (g/ cm^3)	96	96	96
Percent Compacted (%)	89.7	89.8	83.4
Average Percent Compacted (%)		87.66%	

Collected Sediment Loss

Sample Number	**A**	**B**	**C**	**D**
Settling Time (hr)	24	24	24	24
Wet Weight of Sediment + Container, lb	40.1	163	25	334.9
Container Weight, lb	1	5	1	7
Wet Weight of Sediment, lb	39.1	158	24	326.9
Dry Weight, lb	28.82	153.84	16.71	289.18
Moisture Content, %	35.67%	102.70%	43.60%	113.04%

Sample Number	E	F	G	H
Settling Time (hr)	24	24	24	24
Wet Weight of Sediment + Container, lb	87.7	166.7	611.8	72
Container Weight, lb	2	3	12	2
Wet Weight of Sediment, lb	85.7	163.7	599.8	70
Dry Weight, lb	64.21	113.74	316.63	40.35
Moisture Content, %	33.46%	43.9%	89.43%	73.47%
Total Dry Weight of Sediment, lb	1023.49			

TSS and Turbidity Data

Sample ID	Time (min)	Dilution Factor	Turbidity Reading (NTU)	Filter + Crinkle Dish (g)	Dry Filter + Soil + Crinkle Dish (g)	Turbidity (NTU)	TSS (mg/L)
1	3						
2	6	13	3521	1.4227	1.8128	45773	39010
3	9	11	4082	1.3920	2.3746	44902	81883
4	12	15	2949	1.4095	2.2442	44235	69558
5	15	15	4184	1.3992	2.0506	62760	65140
6	18	21	2642	1.4259	2.2189	55482	66083
7	21	21	3256	1.4262	2.0659	68376	63970
8	24	17	1076	1.4030	2.1234	18292	72040
9	27	17	3588	1.4070	2.0540	60996	64700
10	30	21	3441	1.4298	2.2102	72261	78040
11	33	21	3708	1.4105	2.3369	77868	92640
12	36	21	3064	1.4127	2.1533	64344	74060
13	39	21	3131	1.4250	2.1344	65751	70940
14	42	22	2869	1.4112	1.9770	63118	56580
15	45	22	2520	1.3980	1.9258	55440	52780
16	48	22	2419	1.4146	2.0592	53218	64460
17	51	21	2529	1.396	1.9041	53109	50810
18	54	21	2785	1.3990	2.1215	58485	72250
19	57	22	1599	1.4237	1.8311	35178	40740
20	60	21	1320	1.4314	1.8267	27720	39530

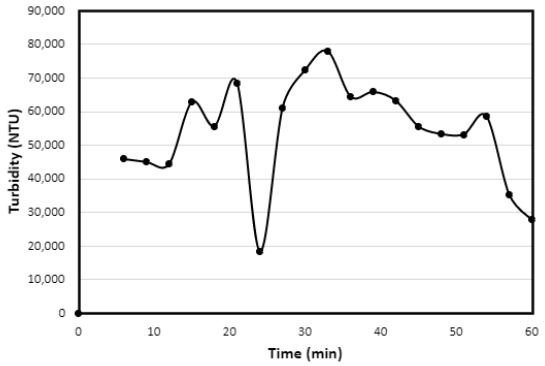

(a) Verification 1 Turbidity Results

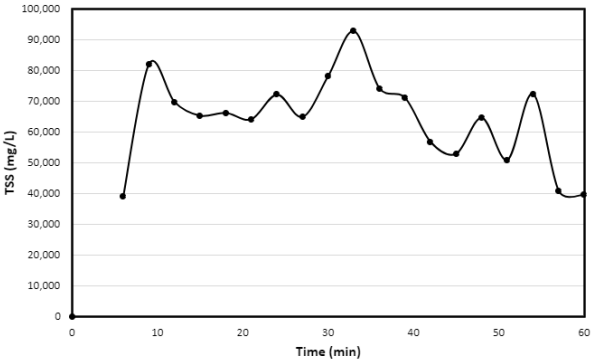

(b) Verification 1 TSS Results

TABLE C.0.19: Original AU-SRF Rainfall Simulator Verification Bare Soil Test 2

Date:	6/21/2022		**Weather**		
Operator:	JE		**Temperature:**	89	F
Operating Pressure:	36	psi	**Wind Speed:**	1	mi/hr
Test Total Intensity:	3.70	in./hr	**Wind Direction:**	N	
Test Start Time:	9:30	AM	**Humidity**	79	%
Test Finish Time:	11:00	AM			

Drive Cylinder Compaction Data

Cylinder Number	**1**	**2**	**3**
Test Location Number	11	34	20
Depth of Soil Sample (in)	5	4.3	5
Volume of Soil in Drive Cylinder (in^3)	58.97	50.71	58.97
Weight of Drive Cylinder Soil (g)	1457	1218	1465
Wet Weight of Soil (g)	105	106.0	71.0
Dry Weight of Soil (g)	86	88.0	59.0
Water Content (%)	18.1%	17.0%	16.9%
Wet Density (lb/ft^3)	94.13	91.50	94.65
Dry Density (lb/ft^3)	79.71	78.22	80.96
Maximum Dry Density (g/ cm^3)	96	96	96
Percent Compacted (%)	83.03	81.48	84.34
Average Percent Compacted (%)		82.95	

Collected Sediment Loss

Sample Number	A	B	C	D
Settling Time (hr)	24	24	24	24
Wet Weight of Sediment + Container, lb	17.3	138.6	50.9	138.7
Container Weight, lb	1	5	2	5
Wet Weight of Sediment, lb	16.3	133.6	48.9	133.7
Dry Weight, lb	28.82	153.84	16.71	289.18
Moisture Content, %	37.42%	69.30%	66.89%	47.00%

Sample Number	E	F	G	H
Settling Time (hr)	24	24	24	24
Wet Weight of Sediment + Container, lb	133.9	184.9	717.3	302.7
Container Weight, lb	4	6	17	7
Wet Weight of Sediment, lb	129.9	178.9	700.3	295.7
Dry Weight, lb	64.21	113.74	316.63	40.35
Moisture Content, %	26.18%	68.2%	38.69%	23.72%
Total Dry Weight of Sediment, lb	1471.6			

TSS and Turbidity Data

Sample ID	Time (min)	Dilution Factor	Turbidity Reading (NTU)	Filter + Crinkle Dish (g)	Dry Filter + Soil + Crinkle Dish (g)	Turbidity (NTU)	TSS (mg/L)
1	3	61	2609	1.3848	3.2341	0	46233
2	6	61	1221	1.4309	2.3880	74481	95710
3	9	61	1015	1.3782	2.3270	61915	79067
4	12	61	876	1.3938	2.0106	53436	51400
5	15	61	1018	1.4157	2.2794	62098	86370
6	18	61	831	1.3949	2.2682	50691	72775
7	21	61	823	1.3923	2.1889	50203	79660
8	24	61	755	1.3823	2.3860	46055	100370
9	27	61	835	1.3754	2.3385	50935	96310
10	30	61	989	1.3896	2.3943	60329	100470
11	33	61	936	1.4063	2.2743	57096	86800
12	36	61	826	1.3900	2.3394	50386	94940
13	39	61	799	1.3927	2.2835	48739	89080
14	42	61	699	1.4033	2.2623	42639	85900
15	45	61	751	1.3920	2.1857	45811	79370
16	48	61	923	1.4052	2.4141	56303	100890
17	51	61	1210	1.3878	2.2609	73810	87310
18	54	61	979	1.3855	2.4164	59719	103090
19	57	61	865	1.4129	2.1903	52765	77740
20	60	61	893	1.4014	2.3971	54473	99570

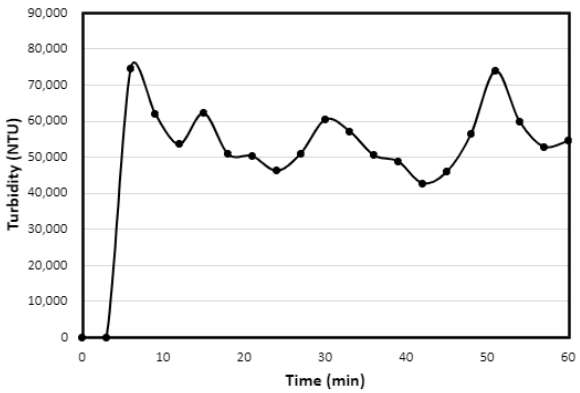

(a) Verification 2 Turbidity Results

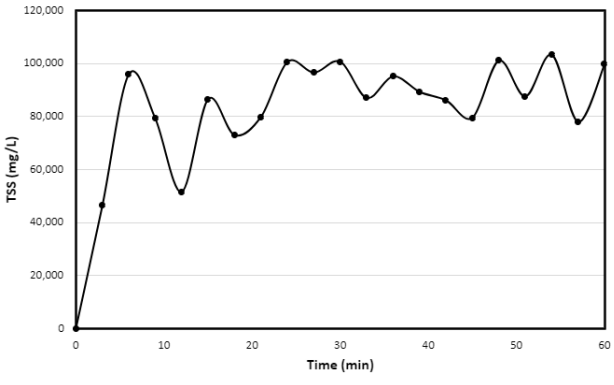

(b) Verification 2 TSS Results

TABLE C.0.20: Sand Bare Soil Test on 4H:1V Plot 3

Date:	1/20/2023		**Weather**		
Operator:	JE		**Temperature:**	56	F
Operating Pressure:	32	psi	**Wind Speed:**	1	mi/hr
Test Total Intensity:	4.23	in./hr	**Wind Direction:**	NNW	
Test Start Time:	9:30	AM	**Humidity**	60	%
Test Finish Time:	11:00	AM			

Drive Cylinder Compaction Data

Cylinder Number	**1**	**2**	**3**
Test Location Number	10	17	23
Depth of Soil Sample (in)	2.77	2	3.826
Volume of Soil in Drive Cylinder (in^3)	32.67	23.59	45.12
Weight of Drive Cylinder Soil (g)	953.4	731.2	1308.7
Wet Weight of Soil Sample (g)	138	168.2	107.2
Dry Weight of Soil Sample (g)	115.3	147.9	90.3
Water Content (%)	16.4%	12.1%	15.8%
Wet Density (lb/ft^3)	111.18	118.10	110.49
Dry Density (lb/ft^3)	95.48	105.38	95.45
Maximum Dry Density (g/ cm^3)	112	112	112
Percent Compacted (%)	85.25	94.09	85.22
Average Percent Compacted (%)		88.19	

Collected Sediment Loss

Sample Number	**1A**	**1B**	**2A**	**2B**
Settling Time (hr)	24	24	24	24
Wet Weight of Sediment + Container, lb	72.7	34.0	154.7	195.7
Container Weight, lb	7	4	10	9
Wet Weight of Sediment, lb	65.7	29.0	144.7	186.7
Dry Weight, lb	45.00	91.41	90.98	143.83
Moisture Content, %	46.00%	31.73%	59.05%	29.81%

Sample Number	2C	3A	3B	3C
Settling Time (hr)	24	24	24	24
Wet Weight of Sediment + Container, lb	42.5	302.2	67.4	63.4
Container Weight, lb	2	20	4	3
Wet Weight of Sediment, lb	40.5	282.2	63.4	60.4
Dry Weight, lb	33.25	139.12	44.45	49.06
Moisture Content, %	21.82%	102.8%	42.62%	23.13%

Sample Number	4A
Settling Time (hr)	24
Wet Weight of Sediment + Container, lb	488.9
Container Weight, lb	20
Wet Weight of Sediment, lb	468.9
Dry Weight, lb	387.85
Moisture Content, %	20.90%
Total Dry Weight of Sediment, lb	1024.9

TSS and Turbidity Data

Sample ID	Time (min)	Dilution Factor	Turbidity Reading (NTU)	Filter + Crinkle Dish (g)	Dry Filter + Soil + Crinkle Dish (g)	Turbidity (NTU)	TSS (mg/L)
1	3	21	2680	1.4063	1.7975	56280	9780
2	6	21	2333	1.4352	2.0616	48993	62640
3	9	21	2486	1.4349	1.9150	52206	40008
4	12						
5	15	21	2257	1.3945	1.8951	47397	50060
6	18	21	2217	1.4029	1.8656	46557	38558
7	21	21	2344	1.4392	2.2006	49224	76140
8	24	21	2511	1.4070	2.1329	52731	72590
9	27	21	3228	1.4506	1.7533	67788	30270
10	30						
11	33	21	2266	1.4013	1.8942	47586	49290
12	36	21	3462	1.4185	2.0695	72702	65100
13	39	21	1186	1.4295	2.3279	24906	89840
14	42	21	4040	1.4041	2.0455	84840	64140
15	45	31	2761	1.4218	2.4295	85591	100770
16	48	21	3900	1.4129	2.1411	81900	72820
17	51	31	4159	1.4537	4.1538	128929	270010
18	54	31	3667	1.4160	4.1362	113677	272020
19	57	31	4155	1.4475	4.76	128805	331250
20	60	31	3481	1.4271	3.2783	107911	185120

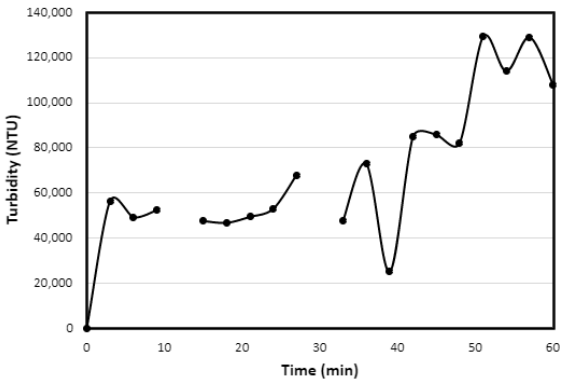

(a) Sand Turbidity Results

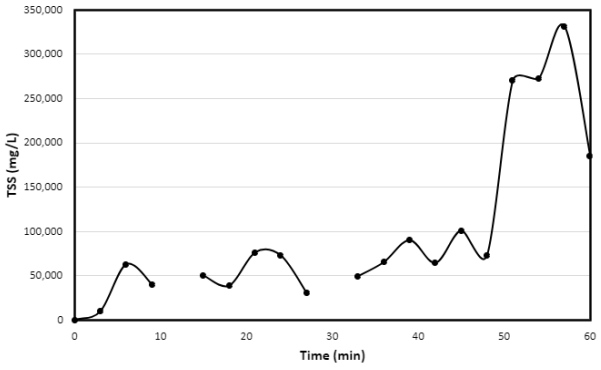

(b) Sand TSS Results

TABLE C.0.21: Loam Bare Soil Test on 4H:1V Plot 5

Date:	1/27/2023		**Weather**		
Operator:	JE		**Temperature:**	47	F
Operating Pressure:	36	psi	**Wind Speed:**	0.5	mi/hr
Test Total Intensity:	4.03	In./hr	**Wind Direction:**	NNW	
Test Start Time:	9:30	AM	**Humidity**	79	%
Test Finish Time:	11:00	AM			

Drive Cylinder Compaction Data

Cylinder Number	**1**	**2**	**3**
Test Location Number	8	17	25
Depth of Soil Sample (in)	3.1	3.2	3.2
Volume of Soil in Drive Cylinder (in^3)	36.56	37.74	37.74
Weight of Drive Cylinder Soil (g)	958	1057.8	1019.2
Wet Weight of Soil Sample (g)	83.2	68.7	114.6
Dry Weight of Soil Sample (g)	69.2	54.2	93.5
Water Content (%)	16.8%	21.1%	18.4%
Wet Density (lb/ft^3)	99.83	106.78	102.89
Dry Density (lb/ft^3)	85.45	88.17	86.89
Maximum Dry Density (g/ cm^3)	99	99	99
Percent Compacted (%)	86.31%	89.06%	87.77%
Average Percent Compacted (%)		87.71%	

Collected Sediment Loss

Sample Number	**1A**	**2A**	**2B**	**3A**
Settling Time (hr)	72	72	72	72
Wet Weight of Sediment + Container, lb	38.2	106.0	26.0	121.0
Container Weight, lb	2	4	1	4
Wet Weight of Sediment, lb	36.2	102.0	25.0	117.0
Dry Weight, lb	18.9	61.6	21.3	101.3
Moisture Content, %	91.2%	65.6%	17.3%	15.5%

Sample Number	4A	4B
Settling Time (hr)	72	72
Wet Weight of Sediment + Container, lb	93.8	36.4
Container Weight, lb	2	1
Wet Weight of Sediment, lb	91.8	35.4
Dry Weight, lb	56.4	35.4
Moisture Content, %	62.6%	14.1%
Total Dry Weight of Sediment, lb	294.97	

TSS and Turbidity Data

Sample ID	Time (min)	Dilution Factor	Turbidity Reading (NTU)	Filter + Crinkle Dish (g)	Dry Filter + Soil + Crinkle Dish (g)	Original Sample	
						Turbidity (NTU)	TSS (mg/L)
1	3	5	454	1.4414	1.4526	0	280
2	6	5	3726	1.4279	1.5233	18630	9540
3	9	8.5	2308	1.4668	1.6388	19618	14333
4	12	8.5	3652	1.4084	1.5911	31042	15225
5	15	8.5	3761	1.4168	1.5822	31968.5	16540
6	18	8.5	3199	1.4154	1.5753	27191.5	13325
7	21	8.5	3561	1.4400	1.6627	30268.5	22270
8	24	8.5	2519	1.4188	1.5677	21411.5	14890
9	27	8.5	2710	1.3860	1.5382	23035	15220
10	30	8.5	3002	1.4086	1.5568	25517	14820
11	33	8.5	2245	1.4043	1.5400	19082.5	13570
12	36	8.5	2395	1.3940	1.5225	20357.5	12850
13	39	8.5	2096	1.4105	1.5310	17816	12050
14	42	8.5	1970	1.4072	1.5325	16745	12530
15	45	8.5	1345	1.4047	1.5193	11432.5	11460
16	48	8.5	1715	1.3899	1.4981	14577.5	10820
17	51	8.5	1623	1.4011	1.5084	13795.5	10730
18	54	8.5	1506	1.4283	1.5223	12801	9400
19	57	8.5	1638	1.4118	1.5143	13923	10250
20	60	8.5	1577	1.4197	1.5107	13404.5	9100

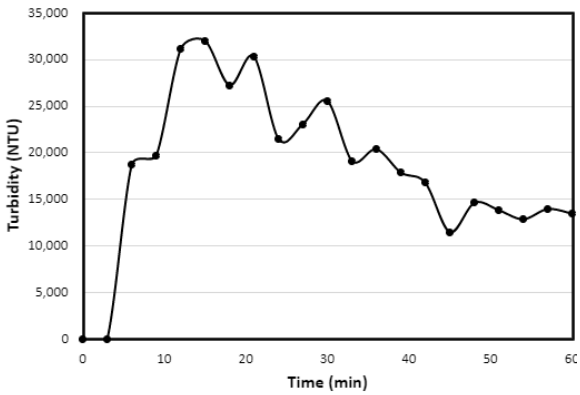

(a) Loam Turbidity Results

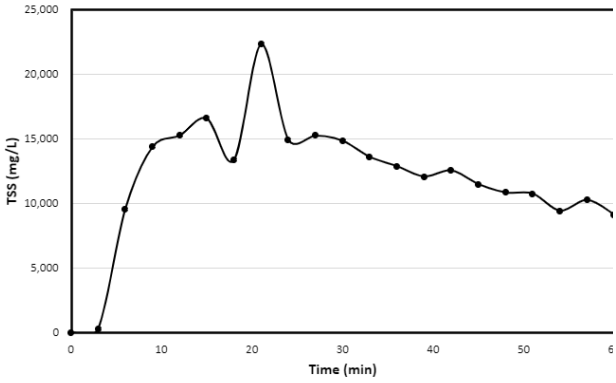

(b) Loam TSS Results

TABLE C.0.22: Clay Bare Soil Test on 4H:1V Plot 1

Date:	2/15/2022		**Weather During Calibration**		
Operator:	JE		**Temperature:**	70	F
Operating Pressure:	40	psi	**Wind Speed:**	3	mi/hr
Test Total Intensity:	4.86	In./hr	**Wind Direction:**	S	
Test Start Time:	9:30	AM	**Humidity**	84	%
Test Finish Time:	11:00	AM			

Drive Cylinder Compaction Data

Cylinder Number	1	2	3
Test Location Number	4	13	27
Depth of Soil Sample (in)	2.1	2.4	2.9
Volume of Soil in Drive Cylinder (in^3)	24.77	28.30	34.20
Weight of Drive Cylinder Soil (g)	649.1	712.2	904.5
Wet Weight of Sample Soil (g)	154.3	164.1	171.3
Dry Weight of Sample Soil (g)	127.4	122.0	132.2
Water Content (%)	17.4%	25.7%	22.8%
Wet Density (lb/ft^3)	99.85	95.86	100.75
Dry Density (lb/ft^3)	85.02	76.29	82.03
Maximum Dry Density (g/ cm^3)	88	88	88
Percent Compacted (%)	96.62%	86.69%	93.21%
Average Percent Compacted (%)		92.17%	

Collected Sediment Loss

Sample Number	1A	2A	3A	4A
Settling Time (hr)	24	24	24	24
Wet Weight of Sediment + Container, lb	9	83.6	123.9	69.8
Container Weight, lb	1	2	3	2
Wet Weight of Sediment, lb	8	81.6	120.9	67.8
Dry Weight, lb	4.31	50.11	68.40	45.46
Moisture Content, %	85.57%	62.85%	76.8%	49.13%

Sample Number	4B
Settling Time (hr)	24
Wet Weight of Sediment + Container, lb	12.6
Container Weight, lb	1
Wet Weight of Sediment, lb	11.6
Dry Weight, lb	9.51
Moisture Content, %	21.93%
Total Dry Weight of Sediment, lb	177.8

TSS and Turbidity Data

Sample ID	Time (min)	Dilution Factor	Turbidity Reading (NTU)	Filter + Crinkle Dish (g)	Dry Filter + Soil + Crinkle Dish (g)	Turbidity (NTU)	TSS (mg/L)
1	3	5	824	1.4061	1.4426	0	913
2	6	5	1145	1.4502	1.4964	5725	4620
3	9	5	1416	1.3968	1.4628	7080	5500
4	12	5	1656	1.4078	1.4824	8280	6217
5	15	5	2493	1.4099	1.4928	12465	8290
6	18	10	2317	1.4234	1.6564	23170	19417
7	21	5	2764	1.4388	1.5274	13820	8860
8	24	10	1984	1.4327	1.6394	19840	20670
9	27	10	1724	1.4000	1.6019	17240	20190
10	30	10	2198	1.4328	1.6256	21980	19280
11	33	10	1607	1.4015	1.5414	16070	13990
12	36	15	1189	1.4241	1.6092	17835	18510
13	39	10	1816	1.4569	1.5975	18160	14060
14	42	10	2418	1.4301	1.6136	24180	18350
15	45	10	2765	1.4313	1.6339	27650	20260
16	48	10	2289	1.4058	1.6039	22890	19810
17	51	10	2776	1.4123	1.5896	27760	17730
18	54	10	2319	1.4054	1.5912	23190	18580
19	57	10	1947	1.4136	1.6019	19470	18830
20	60	10	1970	1.447	1.6386	19700	19160

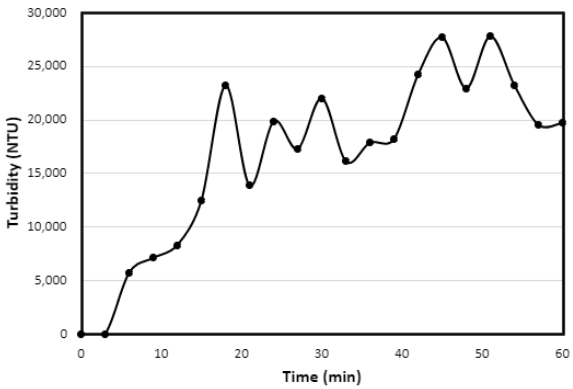

(a) Test 1 Turbidity Results

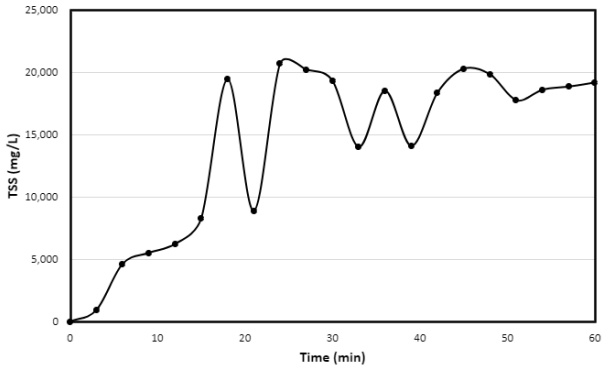

(b) Test 1 TSS Results

TABLE C.0.23: Theoretical R-factor Calculations for Flour Pan Test on New Rainfall Simulators

Target Storm Event	Target Intensity (in./hr)	Particle Diameter Range (mm)	Average raindrop size (mm)	% of rainfall	Fall Vel (m/s)	Fall Vel (ft/s)
2 in/hr	2	4.76+	-	0.00%	2.86	9.38
		4.76-2.38	3.35	38.39%	7.10	23.29
		2.38-2.0	2.31	12.22%	6.18	20.28
		2.0-1.41	1.61	21.50%	5.36	17.59
		1.41-0.841	1.23	19.27%	4.85	15.91
		0.841-0.59	0.79	8.63%	4.20	13.78
4 in/hr	4	4.76+	6.75	1.92%	7.57	24.84
		4.76-2.38	3.48	35.70%	7.19	23.58
		2.38-2.0	2.54	13.32%	6.42	21.06
		2.0-1.41	1.78	21.45%	5.57	18.28
		1.41-0.841	1.17	18.19%	4.76	15.63
		0.841-0.59	0.76	9.42%	4.15	13.63
6 in/hr	6	4.76+	6.34	4.52%	7.72	25.33
		4.76-2.38	3.32	27.95%	7.07	23.21
		2.38-2.0	3.24	31.77%	7.01	23.01
		2.0-1.41	1.78	16.09%	5.58	18.32
		1.41-0.841	1.18	11.98%	4.78	15.67
		0.841-0.59	0.79	7.69%	4.19	13.75

TABLE C.0.24: K-Factor Calculation for Sand

Target Storm Event	Test Intensity	Rainfall Vol (ft^3)	Rainfall Weight (lbf)	Rainfall Mass (slugs)	Incr. Rainfall Mass (slugs)	$KE_{rainfall}$ (ft-lbf)	$KE_{total\ rainfall}$ (ft-tonf)	Incremental E (ft-tonf/ac)	E (hundred ft-tons/ac)
					0.00	0.00	0.00	0.00	0.00
					14.88	4034.98	2.02	274.63	2.75
2 in/hr	2.25	20.00	1248.00	38.76	4.73	973.53	0.49	66.26	0.66
					8.33	1288.55	0.64	87.70	0.88
					7.47	945.05	0.47	64.32	0.64
					3.34	317.35	0.16	21.60	0.22
Average					*38.758*	*7559.45*	*3.78*	*514.52*	*5.15*
					1.44	444.35	0.22	30.24	0.30
					26.75	7436.05	3.72	506.12	5.06
4 in/hr	4.35	38.67	2412.80	74.93	9.98	2212.91	1.11	150.62	1.51
					16.07	2685.33	1.34	182.77	1.83
					13.63	1664.70	0.83	113.30	1.13
					7.06	655.06	0.33	44.58	0.45
Average					*74.932*	*15098.40*	*7.55*	*1027.63*	*10.28*
					4.75	1522.23	0.76	103.61	1.04
					29.37	7908.98	3.95	538.30	5.38
6 in/hr	6.10	54.22	3383.47	105.08	33.38	8840.71	4.42	601.72	6.02
					16.91	2837.42	1.42	193.12	1.93
					12.59	1544.63	0.77	105.13	1.05
					8.08	763.82	0.38	51.99	0.52
Average					*105.077*	*23417.78*	*11.71*	*1593.87*	*15.94*

Target Storm Event	Incremental E (hundred ft-tons/ac)	I_{30} (in./hr)	Incremental EI_{30}	Soil Loss per Intensity (lb)	Soil Loss per Intensity (ton)	A (ton/ac/yr)
2 in./hr	2.25	11.58	136.41	0.07	9.28	2.25
4 in./hr	15.42	3.65	56.29	268.05	0.13	27.53
6 in./hr	31.36	5.52	173.00	620.50	0.31	69.76

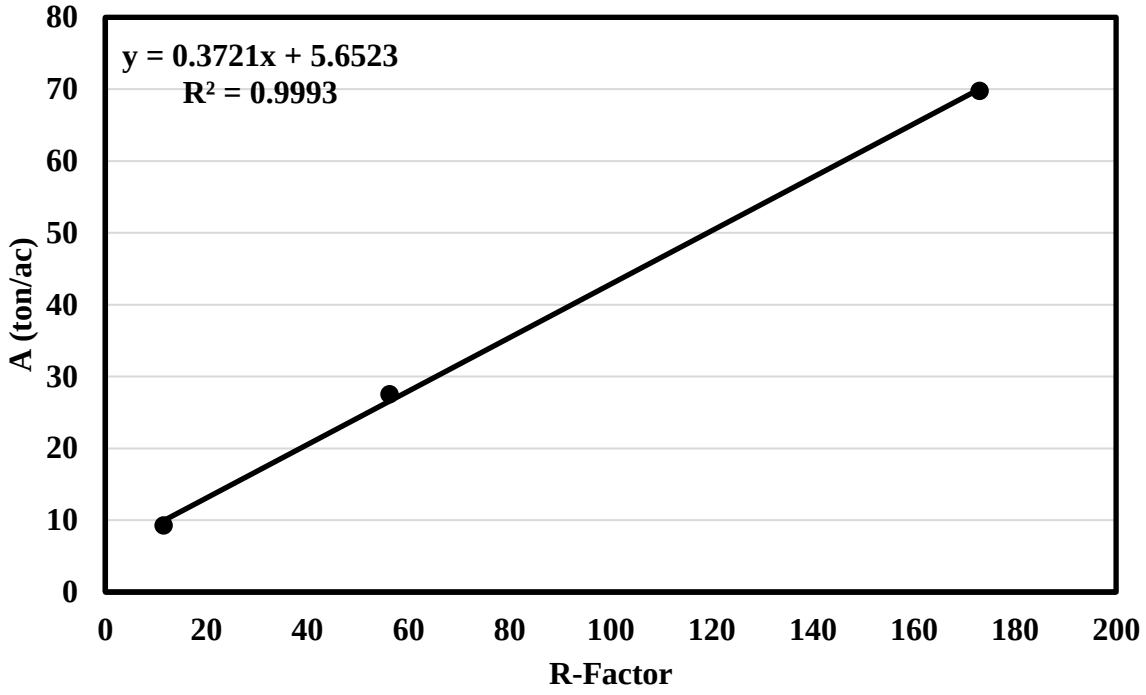

RUSLE Equation Factors

	Slope	Intercept
y =	0.3721	5.6523
x =	148.51	
y =	60.91	
K =	A/RLSCP	
A =	60.91	
Theoretical R =	148.51	
LS Factor =	2.23	
C =	1.0	
P =	1.0	
A/R =	0.4101	
K =	0.18	

TABLE C.0.25: K-Factor Calculation for Loam

Target Storm Event	Test Intensity	Rainfall Vol (ft^3)	Rainfall Weight (lbf)	Rainfall Mass (slugs)	Incr. Rainfall Mass (slugs)	$KE_{rainfall}$ (ft-lbf)	$KE_{totalrainfall}$ (ft-tonf)	Incremental E (ft-tonf/acre)	E (hundred ft-tons/ac)
					0.00	0.00	0.00	0.00	0.00
					14.88	4034.98	2.02	274.63	2.75
2 in/hr	2.25	20.00	1248.00	38.76	4.73	973.53	0.49	66.26	0.66
					8.33	1288.55	0.64	87.70	0.88
					7.47	945.05	0.47	64.32	0.64
					3.34	317.35	0.16	21.60	0.22
Average					*38.758*	*7559.45*	*3.78*	*514.52*	*5.15*
					1.32	408.59	0.20	27.81	0.28
					24.60	6837.75	3.42	465.39	4.65
4 in/hr	4.00	35.56	2218.67	68.90	9.18	2034.86	1.02	138.50	1.38
					14.78	2469.27	1.23	168.06	1.68
					12.53	1530.75	0.77	104.19	1.04
					6.49	602.35	0.30	41.00	0.41
Average					*68.903*	*13883.58*	*6.94*	*944.95*	*9.45*
					4.55	1459.84	0.73	99.36	0.99
					28.17	7584.84	3.79	516.24	5.16
6 in/hr	5.85	52.00	3244.80	100.77	32.01	8478.38	4.24	577.06	5.77
					16.22	2721.13	1.36	185.21	1.85
					12.07	1481.33	0.74	100.82	1.01
					7.75	732.51	0.37	49.86	0.50
Average					*100.770*	*22458.03*	*11.23*	*1528.55*	*15.29*

Target Storm Event	Incremental E (hundred ft-tons/ac)	I_{30} (in./hr)	Incremental EI_{30}	Soil Loss per Intensity (lb)	Soil Loss per Intentisty (ton)	A (ton/ac)
2 in/hr	5.15	2.25	11.58	18.93	0.01	1.29
4 in/hr	14.59	3.42	49.87	82.91	0.04	6.93
6 in/hr	29.88	5.23	156.37	193.10	0.10	20.07

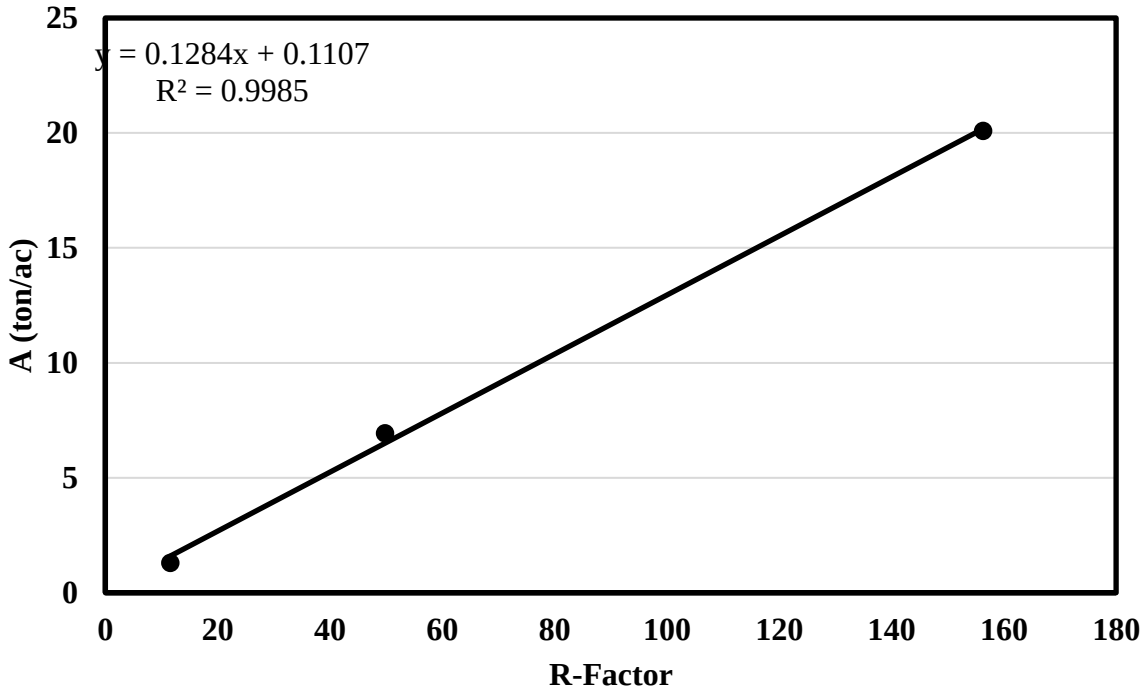

RUSLE Equation Factors

	Slope	Intercept
y =	0.1284	0.1107
x =	148.51	
y =	19.18	
K =	A/RLSCP	
A =	19.18	
Theoretical R =	148.51	
LS Factor =	2.23	
C =	1.0	
P =	1.0	
A/R =	0.1291	
K =	0.06	

TABLE C.0.26: K-Factor Calculation for Clay

Target Storm Event	Rainfall Vol (ft^3)	Rainfall Weight (lbf)	Rainfall Mass (slugs)	Incr. Rainfall Mass (slugs)	$KE_{rainfall}$ (ft-lbf)	$KE_{totalrainfall}$ (ft-tonf)	Incremental E (ft-tonf/acre)	E (hundred ft-tons/ac)
				0.00	0.00	0.00	0.00	0.00
				18.18	4931.64	2.47	335.66	3.36
2 in/hr	24.44	1525.33	47.37	5.79	1189.86	0.59	80.99	0.81
				10.19	1574.89	0.79	107.19	1.07
				9.13	1155.06	0.58	78.62	0.79
				4.09	387.87	0.19	26.40	0.26
Average				*47.371*	*9239.33*	*4.62*	*628.85*	*6.29*
				1.49	459.67	0.23	31.29	0.31
				27.68	7692.46	3.85	523.57	5.24
4 in/hr	40.00	2496.00	77.52	10.32	2289.22	1.14	155.81	1.56
				16.63	2777.93	1.39	189.07	1.89
				14.10	1722.10	0.86	117.21	1.17
				7.30	677.65	0.34	46.12	0.46
Average				*77.516*	*15619.03*	*7.81*	*1063.07*	*10.63*
				5.72	1834.16	0.92	124.84	1.25
				35.39	9529.67	4.76	648.61	6.49
6 in/hr	65.33	4076.80	126.61	40.22	10652.33	5.33	725.02	7.25
				20.38	3418.85	1.71	232.70	2.33
				15.17	1861.15	0.93	126.67	1.27
				9.74	920.34	0.46	62.64	0.63
Average				*126.609*	*28216.50*	*14.11*	*1920.49*	*19.20*

Target Storm Event	Incremental E (hundred ft-tons/ac)	I_{30} (in./hr)	Incremental EI_{30}	Soil Loss per Intensity (lb)	Soil Loss per Intentisty (ton)	A (ton/ac)
2 in/hr	6.29	2.75	17.29	4.31	0.00	0.29
4 in/hr	16.92	3.92	66.27	50.11	0.03	3.70
6 in/hr	36.12	6.40	231.19	123.40	0.06	12.10

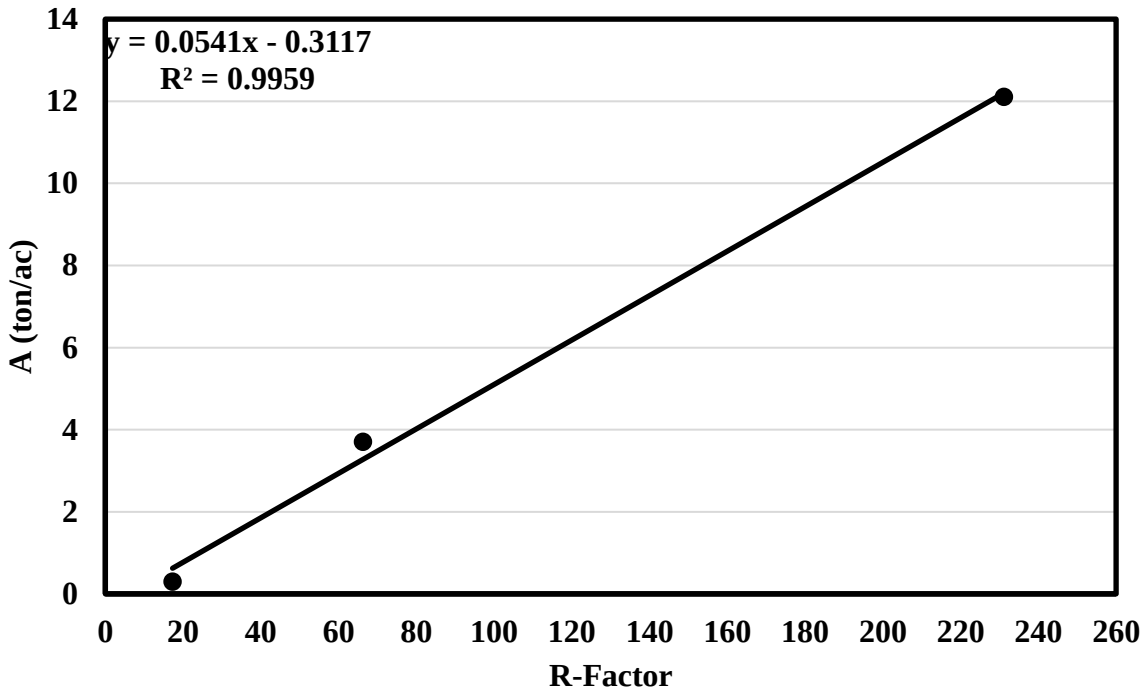

RUSLE Equation Factors

	Slope	Intercept
y =	0.0541	-0.3117
x =	148.51	
y =	7.73	
K =	A/RLSCP	
A =	7.73	
Theoretical R =	148.51	
LS Factor =	2.23	
C =	1.0	
P =	1.0	
A/R =	0.0520	
K =	0.02	